SODOS

- Appendixes -

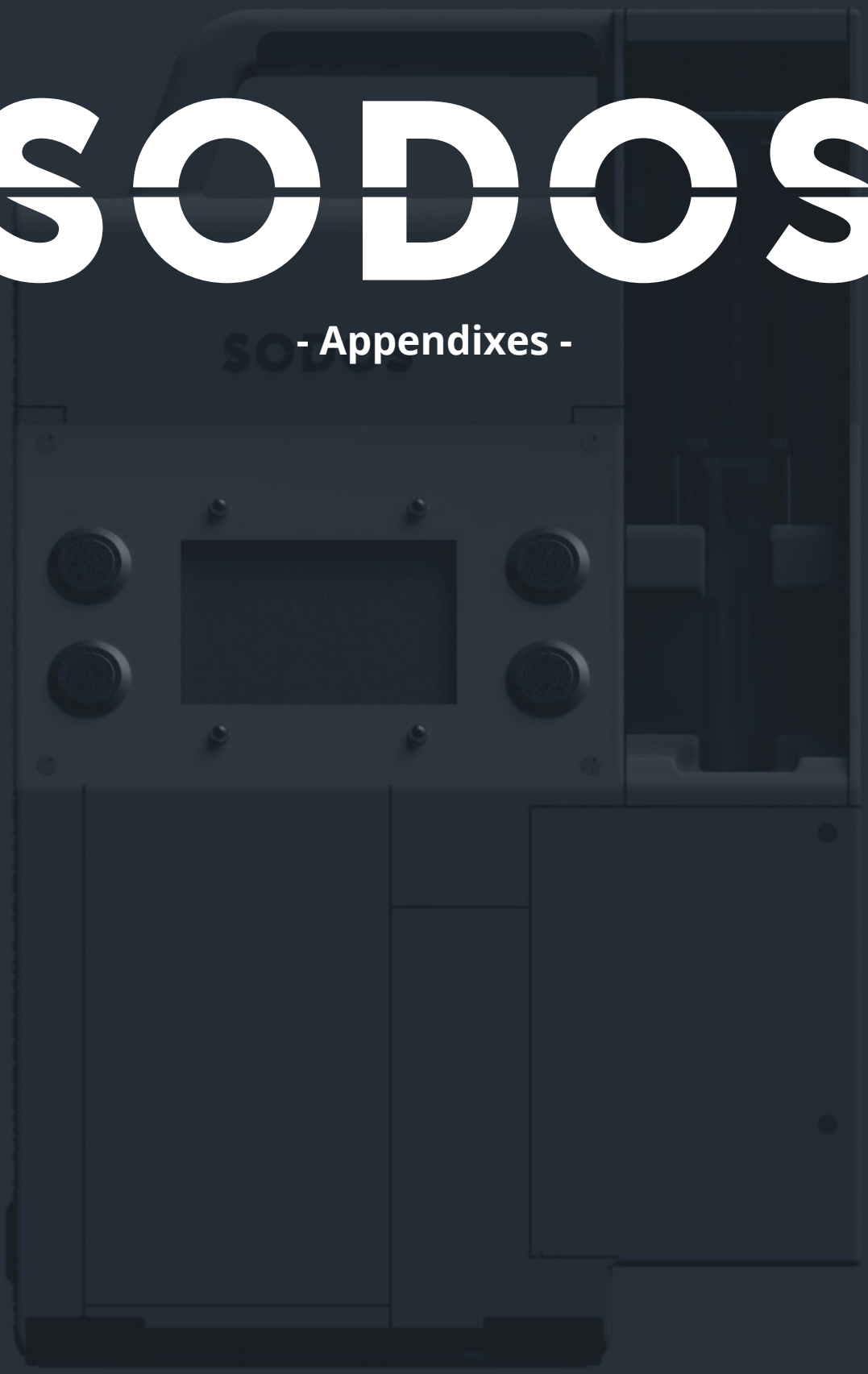

Master Thesis by Max Hoeboer
4207866 - September 2019

Table of Content

Due to both the report and the appendixes serving for two fields, it consists of sections with relevance to either or both fields, as indicated both in the Table of Content and on the bottom of each spread whenever applicable. This is indicated for both Integrated Product Design (IPD) and BioMedical Engineering (BME).

Still, to obtain a detailed overview of the graduation project and the work it entailed, it is recommended to consider the all appendixes. To maintain consistency, reference numbering in the appendix has been kept consistent with that of the report.

Integrated Product Design (IPD)

BioMedical Engineering (BME)

Appendix A. Summarizing Research Paper

In this appendix, a summarizing research paper on the report has been included. In this, the graduation project is globally and briefly discussed and an academic structure is maintained.

At the time of this report, no attempts were made to publish the presented paper. Still, another publication discussing the design is in the process of being submitted.

Automated Diagnostic Device for Urinary Schistosomiasis Using In-Line Digital Holography

Max D.B. Hoeboer
Delft University of Technology, maxhoeboer@outlook.com

Abstract – **Current diagnostic methods of urinary schistosomiasis are often unavailable in rural endemic areas. Therefore, a new diagnostic method using in-line digital holography has been proposed. Continuing on prior development by fellow students, the first both functional and interactive prototype of the diagnostic device was developed. After this, interaction evaluation and functional evaluation of the created prototype were performed in the envisioned context of rural endemic areas in Africa using users tests and 95 local urine samples respectively. Though this, valuable data has been obtained that will be used to evaluate the diagnostic potential of in-line digital holography and optimize the reconstruction and classification algorithms of the device, turning it into a fully automated diagnostic solution.**

Index Terms – Automated diagnostic, Digital holography, Schistosoma haematobium, Urinary schistosomiasis

INTRODUCTION

Urinary schistosomiasis is with over 110 million infected people one of the most common parasitic infections worldwide amongst humans [1]. It is caused by matured parasitic flatworm of the species S. haematobium of the genus schistosoma, most commonly found in Sub-Saharan Africa [2]. These flatworms manifest themselves in the urinary tract of their mammalian host and lay their eggs there [2]. These eggs are either released during urination to complete their life-cycle or retained in host tissues [2,3]. Eggs retaining in host tissues induce inflammation and die. This can result in a range of symptoms, including haematuria, anaemia, and kidney failure [2,3]. In addition, it is often associated with bladder cancer, and may result in impaired growth and cognitive development for children [4,5].

The current gold standard for diagnosing urinary schistosomiasis is manual microscopic eggs counting [2]. In this method, shown in Figure 1, an urine sample is centrifuged or stained, after which it is manually examined using a microscope for the presence of S. haematobium eggs, as shown in Figure 2. The method requires well-trained staff, an expensive microscope, and disposables, and is therefore often not available in the rural conditions of Sub-Saharan Africa. Existing alternative methods are often considered inaccurate or are unavailable, and better diagnostic tests for schistosomiasis are deemed necessary [3,6].

Therefore, a new diagnostic method has been proposed with the potential of automatically performing optical diagnosis of urine in endemic areas of Africa. This method is based on the in-line digital holographic recording of flowing urine. In this, urine can be directly and automatically analysed after placing a filled syringe, thus eliminating the need for filtration and staining. Instead, algorithms developed by fellow graduate student Patrick Nijman are used to automatically reconstruct and classify objects observed in the flowing urine. An example of S. haematobium eggs as seen both through manual microscopy and digitally reconstructed holography in saline solution using these algorithms can be seen in Figure 2.

Figure 1. Diagnosis of urinary schistosomiasis through microscopy during field research. Front; a filter is being removed from the filter holder for examination. Back; a stained filter is being examined.

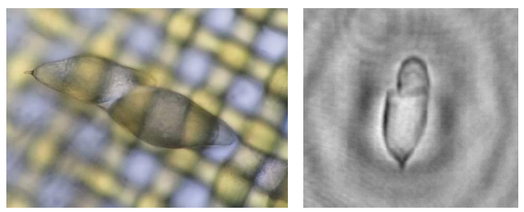

Figure 2. S. haematobium eggs as seen through microscopy with a 40x objective (left), and digital holography using the Sodos prototype and reconstructive algorithms by Patrick Nijman (right).

Up to this point, the experimental setup developed by Patrick Nijman and PhD candidate Temitope Agbana used to capture holographic footage served to provide a proof of principle, and could not be used to provide validation of the diagnostic technology in the envisioned context of endemic areas in Africa. For this, an embodiment design and prototype was to be developed.

To establish the context and user specific requirements for the proposed diagnostic method and its embodiment, a context analysis was performed by fellow graduate student Mirte Vendel. This resulted in lists of requirements and wishes for the diagnostic device and its interaction, and a conceptual interactive design [6].

The performed context analysis and advancements made in the development of the diagnostic method allowed the next steps in the development process to be performed, being the development of a both functional and interactive design and prototype for the diagnostic device and to gain validation of this prototype in the envisioned context of rural endemic areas in Africa. These were set to be the project goals, and will be further discussed. Besides this, it was decided to name the diagnostic device the Smart Optical Diagnostic of Schistosomiasis, or "Sodos" in short.

METHOD

There were two main goals to be individually addressed within the project, subdividing the project into two phases.

I. Developing a both functional and interactive prototype

The first phase consisted of developing and designing a both functional and interactive prototype of the Sodos. This required the development of multiple components in various areas of the envisioned Sodos design, as can be seen in Figure 3.

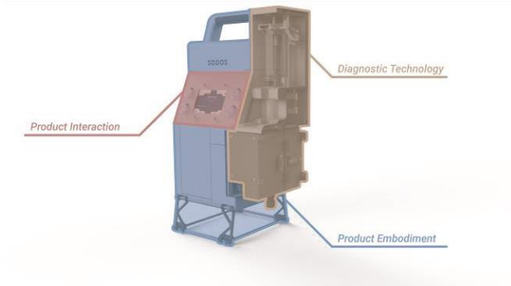

Figure 3. Areas of development for the Sodos, shown on the resulting both functional and interactive design.

In this, the development of the diagnostic technology and the accompanying components required for a fully functioning prototype was considered leading in the development. As the required diagnostic embodiment and the accompanying components required both physical and digital interaction with the user, the process of developing the product interaction was performed in parallel to the diagnostic technology development.

To ensure rapid development in both areas, parallel design cycles were adopted for each individual components within the areas. In these iterative design processes, requirements were established, designs were created, prototyped, and validated. In this phase, validation was primarily performed at the facilities of the Delft University of Technology. Validation of the diagnostic technology was performed using S. haematobium eggs in saline solution provided by the Leiden University Medical Center (LUMC). For the product interaction, validation was primarily performed using user tests. If it was found during validation that not all requirements were met, or new requirements were identified, an additional design cycle was performed.

Once all requirements were sufficiently met and no new requirements could be identified, a product embodiment design and prototype was to be created. Based on requirements set out in literature and during the context analysis, the individual components of the diagnostic technology and product interaction, and general elements of the product embodiment were developed for integration.

II. Validating the prototype in the envisioned context

The second phase consisted of the validation of the created prototype in the envisioned context of rural endemic areas in Africa. For this, a two week field trip to Ivory Coast was organized in collaboration with the Centre Suisse de Recherches Scientifiques en Côte d'Ivoire (CSRS).

The primary goal of the field trip was to evaluate the performance of the diagnostic embodiment and the technology in general. To do this, it was decided to collect high quality footage of 100-120 actual urine samples using the created prototype. In addition, the urine samples were also examined using manual microscopic egg counting, as this allows us to determine the accuracy of the prototype and the reconstruction and classification algorithms following this graduation project. Still, it was decided to not directly run the reconstruction and classification algorithms developed by Patrick Nijman in their current state, but instead only record the highest quality of footage available. This, as the algorithms were not yet optimized for the actual samples found in the field, as we do not yet have any footage of this. By recording the maximum quality of footage available and by determining the number of eggs that could be found in each sample via microscopy, it becomes possible to perform accurate optimization of the algorithms long after the field research.

The required urine samples were obtained from the endemic village of Mopé. The analysis of these samples was performed at the local health centre, called Centre de Santé Urbain d'Azaguié. For the functional evaluation, a local team was hired for five days. This included a lab technician, a lab assistant, a driver, and two urine collectors from the village of Mopé. In addition, local researchers Jean Coulibaly and Kigbafori Silue from the CSRS were actively involved throughout the field trip.

The processing of the urine samples was standardized to consistently analyse 12ml of urine in accordance with the WHO guidelines for urinary schistosomiasis [7]. In this, 20-25 urine samples were obtained every morning by the urine collectors and taken to the health centre in Azaguié by the team. Here, photos were taken of the individual urine samples in similar lightning conditions for future colour comparison. During analysis, the urine was first analysed by the prototype in accordance with the urine handling procedure set out during the first phase. After this, both the analysed sample and the water used for cleaning the prototype after a measurement were analysed by the lab technician using microscopy to determine the number of eggs that could have been observed by the prototype. The flow cell used by the prototype was replaced by a new sterile one every ten measurements and at the start of a day, and captured footage and statistics were transferred to USB sticks between measurements. In addition, all actions

performed on the prototype, anonymous participant information, and relevant observations were digitally recorded for future analysis.

For the field research, a local ethical approval was obtained. In accordance with this ethical approval, standard Praziquantel treatment was provided to all participants found to be positive for urinary schistosomiasis on the last day of measurements. This was done upon consultation with local medical professionals, and additional medication was made available to the other participants due to the possibility of false negatives.

The secondary goals of the field trip were to evaluate the interaction with the device with the envisioned user and the overall performance of the prototype in the envisioned context. For evaluating the interaction, informal user tests were to be performed throughout the field trip whenever possible. For this, the fully interactive programmed English interfaces of the prototype were to be used, and have been made bilingual by including French translations for this purpose. By performing both functional and interactive evaluation of the prototype, the overall performance of the prototype could be evaluated in the process.

Participants

For the functional and interaction evaluation, different participants were required. For the functional evaluation, a list of 200 potential voluntary participants was created by the urine collectors prior to the field research. This included participants of all ages and both sexes living in the village of Mopé. The activities and goals of the field research were communicated to the village representatives during the first visit and permission for performing these activities was obtained, as is local custom.

For the interaction evaluation, the only requirement for participants was that they should be able to read in English or French, and be working in local healthcare. For these informal user tests, no ethical approval was deemed necessary, and the purpose of the research would be explained prior to the tests.

Materials

For the functional and interaction evaluation the following materials were required:

1. The prototype with accessories
2. 100-120 urine samples
3. 130 cups, to be used by urine collectors
4. 25 cups, used and cleaned during analysis every day
5. 150 syringes, disposed after analysis
6. 15 flow cells (Ibidi µ-Slide I Luer 0.8 mm)
7. 2 external hard drives (1TB) and USB sticks (8GB)
8. 2 external power banks (10400mAh)
9. Disposable gloves in various sizes
10. Cotton buds, for cleaning the measurement box
11. 90% ethanol, for cleaning the measurement box
12. 480 tablets of Praziquantel

RESULTS

I. Developing a both functional and interactive prototype

The development of the diagnostic technology and product interaction had a total of five components that were individually developed in parallel, using two to four design cycles per component. For the diagnostic technology, three components were developed.

As previously discussed, the first component was the embodiment design for the diagnostic setup, as seen in Figure 4. This component replaced the previously developed experimental setup, and holds the optical sensor, the flow cell through which urine flows, and a suitable laser module. It also maintains accurate alignment, offsets the components, and blocks out all external light, enabling the capturing of flow-based in-line digital holographic footage. As shown, the setup can be opened for replacement of the flow cell and cleaning, and can only be activated when correctly locked to prevent accidental exposure to the laser light.

Besides this, two accompanying components were developed. This included the fluid insertion system, as seen in Figure 5. This system was developed due to the quickly identified need for a highly controlled method for inserting fluids into the flow cell of the diagnostic setup embodiment.

Figure 4. Diagnostic setup embodiment

Figure 5. Fluid insertion system

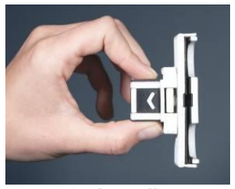

Figure 6. Flow cell placement tool

Figure 7. Digital interaction design and embodiment design

The final system is capable of reliably inserting and retracting fluids at a high accuracy using standard syringes. In combination with the setup, it is capable of automatically detecting and removing air bubbles from the flow cells.

The second accompanying component developed was a flow cell placement tool, as seen in Figure 6. This was developed, as it was quickly noticed that the flow cells used were very easily damaged. Therefore, a small tool was developed that can hold a flow cell without relying on external forces. This tool can be used to place or remove a flow cell from the setup without causing damage or contamination.

For the product interaction, two highly interdependent components were developed in parallel, being the digital interaction design and its embodiment, as seen in Figure 7. These designs were developed to enable all potentially desirable interactions with the diagnostic device within the envisioned context. The bilingual digital prototype contains all interactive functionalities and has been validated with multiple user tests. Besides this, the fluid handling protocol was detailed and made suitable for in-field validation.

After the individual components were sufficiently developed, an integrated design and prototype of the Sodos was created that is both functional and interactive, as seen in Figure 8. In this, general product requirements and elements were implemented, including a handle and a retractable stand for transportation. In addition, general electroncis including power supply and secondary sensors were implemented. After functional and interactive validation of the resulting prototype at the Delft University of Technology, validation could be performed in the envisioned context.

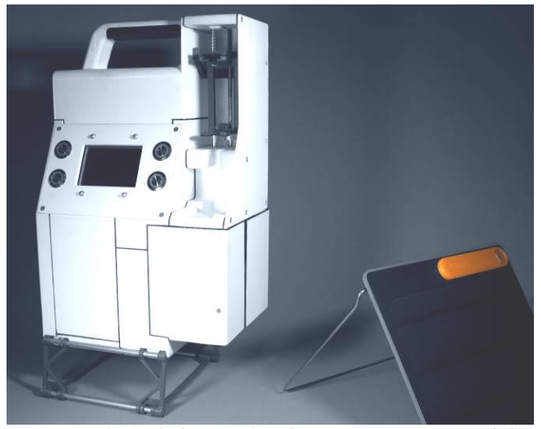

Figure 8. The both functional and interactive prototype of the Sodos

II. Validating the prototype in the envisioned context

For the functional evaluation of the prototype, a total of 102 urine samples were obtained upon request from the voluntary participants in the village of Mopé. Of these, 95 samples were photographed for colour comparison and analysed using both the prototype and manual microscopy. The remaining 7 samples were only analysed by manual microscopy due to unanticipated time restrictions. In total, 64425 holographic images were taken during the field research with a total size of 198.7Gb. For this, the prototype had been actively running for over 53 hours in 5 days. All footage has been made available to those developing the reconstruction and classification algorithms with additional statistics.

Namely, of the 95 participants, 52% was male compared to 48% female. The average age was 36.6 years (range 6-79). Using manual microscopy, it was found that 66% of the 95 participants had no infection, 30% had a light infection (1-50 eggs/10ml), and 4% had a heavy infection (>50 eggs/10ml).

Comparing manual microscopy with the currently used prototype, it was clear that manual microscopy required a lot less time to perform a diagnosis, with 174 seconds on average (range 62-310s) compared to 1440 seconds on average (range 1287-2006s). This large difference can be contributed to the increased file size of the footage due to contamination, the low writing speed of the prototype to its storage memory, and the extensive experience of the local lab technician in performing manual diagnoses of urinary schistosomiasis through microscopic egg counting. Still, the automated process of the prototype required little interaction with the user, and the duration of interaction seemed to be less than that of manual microscopy with room for further optimization.

For the evaluation of the prototype's interaction, fewer user tests could be performed than anticipated due to practical limitations. Still, during the user tests that were performed, improvements for both the digital interface design and physical embodiment design were identified. In addition, the handling of fluids during the functional evaluation was executed by the lab assistant without problems. Replacement of the flow cells was considered the main difficulty in terms of interaction.

When evaluating the overall performance of the prototype, various points of improvements were identified in the design. For both interaction and overall performance evaluations, possible solutions were envisioned as recommendations for future design iterations.

DISCUSSION

The development of a both functional and interactive prototype of the Sodos was a more complex process than anticipated. The decision to perform parallel design cycles was effective, but turned out to require five parallel design cycles instead of three. In addition, the development of the required software was more complex than expected due to new programming languages, limited documentation, and the excessive functionalities of the device. Currently, over 6400 lines of personally written code are being used to enable the on-board functionalities of the Sodos.

The resulting prototype is able to record high quality in-line digital holographic footage of flowing fluids, and enables all interactions required for intuitive usage via interfaces. The prototype has been validated both at the Delft University of Technology via simulations, and during a field trip to Ivory Coast.

This consisted of functional evaluation via direct measurements on actual urine samples, and interaction evaluation via user tests with the envisioned user. For the functional evaluation, footage was recorded at the maximum quality and the number of eggs that could be found in each sample was determined via microscopy, enabling accurate evaluation and optimization of the reconstruction and classification algorithms in the coming future.

Besides this, the potential of the method can already be discussed based on initial observations. In Figure 9, typical unprocessed in-line digital holographic footage recorded during the field research is shown. In this, it can be seen that the level of contamination greatly varied between different samples. Currently, the algorithms for diagnosis developed by Patrick Nijman perform background subtraction, followed by object detection and individual consecutive reconstruction and classification of the identified objects. Thus, the number of observable objects is largely determining the computational demands of the system. In addition, the effect of overlapping fringes of objects on the reconstructive capabilities of the algorithms should be assessed. On the other hand, seeing such a large number of objects would suggest that the device is

potentially capable of observing additional indicators of the participants' overall health. This could potentially result in the application of in-line digital holography for the diagnosis of medical conditions other than urinary schistosomiasis. It is important that each of these aspects is further explored in the coming future in order to assess the overall potential of digital holography for diagnostic purposes.

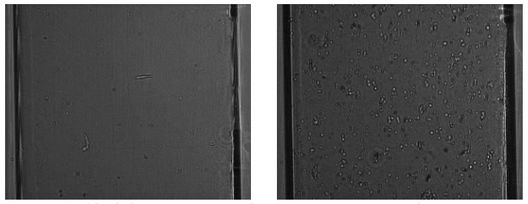

Figure 9. Slightly contaminated negative urine sample comparable to previously simulated measurements (left), and heavily contaminated negative urine sample (right)

For the both the interaction and overall performance of the Sodos, various points of improvements were identified and solutions were envisioned. Originally, an additional optional goal was to create a redesign of the Sodos towards a producible design based on the obtained feedback of the field research. However, as the prototype met the major requirements set out, and assessment of the technology is still to be performed, there was currently no clear need for this redesign. Instead, detailed recommendations for future design changes have been made.

I. Limitations

Throughout the development process of the both functional and interactive prototype, various limitation were present. Due to this project being my graduation project and the large number of components that required development, limited time was available for the development of individual designs. As a result of this and the subjective nature of user experience design [8], it can be stated that the created designs are good solutions, but possibly not the optimal solutions.

During the field research in Ivory Coast, limitations were present for both the functional and interaction evaluation. For the functional evaluation, 95 urine samples were fully analyzed. This is just short of the minimum of 100 samples set out, and therefore not considered a major limitation. In addition, only 12ml of urine could be analyzed by the prototype. Even though this is in accordance with WHO guidelines [7], it is possible to miss very light infections due to not analyzing the whole sample. Therefore, the remaining urine of 22 negatively tested urine samples was analyzed via microscopy. Through this, four additional light infections were found, suggesting a false negative rate of 18%. Therefore, it is recommended to reconsider the 10ml minimum for urine analysis set out by WHO guidelines [7].

For the interaction evaluation, fewer user tests could be performed than anticipated. This was mostly due to practical limitations, including the unexpectedly large language barrier with the envisioned users and the presence of fewer potential participants than expected. Still, the combined user tests performed at the facilities of the Delft University of Technology and in Ivory Coast are deemed sufficient support for the interaction design.

II. Recommendations

The main recommendation for future research is to perform analysis on the high quality data obtained in Ivory Coast to reassess the diagnostic potential of in-line digital holography. Only if the method shows sufficient potential after analysis, the Sodos should be further developed and simplified towards a producible product design. For this, detailed design recommendations have been made available.

CONCLUSION

For this project, the goals set out were to develop the first both functional and interactive design and prototype of the Sodos, and to gain validation of this prototype in the envisioned context of rural endemic areas in Africa. To do so, five iterative design cycles on the individual components of the Sodos were performed in parallel, and the resulting designs were integrated to form a both functional and interactive prototype. This prototype was validated and optimized at the Delft University of Technology, after which field research was performed in Ivory Coast. During the field research, the prototype was validated in terms of functionality and interaction, and data was gathered for future optimization.

ACKNOWLEDGMENT

This graduation project was supported by the Delft University of Technology, Leiden University Medical Centre, Centre Suisse de Recherches Scientifiques en Côte d'Ivoire, Centre de Santé Urbain d'Azaguié, and Delft Global Initiative. I wish to personally thank those who have performed the essential research to enable this graduation project, being Patrick Nijman, Mirte Vendel, and Temitope Agbana, and the supervisors of this project, being Jan-Carel Diehl, Jenny Dankelman, Stefan van de Geer, and Roos Oosting. In addition, I wish to thank local researchers Jean Coulibaly and Kigbafori Silue, and the other members of the local team. Finally, I wish to thank those consulting me throughout this project, including Gleb Vdovin and G-Young Van.

REFERENCES

1. World Health Organization Expert Committee on the Control of Schistosomiasis, *Prevention and control of Schistosomiasis and soil-transmitted helminthiasis*, in *World Health Organization Technical Report Series*. 2002, World Health Organization: Geneva.
2. Gryseels, B., et al., *Human schistosomiasis.* The Lancet, 2006. **368**(9541): p. 1106-1118.
3. Colley, D.G., et al., *Human schistosomiasis.* The Lancet, 2014. **383**(9936): p. 2253-2264.
4. International Agency for Research on Cancer, *Schistosomes, liver flukes and Helicobacter pylori*. Vol. 61. 1994: IARC Lyon.
5. King, C.H. and M. Dangerfield-Cha, *The unacknowledged impact of chronic schistosomiasis.* Chronic illness, 2008. **4**(1): p. 65-79.
6. Vendel, M., *The EC: a device to diagnose urinary schistosomiasis in Ghana*, in *Design Engineering*. 2018, Delft University of Technology: Repository.
7. World Health Organization. *Annex 10: Urine filtration SOP, Diagnosis of Schistosoma Haematobium*. 2017 12-07-2019]; Available from: https://www.who.int/neglected_diseases/training/Session_9.3.2_learners_guide.pdf.
8. Law, E.L.-C., et al. *Understanding, scoping and defining user experience: a survey approach*. in *Proceedings of the SIGCHI conference on human factors in computing systems*. 2009. ACM.

AUTHOR INFORMATION

Max D. B. Hoeboer, Master Student BioMedical Engineering, Department of BioMechanical Engineering, Delft University of Technology. Master Student Integrated Product Design, Department of Design for Sustainability, Delft University of Technology.

Appendix B. IDE Graduation Assignment

In the following appendix, the original IDE Graduation Assignment as submitted in the first phase of the graduation project to the Board of Examiners can be seen.

It must be noted that the information presented here may not correspond to the rest of the thesis and its appendixes.

IDE Graduation Assignment (version 2017.09.21)

incl. the student's study progress (Appendix 3)

TU Delft Delft University of Technology

To be completed by the student
Please save your assignment as (format): IDE Graduation Assignment_family name, name_student number_dd-mm-yyyy
Place the proper document name on each page of your assignment in the headline, number the pages

Name student	Max Daniël Boo Hoeboer	
Student number	4207866	
Address		
Zip- code, City		
Telephone		
E-mail address		
Start at IDE 2012 (year)	Start at TU Delft 2012 (year)	

Bachelor [1]	**Master** [1]	**Specialisation** [1]
✓ TUD Bachelor IO	✓ IPD	✓ Medisign
☐ TU/e or UT Bachelor IO	☐ DfI	
☐ TU Delft non-IO BSc	☐ SPD	**Annotation** [1]
☐ Other Dutch University Bachelor	✓ BioMedical Engineering = 2nd non-IDE master	☐ Techn. in Sustainable Design
☐ HBO Bachelor	✓ Individual programme, date of approval [2] 24-03-2018	☐ Entrepreneurship
☐ Foreign Bachelor	☐ Master Honours Programme	

Name Chair	Jan Carel Diehl

1. Check study progress	*To be completed by the Shared Service Centre O&S after approval of the assignment by the chair. The study progress will be checked for a 2nd time just before the green light meeting.*		
Bachelor degree:	☐ Yes	☐ No	☐ N.A.
Missing 1st year Master courses	1. …… 2. …… 3. ……	4. …… 5. …… 6. ……	
Master electives, no. of EC credits accumulated: ……			
Name:	Date: ….. / ….. / 20…..	Signature:	

2. Formal approval Graduation Assignment by the Board of Examiners	*To be completed by the Board of Examiners*	
Approval of the content of the Grad. Assignment:	☐ Approved	☐ Not Approved
Procedural approval:	☐ Approved	☐ Not Approved
Comments:		

[1] *Tick where appropriate.*
[2] *Date of approval of your individual programme by the Board of Examiners.*

Name:	Date: ….. / ….. / 20…..	Signature:

IDE Graduation Assignment

GENERAL INFORMATION

Title Graduation Project [3]	**The Smart Optical Diagnosis of Schistosomiasis**		
Chair of Supervisory Team [4]	Jan Carel Diehl		
Department / Section	DE / DfS		
Mentor of Supervisory Team [4]	Stefan van de Geer		
Department / Section	ID / DA		
Project commissioned by [5]	☐ Faculty	✓ Company	☐ Other, e.g. entrepreneurial
Project type [5]	✓ Design	☐ Research [6]	☐ Other, e.g. entrepreneurial
Company name, if applicable	Medical Optics fund		
City & Country	Rotterdam, The Netherlands		
Company Mentor	Mirte Vendel		
Start date	17-12-2018		
End date	03-08-2019		

CONTENT

Ascertain that the text of your Graduation Assignment clearly meets and reflects the general and specific requirements for your specific IDE master. [7]
Write your assignment in a neutral form.
When inserting images or schedules in colour, make sure a print in black and white is still readable.

Introduction
Give a sketch of the context of your assignment. Historical developments, if applicable relevant published scientific research results, new trends, status quo; materials, technologies, usage, etc.
- *In case of a faculty project: describe how your assignment reflects the research portfolio of the IDE Faculty* [6].
- *In case of a company project: provide company information.*
- *If other, e.g. entrepreneurial: describe the future enterprise and how your assignment will be of value to the enterprise.*

Include an illustration or visual which depicts the context of your assignment.
In case one or more extra parties are involved in your project, indicate which role they play.

In this project I will focus on developing a functional and interactive design and prototype for a new way of diagnosing the Schistosoma haematobium parasite. As can be seen in Figure 1, this parasite is the major agent of Schistosomiasis, which is with over 250 million people infected worldwide the most prevalent parasitic infection in humans.

This project is performed for the Medical Optics fund, a non-governmental organisation established in the year 2018. The Medical Optics fund focusses on the development of optical diagnostic solutions for parasitic infections, and aims to create functional and applicable solutions as soon as possible. As of now, this young organisation focusses on the parasitic infections Malaria, Trypanosomiasis, and Schistosomiasis.

[3] *Keep the title compact and simple. Do not use abbreviations.*
[4] *Avoid team members from the same section. In case a non-IDE mentor is preferred over an IDE-mentor, the Chair should request so for approval by the Board of Examiners (including a motivation letter and c.v. of the proposed non-IDE mentor).*
[5] *Tick where appropriate. See the IDE Graduation Manual, paragraph 2.5. If necessary, explain at Introduction.*
[6] *See webpage http://www.io.tudelft.nl/en/research/*
[7] *For general master specific requirements, consult article 4 of the Master Teaching and Examination Regulations, and the IDE Graduation Manual, especially paragraph 2.4 and 3.1.4.*

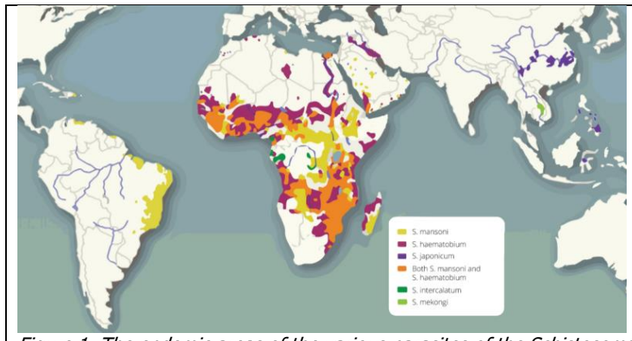

Figure 1. The endemic areas of the various parasites of the Schistosoma genus

Former Integrated Product Design student and current Medical Optics fund employee Mirte Vendel also graduated on this new way of optical diagnosis of Schistosomiasis. In this, a context analysis for the diagnostic method and device was performed in Ghana, requirements were set out, and a conceptual interactive design was created. Simultaneously, 3ME graduation student Patrick Nijman and PhD candidate Temitope Agbana started working on the development of the experimental diagnostic setup and algorithms. Recently, this has resulted in a functional proof of principle, as can be seen in Figure 2.

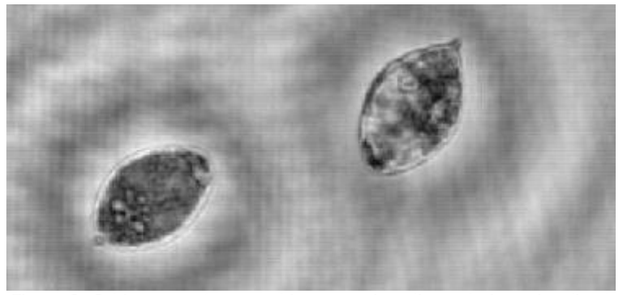
Figure 2. Schistosoma haematobium eggs in saline solution, visualized using the experimental setup.

The completion of a conceptual interactive design by Mirte and the advancements made in the diagnostic development by Patrick and Temitope created an opportunity for performing a next step in the development process; the creation of a functional and interactive prototype of the diagnostic device. For this, sufficient financial means are available and experts are available both within the TU Delft and LUMC.

As I am graduating my individual Double Master's Degree I have two chairs; Jan Carel Diehl for Industrial Design Engineering and Jenny Dankelman for BioMedical Engineering. Still, as this project is mainly initiated via Industrial Design Engineering, Jan Carel will be most actively involved throughout the project. As he and Jenny work closely together in various projects, consultation can easily be initiated between them.

Problem definition
Indicate clearly, what should/could be improved compared to the present situation. When executing a research project: indicate the knowledge gap. What opportunities exist, what contradicting demands should be addressed, etc.

The optical diagnostic technology developed by Patrick Nijman and Temitope Agbana for the Schistosoma haematobium parasite can not yet be validated in and applied to the Schistosoma haematobium endemic areas of Africa. This, as the current experimental setup is only designed to enable a proof of principle for the technology.

Therefore, there is a clear demand for an embodiment design for the diagnostic technology and validation of the diagnostic technology in the endemic areas of Africa. At the same time, the graduation project by Mirte Vendel identified the difficulties in designing such a product and suiting

interactions for the conditions present in these areas of Africa. As the diagnostic technology uses urine to perform its diagnosis, unique problems such as hygiene and repeatability are a major consideration during this project.

Assignment

Briefly and to the point, describe what you are going to design, create or generate to solve (part of) the problem.
In case of a Specialisation and/or Annotation, address specifically how this is/these are included in the assignment.

The assignment in this Master Graduation Project is to develop and design a both functional and interactive prototype for a new method of diagnosing the Schistosoma haematobium parasite using the optical analysis of urine. This prototype will be validated in a Schistosoma haematobium endemic area of Africa and a redesign will be created based on the obtained feedback.

This broad assignment covers both medical, technical, and interactive elements. Therefore, this suits both the Medisign specialisation and both masters of my individual Double Master's Degree.
As this Master Graduation Project is for my individual Double Master's Degree, I have 50 EC (33 full time weeks or 166 working days) to spend on this project. However, a clear distinction should be made within the project and report what aspects will be part of BioMedical Engineering or Integrated Product Design, or will cover both master.

Approach

What will be the approach to deal with the complexity of the assignment? What has to be done to meet the challenges? Indicate the main methodologies to be used. Indicate the same project phases as you distinguish in your planning. If one or more extra parties are involved in your project, indicate which role they play.
In case of a Specialisation and/or Annotation, address specifically how this is/these are dealt with.

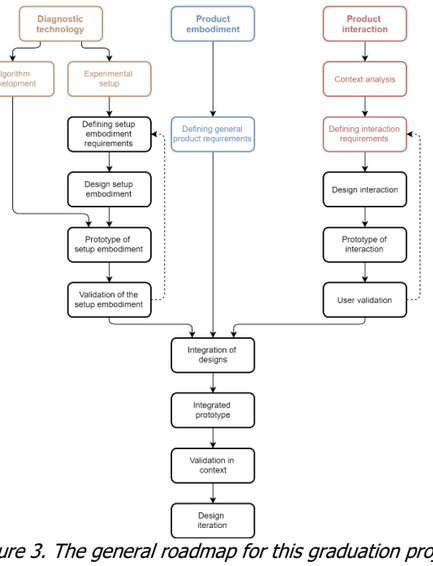

Figure 3. The general roadmap for this graduation project.

In the roadmap presented in Figure 3, the coloured fields in each of the three development areas indicate the work already (partially) done by Mirte and Patrick. It can also be seen that multiple designs and prototypes will be created and validated throughout an iterative design process. This allows me to obtain quick validation of the various design choices that are to be made and to identify new requirements.

Therefore, the first part of the project will consist of two simultaneous rapid iterative design cycles. One design cycle consists of developing a design for the currently experimental diagnostic setup created by Patrick and Temitope. This will be performed in close collaboration with Patrick to ensure a good design and easy implementation of diagnostic algorithms. Validation will be performed at the TU Delft using simulated diagnostic experiments.

In the other design cycle, the product interaction is to be developed using the existing requirements set out and incorporating the diagnostic setup design. In this, validation is performed at the TU Delft using user tests.

After both the diagnostic setup design and product interaction have been designed and validated at the TU Delft, and no more design iterations are required, an integrated design and prototype can be created. This will be a both functional and interactive design and prototype that can be used to perform field research in a Schistosoma haematobium endemic area of Africa that is yet to be determined. For this, local contacts are available at medical facilities in various African countries. In this, both the interaction with the device by the envisioned users and the actual performance of the diagnostic technology can be tested.

After the field research, a redesign can be created using the obtained feedback of the field research. This redesign will be the final deliverable of the Master Graduation Project. As this medical project contains both highly technical aspects in the development of the diagnostic technology, and interaction and embodiment aspects for the product as a whole, it is a good combination of both masters of my individual Double Master's Degree and suits my Medisign specialisation.

Graduation Project results

1. Describe the expected results or outcome of your Graduation Project. For instance, a product, a product-service combination, a strategy illustrated through product or product-service combination ideas.
2. Indicate the expected scientific and/or societal and/or commercial significance of the outcome of your project.
3. In case of a Specialisation and/or Annotation, address specifically the relevant results to be expected.

The end result of this Graduation Project is a both functional and interactive prototype of the diagnostic device and a redesign of this prototype towards a producible product design based on the obtained feedback of the field research. This will include designing the required sub-systems of such a prototype as much as possible, including both technical and interactive elements.

Due to the unique combination of challenges expected in creating such a prototype and redesign, this outcome would suit both the master Integrated Product Design with the Medisign specialisation and the master BioMedical Engineering.

The redesign can be either further validated for application, or further iterated upon. Regardless, the prototype and redesign offer a realistic step towards implementation of the diagnostic device. Hopefully, the diagnostic device will on the long run enable easy and reliable diagnoses of the Schistosoma haematobium parasite to many endemic areas around the world.

Deliverables

List the extra graduation deliverables, if any (apart from the mandatory deliverables being the thesis report, annexes if any, the poster and the representative pictures). For instance, a working prototype or a paper.

A both functional and interactive prototype of the diagnostic device, and a redesign of this prototype towards a producible product design.

Relation and relevance to the domain of Industrial Design Engineering, the chosen master direction and the IDE pillars

Explain the relation of your project with the domain of Industrial Design Engineering and your master direction IPD, DfI or SPD.
1. Relation of you project to the master IPD, DfI or SPD
Furthermore describe the interface of your project with each of the IDE pillars:
2. Business
3. Human Interaction
4. Technology

The project is a good fit to the master of Integrated Product Design due to the broad range of product design related activities involved. This is especially the case for the areas of embodiment design and prototyping.

Apart from this, the project is related to each of the three Industrial Design Engineering pillars. The project is subjected to business related requirements, including cost, durability, and easy systemic implementation. The interaction with the user is also included, as special interaction designs will be created and iterated upon. This will include both the physical and digital interaction. Technology is

most present during this project, as many technical elements are involved in every part of the design process.

Planning

Present your planning in a Gantt Chart, which can easily be made in Excel, see example underneath. Make sure a print in black and white is still readable. Mention the main phases of the project as described at Approach + number of weeks. Indicate only main activities, milestones, meetings. Take notice: 33 EC = 22 full-time weeks! Indicate periods of part-time graduation project activity and/or periods of not spending time on your graduation project, if any, for instance because of holidays [8].

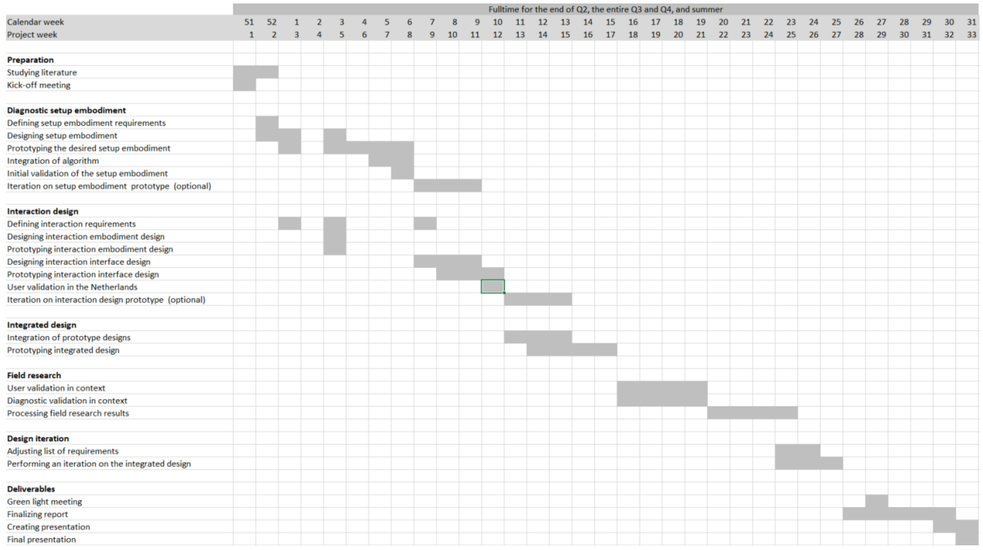

Brief explanatory remarks on the planning, if any.

As this Master Graduation Project is for my individual Double Master's Degree, I have 50 EC (33 full time weeks or 166 working days) to spend on this project.

It can be seen in the planning that the first design iteration of the diagnostic setup embodiment and interaction design are fully described. Depending on the obtained feedback during their validation iterations may be required. Still, as it can not yet be determined which steps are required for these iterations to be performed, a general timeframe has been reserved for now. This can later be specified once feedback has been obtained.

Also, the planning of the field research is difficult to specify at this point. This is due to the current uncertainties surrounding the execution of this phase.
As I intend to finish this project before the during the summer I did not plan any holidays or parallel activities.

Further comments and information

In case your Assignment needs further comments, please add any information you think is relevant.

APPROVAL BY CHAIR

Date of approval	
Signature of Chair	

[8] *Only by approval of the Board of Examiners , a not yet passed course may be combined with the Graduation Project. In such case, show the approval to your Chair and indicate the period of not spending time on your Graduation Project for this reason.*

Appendix C. Initial diagnostic setup embodiment design

To create the initial diagnostic setup embodiment design, a list of requirements and wishes was first created, as can be seen in Part A, section 2.1 of the report. Based on this, an initial design was to be made, validated, and iterated upon if necessary.

The starting point for this was the existing experimental setup developed by Patrick. As the experimental setup was already relatively defined, the freedom of design was fairly limited. Therefore, it was deemed unnecessary to perform an overall conceptual exploration of the diagnostic setup embodiment. Instead, a single embodiment design was to be developed. Where applicable, different options for elements within the design were considered and discussed.

The resulting initial diagnostic setup embodiment design and prototype did not yet have to be completely directly applicable to the product embodiment design. This, as the desired external features of the diagnostic setup embodiment design largely depended on other components of the product embodiment design. In addition, maintaining all relevant product embodiment requirements and wishes would likely limit the creative process of this early stage.

Based on the requirements set out, an initial embodiment design was created suitable for rapid prototyping, as can be seen in Figure C-1. For this design, various design choices were made to suit the requirements and wishes set out.

Figure C-1. Digital design of the initial diagnostic setup embodiment.

As can be seen, the design was a single unit (req. 4) consisting of two box sides connected via a hinge. On one side, the optical sensor was located (left), whilst the other side held the flow cell and laser module. When the box was closed, the optical sensor, flow cells, and laser module were perfectly aligned (req. 7.a). It was decided to combine the flow cell with the laser module side, as the optical sensor was too large to be combined with the flow cell, and the laser module was considered less vulnerable to contamination (wish 2.a).

C.1. Electronic components

When the box was closed the two sides have an overlap, thus preventing light from reaching the optical sensor (req. 5) and preventing the users from being exposed to laser light (req. 8.c). To further prevent the risk of users being exposed to laser light due to the user not correctly closing the box, a small hook was placed on the laser side. Once the box was closed and the hook lowered into its received end on the optical sensor side, a button was pressed. Thus, it became possible to monitor the status of this button, and only activate the laser when the button was pressed by the hook (wish 3). This reduced the risk of users being exposed to laser light due to user error (wish 7).

In order to protect the electronic elements of the optical sensor and laser module against the environmental conditions, they were enclosed as much as possible from all potential means of exposure on all sides (req. 3). This meant that both sides of the box were also enclosed on the surfaces facing each other when the box was closed. The created space contained the flow cell and its connections, and was named the flow space. Enclosing the flow space reduced the potential damage in case of urine leakage (wish 2.b) and other sources of contamination. The back panels of both sides were made removable for maintenance (req. 2) and attached using watertight bolt connections to prevent contamination. Also, in front of both the optical sensor and laser module, watertight transparent windows were created from to allow measurements whilst protecting the electronics. These windows were made from already available PET-G sheets and were easily accessible for cleaning. As the distance between the optical sensor and the flow cell must be both adjustable and less than 5.0 mm (req. 7.b and 7.c), it was decided to only hold the optical sensor from behind using an adjustable structure. This, as the holding structure would require too much space if placed between the optical sensor and flow cell. In addition, a slight deepening was made in the optical sensor side of the box to further reduce the distance.

The electronic connections required for the optical sensor and laser module were guided through standard cable screw glands from Skintop, ensuring reliable

watertight connections. In addition, these connections ensured that forces on the cables were not transferred to the more vulnerable electronic components.

C.2. Urine tubing

The same cable screw glands used for electronics connections were also used to hold the urine tubes at the entry and exit points of the urine pathway. As the interaction between SH eggs and materials was hardly studied up to this point, little requirements could be identified for the urine tubes. Therefore, a silicon tube similar to the one used in the experimental setup was used for the current design. The material can be further specified in a later stage of product development.

C.3. Flow cell connector

As the flow cell needed to removable for cleaning and maintenance (req. 6.a) and the connections to the urine pathway must be reliable and reusable (req. 6.b), a special connection was to be selected. In the experimental setup, silicone tubes were directly pressed around the cylindrical connections of the flow cell. However, this stretched the tubes excessively, was difficult to achieve, and prone to user error. Therefore, this solution was considered insufficient for the embodiment design. As the cylindrical connections of the flow cell do not contain any feature to ease the attachment, the possibilities were limited. Various types of pneumatic connectors were tested and evaluated for this application. Still, these solutions were all found to be unreliable when used in combination with the flow cell and fluids, and contained edges behind which particles may become stuck (req. 1.b). As there were no features on the cylindrical connections for attachment and the diameter of these connections was not standard, it was decided to create a custom press fitting for the connection.

The cylindrical connections are made of a rigid material. Therefore, the press fitting should be made of a slightly compressible, low friction, durable, fatigue resistant, water resistant, water insulating material. It should also be chemically resistant to chemicals potentially used for cleaning, including ethanol. In addition, human urine can have a pH value in the range of 4.5 to 8.0, depending on the patient's physical condition [21]. Therefore, the material should be both alkali-resistant and acidic-resistant.

Based on these properties, a limit was created on the level 2 CES EduPack 2018 database [22]. As slight compressibility was desirable, yet no value for the Young's modulus was determined at this point, metals and ceramic materials were excluded. As the material should insulate against the flow of water, foams were also excluded. The resulting materials were plotted with their Young's modulus over their fatigue strength logarithmically in Figure C-2.

It can be seen that PEEK, POM, and PC had a clear advantage in terms of fatigue strength. Due to the rapid availability of the material and the limited knowledge on SH egg interaction with materials, POM was selected for the current design. Yet, this material could still be further specified in a later stage of product development. The connector was given a chamfer on the side of the flow cell to make placement user friendly, and a straight end on the side of the silicone tube to strengthen the clamping

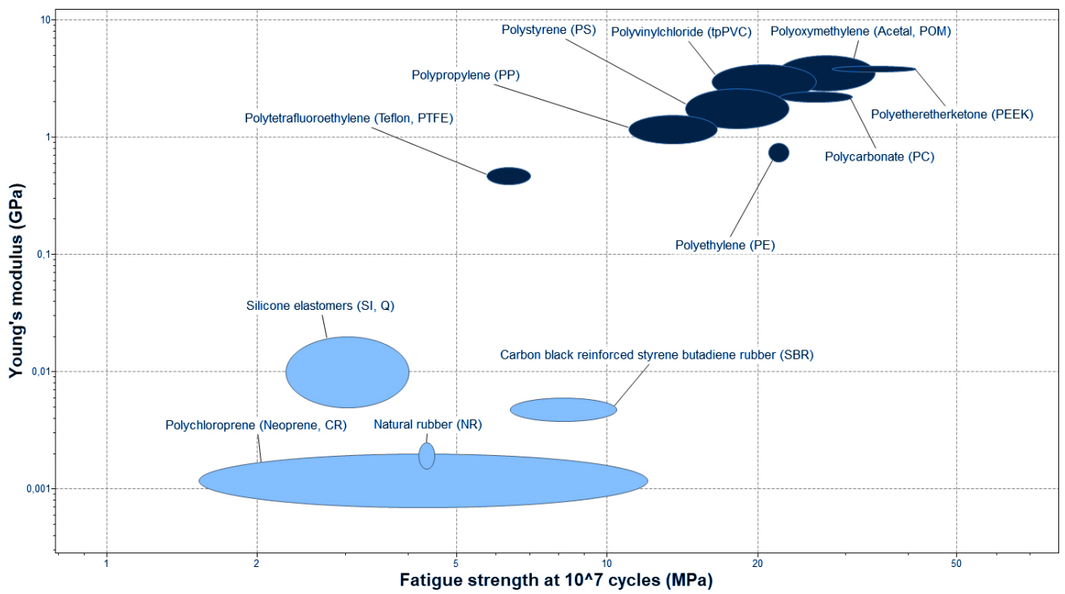

Figure C-2. Initial selection of materials for creating the flow cell connector.

of the silicone tube. As no edges should be present in the urine pathway (req. 1.b), the inner diameter of the silicone tube was made equal to the inner diameter of the cylindrical connections of the flow cell.

To determine the required hole diameter for the desired press fittings, holes were turned in POM rod with an increasing diameter in steps of 0.1 mm until a good press fitting could be achieved. Once both press fitting diameters were determined, the functioning of the connector was validated separately using pressurized water via a syringe. During this initial validation, no leakages occurred.

To keep the flow cell well positioned between the optical sensor and laser module, the flow cell connectors had to be well kept in place by the box side. This was also required to prevent forces of placing and removing the flow cell from being translated to the connection with the urine tubing. This was expected to result in leakage at this location, causing contamination and damage to the laser module. Therefore, experiments were performed with threading both POM and the PLA used in 3D printing at the TU Delft. This, as the box sides will be prototyped using this process. The results were poorly and quickly wore out, and it was decided to place an adjusting bolt perpendicular to the flow cell connector, as can be seen in Figure C-3.

Figure C-3. Digital design for the flow cell connector and its fixation to the laser side of the box.

As can be seen, a hollow cylindrical extrusion was added to the laser side of the box in which the flow cell connector could fit. A perpendicular slot was added to the side of the hollow cylinder in which a nut could be placed. Through this nut and the hollow cylinder, an adjusting bolt could be inserted to fix the flow cell connector without applying stress to the press fitting areas of the connector.

C.4. Initial laser module selection

In the experimental setup, a high-end laser module was used to create a diffuse laser light with an optical output of 5mW at a wavelength of 635nm. Therefore, the laser module in the diagnostic setup embodiment should be able to have a comparable output.

As the laser module must be directly applicable to the product embodiment design for this to be considered relevant, general product requirements and wishes were considered during the selection process.

The laser module used in the experimental setup was a precise, yet expensive device that could only be powered from the electric grid. As the product was to remain functional for multiple hours with an insufficient power supply (Part A, Section 3.1, wish 2) and should be affordable for remote areas (Section 3.1, wish 5), the device should be powerable by the Raspberry Pi used to create the prototype. This introduced a maximum power consumption of 10W for the entire diagnostic device, of which the laser was only to consume a fraction.

Laser types

There are various types of lasers that could theoretically be used to perform measurements. Semiconductor lasers, also denoted as laser diodes are relatively small, commonly used, and affordable [23]. As little optical output is required and laser diodes were already used in the experimental setup, this laser type was used in this prototype.

Parallel and diffuse laser light

As the laser light is the only light source available, having a strongly non-parallel light could cause distortions in the measurements, as objects on the outer edges would appear to be at a different location than would actually be the case. This could even result in the flow cell not being fully observable with the optical sensor.

In the current experimental setup, the laser light was slightly diffuse. Still, by increasing the distance to the flow cell, the angle could be sufficiently reduced. Ideally, parallel laser light was to be used. Still, this required a lens to be placed at a precise distance in front of the laser diode to make the light go parallel. Laser diodes are made both with and without a build-in lens. To determine the exact type of laser light desirable in the device more experiments needed to be conducted. Therefore, laser diodes of both types have been obtained and experimented with.

It was concluded that standard laser diodes with build-in lenses have a beam too narrow for the intended application, as a beam with a diameter of 12 mm was required to fully expose the optical sensor, assuming perfect alignment may not always be achieved due to the tolerances of the prototype. Therefore, a diffused laser diode was implemented in the current prototype.

Laser diode driver

The optical output of a laser diode can best be controlled via a laser diode driver [24]. These drivers maintain a constant current to obtain a desired optical output and wavelength of the laser diode. They are preferred over a constant voltage supply, as the resistance of a laser

diode is not constant and is influenced by the amount of current and temperature being supplied. Therefore, using a constant current supply protects the laser diode and ensures a constant optical output.

There are two main types of laser diode drivers, Automatic Current Control and Automatic Power Control [25]. Automatic Current Control (ACC) maintains a fixed current level, requiring a constant temperature for a constant optical output. Automatic Power Control (APC) uses current over an integrated monitor diode to close its control loop. This ensures a constant optical output power, but risks over-current with self heating or aging effects.

For this prototype, a constant current supply capable of both ACC and APC was purchased. Due to the risks of over-current and the lacking experience with laser diode drivers, it was decided to use ACC in the prototype. However, this required a constant temperature to ensure a good optical output.

Overheating of the laser diode

To prevent overheating of the laser diode, a heatsink was created from aluminum. Using this heatsink, the laser diode was activated for a prolonged duration of one hour, without any observable loss in optical output. Therefore, the heatsink was considered sufficient for the current prototype.

In the case that the heatsink turned out to be insufficient for more tropical environmental conditions, cooling fans were obtained and tested for additional cooling.

Selected laser module

For the current prototype, it was decided to use a diffused laser diode controlled by an ACC laser diode driver and cooled using a heatsink. Upon comparing different possibilities, a laser diode of the type U-LD-630551A was obtained. This laser diode has a wavelength of 635nm with a maximum optical output of 5mW [26].

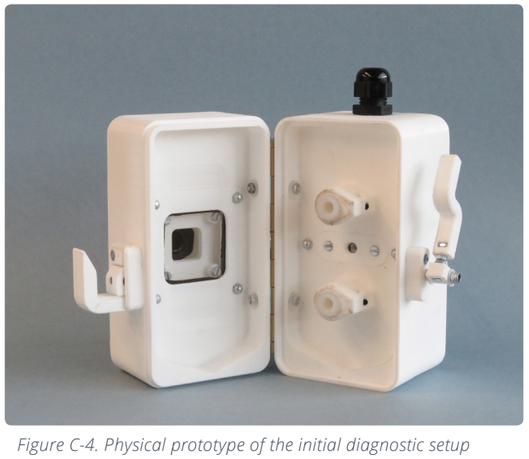

Figure C-4. Physical prototype of the initial diagnostic setup embodiment.

C.5. Initial prototype creation

The initial prototype was mostly realized using the 3D printers available at the faculty of IDE at the TU Delft. As mentioned, this was performed using regular white PLA filaments. All other materials other than the flow cell connectors were standard of-the-shelf materials that required little adjustment. The flow cell connectors were handmade using a turning lathe. Watertight sealing was achieved using nylon rings around all material connections and compressible rubber foam. The resulting prototype can be seen in Figure C-4.

C.6. Validation of initial embodiment design

Even before the initial validation was performed, it could be noticed that the flow cells were relatively easily contaminated at the area of interest, and vulnerable to mishandling. This was especially the case when the flow cells were frequently placed and removed from the flow cell connectors. Therefore, the need was identified for creating a specially designed flow cell placement tool. The development of this tool is further discussed in Part A, section 3.3 of the thesis and Appendix J.

Besides this, the flow cell connectors functioned well, as no leakages occurred. Alignment of the sensor, flow cell, and laser diode was accurate with an observable deviation not exceeding 1.0mm.

Still, it was noticed that the laser diode window was too small for easy cleaning and not the entire optical sensor area was evenly illuminated. It was also noticed that the white filament used in 3D printing was partially translucent, resulting in distortions in the footage obtained when connecting the optical sensor to a computer running the uEye Industrial Cameras Software Suite for Windows [27].

Recommendations for the next design iteration

For the next iteration, the main recommendations were to improve the laser diode illumination and window size, and to make the embodiment of a less translucent material.

It was also recommended to quickly start controlling the optical sensor using the Raspberry Pi that the Sodos was to be based on, as this might introduce new limitations to the system.

In addition, it was also recommended by advising professor Gleb Vdovin to use parallel laser light using cheap lenses rather than the current diffuse light, as this can be relatively easily obtained and would potentially improve the quality of the raw footage obtained.

Appendix D. Improved diagnostic setup embodiment design

The improved embodiment design had four major changes. First, the laser module's window size had been increased to ease cleaning and improve illumination.

The second major change was made to the laser module itself. In this, a Google Cardboard lens was added between the laser diode and laser module window in order to create a laser beam. The exact distance between the lens and laser diode was still to be determined during prototyping. In addition, a larger heatsink was added to ensure no problems would occur due to temperature changes.

The third major change was using a less translucent filament for creating the prototype. In this, a gray filament was selected as this was easily available and had shown to be capable of blocking out all external light.

D.1. Software control of the optical sensor

The fourth major change was to switch the control of the optical sensor to the Raspberry Pi that the Sodos was to be based on. In order to do this, software had to be developed. The UI-1492LE-M by IDS came with the uEye Industrial Cameras Software Suite [27]. This allowed control of the optical sensor via both Windows and Linux based systems.

The software algorithms developed by Patrick have been written in Python 3, a powerful programming language that is also one of the main programming language used on the Linux based Raspberry Pi [28]. By default, the uEye Software Suite for Linux is written in C. However, a Python 3 lean wrapper called PyuEye has also been developed for the uEye Software Suite, and can be used to communicate with the optical sensor [29]. In order to do this, an online course on the use of Python 3 was followed.

With the limited documentation and examples available on the usage of PyuEye, creating the desired communication protocol with Patrick was a difficult and time consuming process. Due to this, little optimization was performed at this stage of development, and a continuous capture mode was implemented which had a varying frame rate. In this mode, the maximum observable frame rate of the UI-1492LE-M was approximately 3 frames per second when configured at the desired 10 megapixel resolution.

As this is a relatively low frame rate, and as the exact timing of the optical sensor could not be predetermined by the system, having a constant flow of the urine sample could result in eggs not being observed. Therefore, it was decided to interrupt the movement of the stepper motor incrementally, and to temporarily freeze the optical sensor when the stepper motor of the fluid insertion system was moving. The algorithms used for the fluid insertion system at this stage of development are discussed in Appendix F.4.

Due to the maximum observable frame rate being approximately 3 frames per second when configured at a 10 megapixel resolution, a delay of up to 1/3th of a second may be present after unfreezing the optical sensor. This was far from ideal, but considered acceptable as a starting point for further development.

Object counting at large increments

During the development of the software for the optical sensor, the choice was made for the current system to only perform measurements at a relatively large interval in which an object was likely to be only observed once. This, to reduce the computational demand on the Raspberry Pi and therefore to allow a complete measurement to be performed in a reasonable amount of time. This, as a large number of samples must be processed per day (Part A, section 3.1, req. 5 and wish 4.a). The alternative of using small intervals between measurements would either increase the duration of a measurement significantly, or potentially require the resolution and quality of reconstruction to be lowered.

The observable amount of urine in a single measurement was 0.0174 ml. However, as SH eggs have the tendency to sink in urine, and the urine flowed downwards, it was decided to move in increments of 0.016 ml.

Still, it could be that a single object is observed in multiple measurements, due to internal variations in flow rate within the observable part of the flow cell. Due to the large increments between measurements, it is difficult to track objects and prevent objects from being analyzed twice. Still, as the main goal of the device was to determine whether SH eggs are present within a given urine sample and to provide a rough indication of the number of eggs, the effect of counting an object multiple times is open for discussion.

If the frame rate could be increased sufficiently by changes to either the hardware or resolution, it could become possible to decrease the increments between measurements without resulting in an unreasonable amount of time per sample. This could enable the tracking of objects within the channel and thus prevent objects from being counted more than once.

D.2. Improved prototype creation

As no changes were required to the camera side of the box other than a change in material, no new prototype had been made of this part. This to safe both time and resources. The effect of the translucent material was expected to be limited due to the translucent material not being in the sensitive area of the optical sensor.

The laser side of the box had again been realized using the 3D printers available at the TU Delft using gray filament. Most other parts could simply be disassembled from the initial prototype and reassembled on the improved prototype.

The main exception to this was the laser module, for which a new design was created. First, cheap Google Cardboard lenses were obtained, and a frame was made to accurately tune the distance between the lens and laser diode, as can be seen in Figure D-1. This included a larger and more suitable heatsink for the laser diode. After this, the distance was adjusted until a parallel laser beam could be observed. Consecutively, an embodiment design was made to accurately maintain this distance and to block out external light, as can be seen in Figure D-2.

Figure D-1. Adjustable laser module frame.

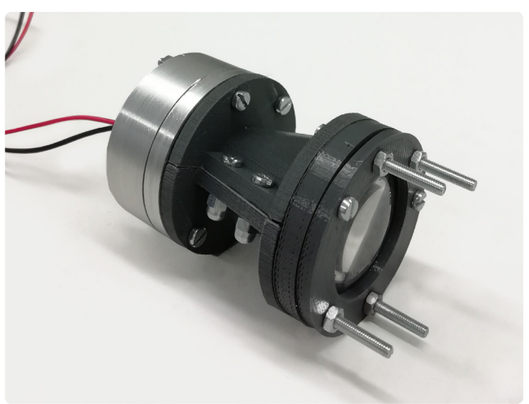

Figure D-2. Improved laser module embodiment design.

D.3. Validation of improved design

The validation of the improved diagnostic embodiment design was performed together with the validation of the improved fluid insertion system to assess the combination of the components, as can be seen in Figure D-3.

The improved prototype performed substantially better than the initial design. Disturbances due to external light were significantly reduced due to the changed filament type. Still, some light was still able to reach the optical sensor via the camera side of the box that was still made of the translucent white filament. Regardless, the flow channel could be clearly seen in a stable manner using the new laser module.

Still, there seemed to be variations in the exact position of the flow cell relative to the optical sensor, due to small variations in the relative position of the two sides of the box and variations in the placement of the flow cell in its connectors. The first was likely caused by a combination of imperfections in the prototype creation and vulnerability of the hook and hinge used to keep the two sides together. The resulting variations caused inconsistencies between measurements and should be avoided. Besides this, it also became more apparent that the distance between the optical sensor and flow cell should be further reduced to improve the reconstruction of raw footage.

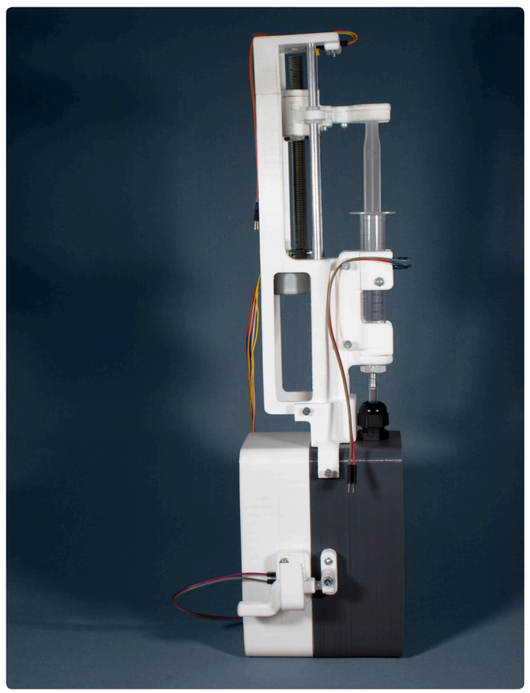

Figure D-3. Combined improved diagnostic setup embodiment and improved fluid insertion system.

Besides these inconsistencies, there seemed to be uneven illumination of the flow cell. Increasing the current supplied to the laser diode seemed to improve the distribution of light and increase the quality of the raw footage obtained. To reduce heating of the laser diode due to the increased current being supplied, the software controlling the optical sensor was adjusted to only activate the laser diode when a measurement was to be performed. However, this resulted in a varying level of illumination between measurements, indicating an inconsistent timing the measurements. After further testing together with Patrick it was concluded that temporarily freezing the optical sensor in its continuous capture mode, as discussed in Section D.1, did not result in the desired level of control and timing capabilities. Therefore, a switch was to be made to a trigger based system as soon as possible.

Recommendations for the next design iterations

The main recommendations for the next design iteration were to completely make the embodiment of the gray filament to fully eliminate the external light, to reduce the complexity and vulnerability of the hook and hinge used to keep the two sides together, to create a system capable of automatically adjusting for variations in the position of the optical sensor relative to the flow cell, and to switch the control of the optical sensor to a trigger based system. As these changes were expected to ensure the diagnostic setup embodiment meeting its requirements, this next design iteration was performed to be an integrated design.

Appendix E. Integrated diagnostic setup embodiment

For the diagnostic embodiment design, several recommendations remained at the end of the previous design iteration. Still, it was decided that the design was sufficiently developed to perform this design iteration as an integrated design. This meant that this design of the diagnostic embodiment was combined with the other separately developed sub-system designs to form a single functional and interactive prototype.

The general design process of this single design and prototype towards product embodiment is discussed in Part C of the thesis. In this appendix, the previously made recommendations for automatically adjusting for variations in flow cell placement, simplifying the hinge and hook design, and improving the software control of the optical sensor are addressed.

E.1. Automatic adjustment for variations in flow cell positioning

For the diagnostic embodiment design, the main design challenge still being presented was to create a system capable of automatically adjusting for variations in the positioning of the optical sensor relative to the flow cell.

The most important variation to adjust for was the distance between the optical sensor and flow cell, as this caused inconsistencies between measurements. Besides this, the distance between the two was to be minimized to improve reconstruction capabilities, whilst still protecting the optical sensor from potential contamination (req. 3).

To ensure a constant distance, a system was designed that used multiple springs to maintain a constant distance, a digital cross-sectional view of this can be seen in Figure E-1. In this, the optical sensor was placed in a separate container that could move relative to the camera side of the box surrounding it. This container completely protected the optical sensor from external contaminations and potential damage (req. 3).

The cable used to connect the optical sensor to the Raspberry Pi was substituted with a relatively flexible cable that was compressed into the container of the optical sensor. The cable was guided through an opening on the side of the camera side of the box, which also provides strain relief for the cable. This ensured that tension on the cable outside of the embodiment design would not negatively affect the optical sensor. It also allowed the cable inside the diagnostic to have a constant length and force on the optical sensor container.

In this design, the minimum distance between the optical sensor and flow cell was determined by the protective PET-g sheet used in the container of the optical sensor, which has a minimum thickness of 1.0mm. Besides this, a small gap should be present between the protective sheet and both the optical sensor and flow cell, as direct contact might cause damage to their surfaces. Therefore, a gap of 0.25mm was included in the design on both sides of the protective sheet, resulting in a total distance of 1.5mm.

As can be seen, springs were placed on two locations within this design. There were four compression springs inside the optical sensor container on the back of the optical sensor. These springs assured that the bolts holding the optical sensor were pressed against the

protective sheet in front of the optical sensor, ensuring a constant distance of 0.25mm between the optical sensor and protective sheet. There were also four tension springs on the outside corners of the optical sensor container being attached to the according corners of the camera side of the box. These pulled the optical sensor container towards the flow cell. The optical sensor container had two 0.25mm deep extruding edges towards the flow cell on the height of the flow cell connectors. This ensured that when the tension springs pull the optical sensor container towards the flow cell that there was a constant distance of 0.25mm between the flow cell and the protective sheet.

The inside of the camera side of the box contained geometries designed to guide the optical sensor container such that it was directly in front of the flow cell. In addition, the geometries also limited the movement on both the front and back side of the optical sensor container. This was designed such that the optical sensor container could always reach the flow cell, regardless of how deep it was placed in the flow cell connectors. It also automatically pressed the flow cell into the flow cell connectors if the flow cell was placed insufficiently deep into the connectors. Preventing potential leakages.

E.2. Simplification of the hinge and hook design

The hook design created for the initial embodiment design was created with adjustability in mind. As a result, the system was overcomplicated and vulnerable at the same time. The hinge used in the initial design was an off-the-shelf component attached to the sides of the box using bolts. As the alignment and fixation of the hinge was done manually, it was possible for the two sides of the box to become misaligned due to play in the connections. Therefore, it was decided to include the hinge into the design of the two sides of the box that were to be made using 3D printing. This reduced the possibility of misalignment by reducing the play between the parts.

During the product embodiment development, discussed in Part C of the thesis, it was decided that the diagnostic embodiment was to be placed on the lower side of the integrated design with the camera side of the box rotating open towards the outer side of the integrated design. This allowed the flow cell and protective sheets to be reachable for cleaning and maintenance purposes without reducing the usable space within the integrated design (req. 6.a). However, this also meant that the side currently holding the hook would not be reachable within the integrated design.

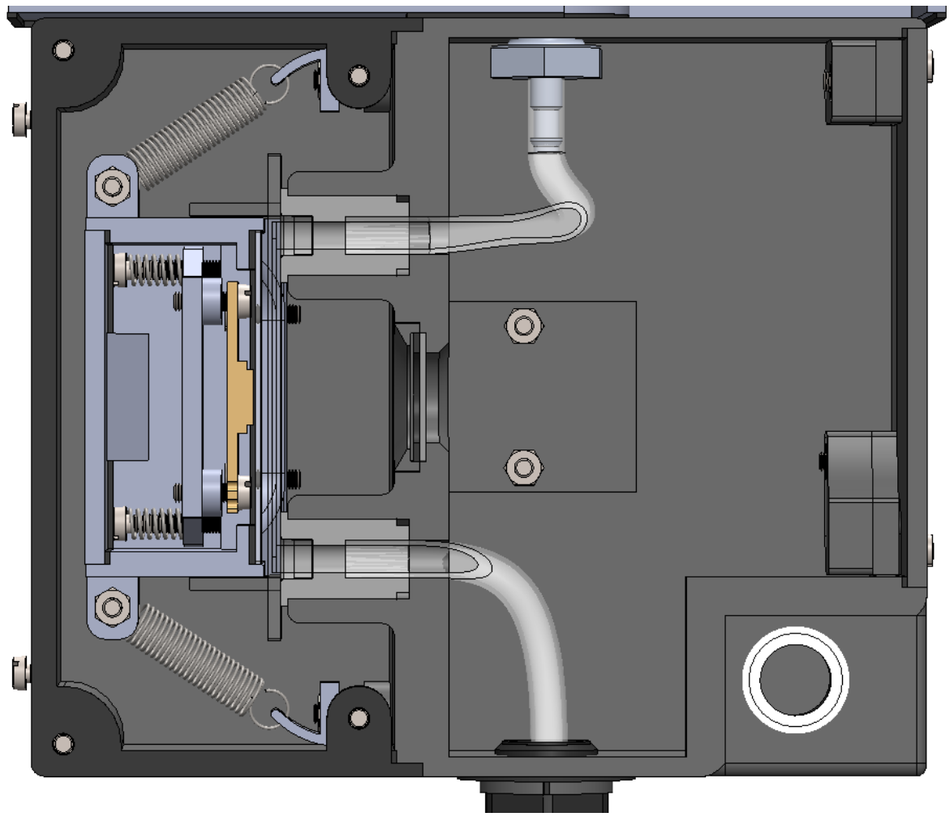

Figure E-1. Cross-sectional view of the integrated diagnostic embodiment design excluding the laser module and electronic wiring.

Within the integrated design, there was limited space available on both the bottom and back of the camera side of the box, whilst there is sufficient place on the side containing the hinge. Therefore, it was decided to place the hook on the same side as the hinge. Due to the complexity and space required for the hook and its receiving end, it was decided to replace this system with a more simplistic yet effective slide lock, as can be seen in Figure E-2. In this, a momentary switch was placed in the receiving end of the slide lock, allowing the system to detect correct closure of the box. The slide itself is 3D printed using white filament. As it is the only part of the box that is made in this color, it suggests the possibility of interaction.

E.3. Integrated prototype creation

Creating the integrated diagnostic embodiment prototype was a long process. This was mostly due to the increased complexity of the design by introducing the automatic adjustment system with springs. In addition, an increasing amount of 3D printed parts was required, as can be seen in Figure E-3. Still, experience obtained from previous prototyping iterations increased productivity significantly and resulted in the envisioned prototype. The partially assembled box and the optical sensor container can be seen in Figure E-4.

E.4. Trigger based software control of the optical sensor

As discussed in Appendix D.1, the optical sensor is currently controlled by a continuous capture mode. In this, a maximum frame rate of 3 frames per second at a resolution of 10 megapixel could be achieved. It was found during validation of the improved diagnostic setup embodiment (Appendix D.3) that temporarily freezing the optical sensor when the stepper motor was moving did not result in the desired level of control and timing capabilities. Therefore, it was recommended to switch to a trigger based system as soon as possible.

This was enabled after a long and tedious process, together with Patrick. In this, a command was sent to the optical sensor that a measurement was to be performed. Upon receiving the command, a measurement was performed and communicated to the Raspberry Pi via its USB 2.0 connection.

In this mode, performing a measurement could fail, after which a second measurement could be performed within a few milliseconds. To prevent potentially missing

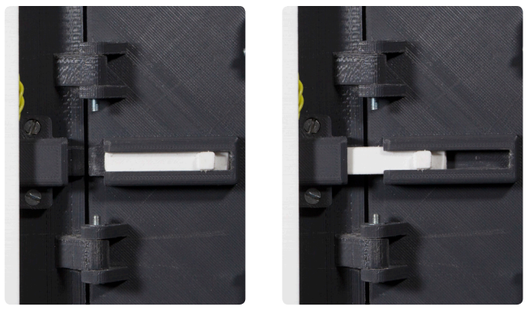

Figure E-2. 3D printed slide lock and hinge used in the integrated diagnostic embodiment.

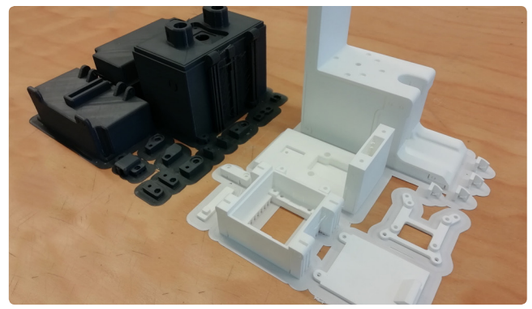

Figure E-3. Unprocessed 3D printed parts for the integrated prototype.

Figure E-4. Partially (Top) and fully (Bottom) assembled integrated diagnostic embodiment box with assembled optical sensor container.

eggs whilst taking measurements of a constant flow, and to prevent moving objects from appearing blurry, the stepper motor was still moved incrementally and interrupted during measurements. This increment was again set at 0.016 ml, for the reasons discussed in Appendix D.1.

It was determined that storing the footage accordingly on the Raspberry Pi could take up to 0.7 seconds. Therefore, the speed of the stepper motor could be kept low when moved whilst the footage was being stored. As the measurement was taken at a precise moment, the laser diode could now be deactivated between measurements to reduce power consumption and to prevent overheating. In contrast to the previously used continuous capture mode discussed in Appendix D.3, this did not result in inconsistent levels of illumination between measurements.

E.5. Validation of integrated embodiment design

During initial testing, the integrated embodiment design directly showed great improvement in terms of maintaining a constant distance and alignment. During repetitive opening and closing of the box and readjustment of the flow cell positioning, no significant differences in alignment were observed.

Besides this, the slide lock and hinge were well functional after some minor sanding, and reliably activated the momentary switch inside. Due to the entire box now being made from gray filament, external light did no longer influence the optical sensor.

However, during consecutive testing with SH eggs in saline solution, it was noticed that the laser light was overly saturating the optical sensor. As a result, SH eggs were not correctly measured. Reducing the amount of current being provided to the laser diode improved this saturation problem, but reintroduced the uneven illumination observed earlier during the validation of the improved embodiment design (Appendix D.3).

Recommendations

The main recommendation was to optimize the laser module and optical sensor configuration to eliminate the uneven illumination. As this required relatively small changes to the design, no new iteration was performed to perform this optimization.

E.6. Improving illumination consistency

To identify the source of the uneven illumination, tests were performed in collaboration with Patrick. In this, the laser module was disassembled, and the laser diode was tested separately. After it was established that the laser diode itself was not the cause of the problem, the other components of the laser module and diagnostic embodiment were tested one by one. It quickly became clear that the problem was caused by both the Google cardboard lens and the protective PET-G sheets. By removing the Google cardboard lens from the setup, the quality of illumination improved significantly.

As introduced before, using a strongly non-parallel light could cause distortions in the measurements. However, with the size of the optical sensor and current distance between the laser diode and optical sensor being 74mm, this angle was currently limited to a maximum of 2.6°. This was considered acceptable for the current prototype and was not expected to significantly influence the measurements.

Besides this, the protective PET-G sheets have been replaced by PMMA sheets of the same thickness, which were of higher quality and more durable. Experiments with the setup did show that these sheets did not negatively affect the level of illumination.

These changes resulted in clear improvements of the raw footage, as can be seen in Figure E-5. When again performing measurements on SH eggs in saline solution, most objects were now clearly visible. However, when moving the syringe, a lot of the objects became blurred. To solve this problem, solutions were explored in two directions: improving the smoothness of the fluid insertion system, which is addressed in Appendix I, and optimizing the level of illumination by the laser diode and the exposure time of the optical sensor.

E.7. Laser output and exposure time optimization

When looking into the exposure time configurations of the optical sensor, it was found that the minimum exposure time was just 0.5ms, but the default value was 500ms. This was a clear cause of the blurry objects observed and indicated a need for optimization.

For optimizing the level of illumination by the laser diode and the exposure time of the optical sensor, experiments were performed with the diffused laser light source used in the experimental setup. This, as it allowed precise control of the optical output. During the experiments, the output location of the laser light source was held at the same location as the laser diode in the integrated embodiment design.

Table E-1. The relation between exposure time and optical output.

Exposure time	Optical output required
1.0ms	0.3mW
10.0ms	0.045mW
20.0ms	0.025mW
100.0ms	0.01mW

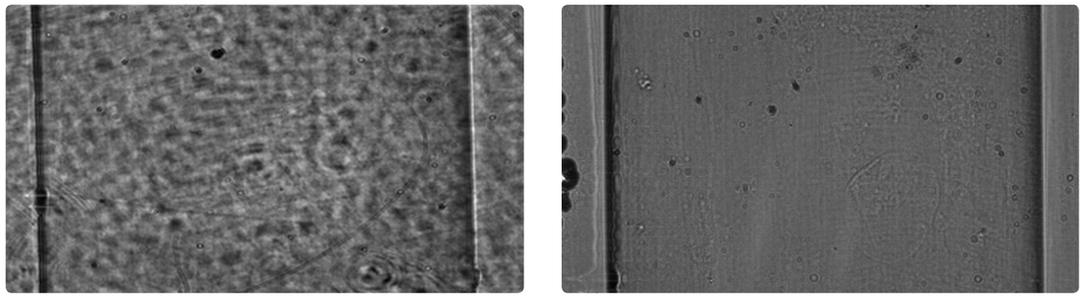

Figure E-5. Raw footage obtained from the optical sensor before (Left) and after (Right) removing the lens and replacing the PET-G sheets with PMMA sheets.

The experiments consisted of incrementally adapting the exposure time of the optical sensor and visually determining the corresponding required optical output. The corresponding optical output was determined by observing the direct raw output of the optical sensor and visually comparing this to earlier results. In this, it was important that no completely black or white areas were present on the screen, as saturation of the sensor eliminates important information. Based on the measurements performed, Table E-1 was constructed.

When selecting the exposure time for the optical sensor, the only requirement was that the resulting footage no longer contained blurry objects. Aside from this, it was important to take the maximum optical output of the laser diode into account. When again placing the laser diode, it could clearly be seen that the maximum output of the laser diode with the ACC laser driver was only sufficient for an exposure time of 125ms. This was mainly attributed to the relatively large beam divergence of the current laser diode with 7.5° perpendicular ($\theta_{\perp FWHM}$) and 33° parallel ($\theta_{\parallel FWHM}$) at its full width at half maximum [26], in combination with the relatively large distance between the laser diode and the optical sensor. As a result, only a small part of the emitted laser light reached the optical sensor. As discussed in Appendix E.6, this distance of 74mm was required to maintain a low maximum angle between the laser light and the optical sensor.

With the exposure time set at 125ms, objects still appeared slightly blurred. Therefore, it was decided that a different laser diode should be implemented. The most important change in this would be to have a smaller beam divergence so more light would reach the optical sensor.

As mentioned in Appendix C.4, both diffuse and parallel laser diodes were obtained to experiment with. It was quickly discovered that the parallel laser diodes gave a laser beam too narrow for the intended application. Still, it was found now that upon removing the lens from the lens cap in the laser diode KY-008, a laser light with a small beam divergence was obtained. Due to this, the laser diode provided sufficient light to the optical sensor to enable an exposure time of just 20ms when powered with a constant 3.3V.

The laser diode KY-008 has a wavelength of 650nm and operates on a voltage supply of 2.5-5.0V, with little other information being available. This change in wavelength required some adaptations in the algorithms by Patrick, but no major changes were required.

As discussed earlier, laser diodes normally require a laser diode driver to maintain a constant output. This, as the resistance of the laser diode is depending on its temperature. Therefore, this could also be required for the KY-008. However, the current drawn by the KY-008 when provided with a constant 3.3V is just 10.03mA. In comparison, the currently used U-LD-630551A draws approximately 55mA when powered by the constant current supply, which has a minimum of 50mA.

Still, partially due to this reduced amount of current, no heating could be observed with the KY-008, whilst this was a major concern with the U-LD-630551A. To confirm this, prolonged testing of the KY-008 was performed with a constant 3.3V supply. After over a hour, the current being draw was still constant at 10.03mA, indicating a constant resistance. Due to this and online examples with the KY-008 never using a constant current supply for Automatic Current Control (ACC), having a constant current supply was not deemed necessary for the this laser diode. Instead, the constant voltage supply of the Raspberry Pi was used. Upon adapting the heatsink to fit the KY-008, stable raw footage could be obtained. Due to this, the diagnostic setup embodiment meets the requirements set out and does not require further development.

Appendix F. Initial fluid insertion system design

To create the initial fluid insertion system design, a list of requirements and wishes was first created, as can be seen in Part A, section 3.1 of the thesis (p.30). Based on this, an initial design was made, validated, and iterated upon if necessary.

The resulting initial fluid insertion system design and prototype was to be directly combinable with the diagnostic setup embodiment design and prototype, but not yet with the product embodiment design. This, as it was not yet certain how the fluid insertion system would be positioned and designed for in the product embodiment design, and protective features could still be introduced during this phase.

F.1. Conceptual exploration

There were various options available for controlling the flow of a fluid. Still, as the system must be fully cleanable internally (req. 4) and must not contain internal edges behind which particles can get stuck (req. 4.a), only a few options remained.

The wish of being able to use the system in combination with syringes (wish 6), further limited the number of options. This was preferable, as syringes were currently commonly used to dose and transport fluids and were commonly available and reusable. It meant that either a syringe could be used to insert the fluid directly, or a syringe could be emptied in a collector with a separate system performing the insertion of the fluid.

For the latter, options potentially meeting the requirements could be found. Examples of these potentially viable solutions can be found in the patents by Wong [30] and Philbin [31]. In the system by Wong, a combination of control valves and a hydraulic piston is used to achieve a pressure based flow rate [30]. Different to this is the system by Philbin, where the position of a control valve is adjusted to achieve a certain desirable pressure and flow rate [31]. This system still requires a driving force for the fluid, for which gravity could potentially be used. These and similar systems were relatively complex, potentially required the use of disposables, and were often pressure based rather than position based (wish 9).

When a syringe or cartridge was directly used to insert the fluid, various relatively comparable options potentially meeting the requirements could be found. Examples of this can be found in the patents by Michaels et al. [32] and Blomquist and Bynum [33]. In addition, the publication by Wijnen et al. proposes and validates relatively cheap position based syringe control systems that could be controlled using a Raspberry Pi [34].

Position and pressure based systems

Fluid insertion systems can be either pressure or position based. Pressure based solutions approximate a flow rate by exercising a certain pressure on the fluid. In position based solutions, the flow rate is approximated by forcing a certain positional change over time. As the properties of urine can vary depending on the patient's physical condition, its viscosity may vary. This could result in deviations in pressure based systems, if the flow rate is not measured to create a feedback loop. As this would unnecessarily increase the complexity of the system, the use position based systems was preferred and included in the list of wishes discussed in Appendix F.

Concept selection

As syringe controlling systems can be made relatively cheap, simple, and position based, this type of system was preferred. This syringe control system could potentially meet all requirements and wishes set out.

F.2. Initial embodiment design

As discussed above, a position based, syringe controlling insertion system was to be designed. For this, a linear motion was required which can be easily achieved using a lead screw rod and guiding optical axes. As the exact required forces and flow rate were yet to be determined, the required pitch on the lead screw rod was not yet known. Therefore, regular threaded rods and nuts of size M10 were used for the current design. Once the exact requirements would be determined, a suitable lead screw rod could be selected. A suitable method for controlling the rotation of the threaded rod was using a small and common stepper motor with an internal gearbox to allow high accuracy positioning and a high torque at a low speed. As the stepper motor would not be not aware of the position of the syringe, a momentary switch was placed on the far side of the syringe system. When starting up the system, the syringe would move until the switch was pressed, allowing calibration to be performed.

To minimize the risks of urine spillage and to prevent eggs from remaining stuck in the syringe, the syringe was to be placed vertically with the nozzle pointing downwards. A small funnel was made to automatically guide the syringe nozzle to the entry of the urine pathway. As the main goal of the initial design was to provide a proof of principle and to allow optimization of the design, protection of internal components was not yet included. The resulting embodiment design can be seen in Figure F-1.

It must be noticed here that the earlier introduced publication by Wijnen et al. was discovered after the creation of the initial embodiment design and prototype, and the large similarities between the two designs was purely coincidental [34]. Still, the large similarities with this validated design confirmed the potential of the embodiment design.

F.3. Initial prototype creation

The prototype for the fluid insertion system was mostly created using the 3D printing of regular PLA at the TU Delft. Besides this, cheap off-the-shelf components were used. This included aluminum round rods for the guiding optical axes, a threaded rod for the lead screw rod and nylon plain bearings. The threaded rod had to be turned in order to be connected to the stepper motor. In this, a hole was turned to receive the stepper motor's shaft. Perpendicular to this hole, a hole was drilled through the rod and threaded for M3 bolts. This allowed coupling between the stepper motor's shaft and rod by placing adjusting bolts against the flat surfaces of the shaft.

The stepper motor used was an unipolar motor of the type 28BYJ-48 with a ULN2003 motor driver board. In addition, a momentary switch was placed on the far side of the syringe system for calibration purposes. The resulting prototype can be seen in Figure F-2.

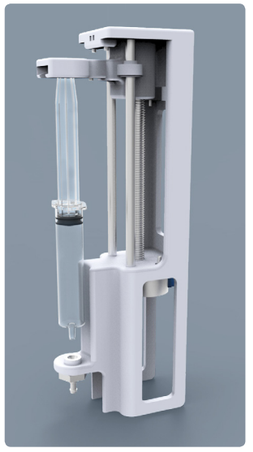

Figure F-1. The digital design of the initial fluid insertion system.

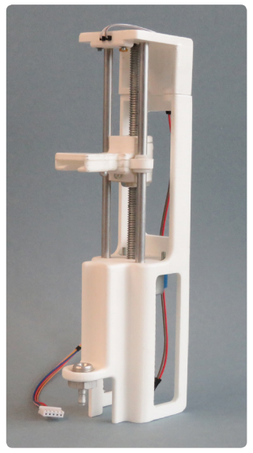

Figure F-2. The physical prototype of the initial fluid insertion system.

F.4. Software control of the fluid insertion system

As the fluid insertion system was to be controlled by the same Raspberry Pi used for all other digital applications, an algorithm had to be developed. As discussed in Appendix D.1, both the existing algorithms by Patrick and the algorithms for controlling the optical sensor were created in Python 3. To ensure a functional and effective cooperation of the algorithms, the fluid insertion system algorithms were also made in Python 3.

These algorithms needed to control both the calibration process and the flow rate. Calibration was performed by moving the syringe holder up to the precise moment that the momentary switch on the far side of the syringe system was pressed. In addition, if the momentary switch was already pressed when the calibration procedure started, the syringe holder was first moved away from the momentary switch before moving back towards the button. This was to ensure that the exact same calibration point was used for every calibration.

The algorithms contained various classes that each had their own specific tasks. The syringe class was responsible for controlling both a motor class for the stepper motor and a switch class for the momentary switch. As the syringe class must be able to control multiple components simultaneously, multithreading was implemented. These and other required classes contained all potentially required functionalities, and constantly validated whether the requested action would endanger the functionality of the device. For example, it was not possible to move the syringe holder to a specific position before calibration was performed, and moving beyond the digitally programmed minimum and maximum position after calibration resulted in the action being terminated.

The code layout was designed such that multiple syringes and stepper motors could be configured, and parameters could be easily adapted during future iterations. In addition, a rough interface design was created to facilitate the validation process, as can be seen in Figure F-3.

As discussed in Section D.1, the syringe was required to move a predetermined amount of fluid of 0.016ml between two measurements. This could easily be achieved using the functionalities of the syringe class. In this, the configured dimensions of the syringe and the configured properties of the stepper motor and the

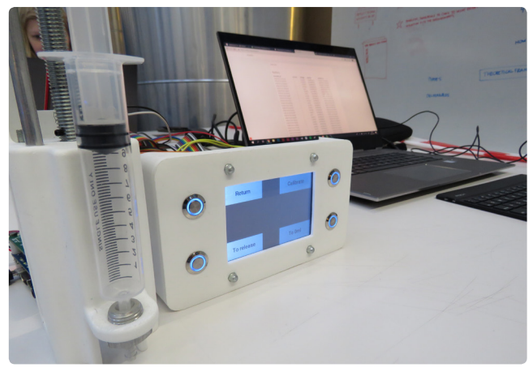

Figure F-3. Controlling the fluid insertion system using rough interface designs

connected lead screw rod were used to determine how many actions were to be send to the stepper motor at which rate. The result is a highly accurate fluid insertion system, well capable of moving exactly 0.016 ml of fluid between the capturing of two frames.

F.5. Validation of the initial fluid insertion system

The initial validation of the prototype consisted of simple testing of the calibration algorithm, and the compressing and releasing of an empty 10ml syringe. This resulted in optimization of the algorithm parameters, validation of the working principle, and small design improvements for future redesigns.

After this, the prototype was connected to the 0.8mm flow cell using the prototyped flow cell connector, and the 10ml syringe was filled completely with water. The optimized algorithms were now used to validate both the capabilities of the fluid insertion system prototype and flow cell connector prototype. In this, the already optimized algorithms only required minor adjustments. This also provided validation for the flow cell connector, as no leakages occurred at various flow rates.

Finally, the prototype was connected to the 0.8mm flow cell using the prototyped flow cell connector and was tested twice with the experimental setup created by Patrick, as can be seen in Figure F-4. In the initial test, samples of SH eggs in saline solution were tested to confirm the basic functioning of the fluid insertion system and to roughly assess the different flow rates. In this, the fluid insertion system worked completely as expected and typical footage could be obtained.

In the second test, SH eggs were placed in urine and the measurements were again performed using varying flow rates. However, in these tests the fluid insertion system was unable to move near the fully extended and compressed syringe positions. This, as there was more resistance in these part of compression due to the stiffness of the syringe and the potentially increased viscosity of urine compared to saline solution. Still, it was possible to obtain raw footage of the SH eggs by using the middle part of the syringe. The resulting raw footage can be seen in Figure F-5.

Recommendations for the next design iterations

The most vital recommendation for the next design iteration was to increase the force the fluid insertion system could exert on the syringe. This, as the current prototype was not powerful enough to compress near the fully extended and compressed syringe positions. In addition, the maximum forces exerted on the syringe should be measured in order to determine the maximum pressure that may be exerted on the entire

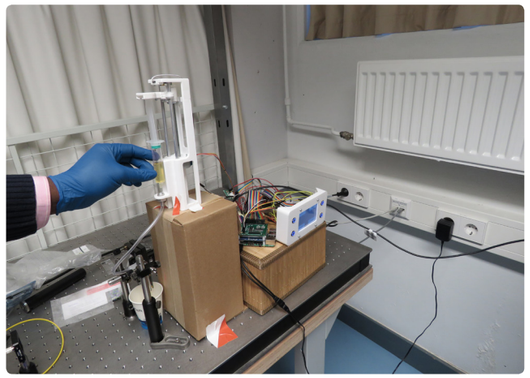

Figure F-4. Setup for validating the performance of the initial fluid insertion system.

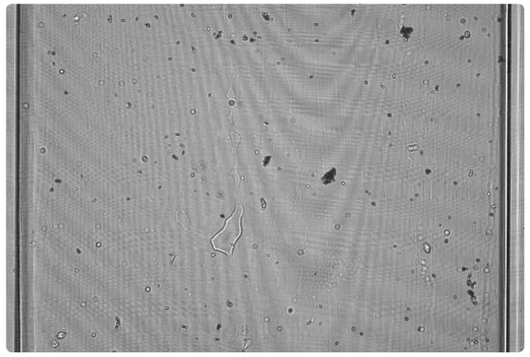

Figure F-5. Typical unprocessed footage of SH eggs in urine obtained using the experimental setup and initial fluid insertion system.

urine pathway. This may occur in the worst-case scenario of an obstructed pathway.

It was also noticeable that when a fully filled and extended syringe is compressed, the syringe deflected undesirably at the connection between the barrel and plunger, as there is no support at this point. Also, the funnel used in the prototype was too small to consistently guide the nozzle of the syringe. Therefore, a redesign of the fluid insertion system was to include a larger funnel and additional support for the syringe barrel. The latter came with the disadvantage that the redesign would only fit a specific syringe size. In this, it was recommended to use a slightly larger syringe than the required 10ml. This, as the urine remaining in the pathway to the sensor when fully compressed could not be analyzed. Therefore, a standard 12ml syringe was recommended to always measure the minimum recommended amount of 10ml.

In addition, it was suggested to design the embodiment of the fluid insertion system in such a way that the user would be completely protected from potential spillage of urine. This additional requirement will be further elaborated on in the final design cycle of the fluid insertion system.

Appendix G. Improved fluid insertion system design

There were three main recommendations for the initial fluid insertion system design; increasing the maximum force that could be exerted, providing support and guidance to the syringe, and protecting the user against potential spillage. Of this, the latter will be further elaborated on during the final design cycle of the fluid insertion system.

There were three logical approaches for increasing the maximum force that could be exerted on the syringe; the torque of the stepper motor could be increased, the resistance of the system could be decreased, and the pitch of the lead screw rod could be decreased. To ensure a fully functioning redesign, all three approaches were explored and evaluated.

G.1. Evaluating the effect of motor mode and driver on performance

To increase the torque that could be provided by the stepper motor, a simply more powerful motor could be obtained. However, the current motor was still highly preferable for the application as it was cheap, had a good internal gearbox, already suited the current design, and used a relatively small amount of current that could be provided by the Raspberry Pi's regular power supply. Therefore, an attempt was made to increase the torque of the 28BYJ-48 stepper motor by changing it from a unipolar to a bipolar stepper motor and accordingly replace the ULN2003 motor driver with the L293D motor driver.

There were various online tutorials on how to make the simple changes required [35]. To easily use the L293D motor driver chip a small circuit board was made, as can be seen in Figure G-1.

To assess whether these adaptation had actually improved the performance the of the fluid insertion system, a comparison was made between the unipolar and bipolar stepper motors. For this, the maximum force that could be exerted on a syringe and the current draw of the motor were measured for different rotational speeds of the lead screw rod. The current draw was interesting to know as well, as the final system would only have a limited amount of power available. The setup for this experiment can be seen in Figure G-2. In this, a force gauge was held against the syringe holder. A current sensor was placed on the ground side of the motor driver board. This, as there were multiple 5V input signals, but only one ground.

During the experiment, the lead screw rod turned at a predetermined speed, causing the syringe holder to

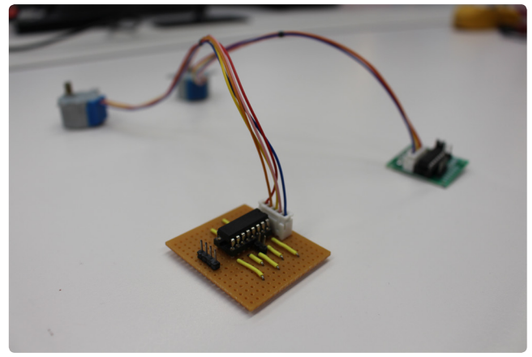

Figure G-1. Front: Custom circuit board made for housing the L293D motor driver chip connected to the bipolar 28BYJ-48. Back: ULN2003 motor driver PCB connected to the unipolar 28BYJ-48.

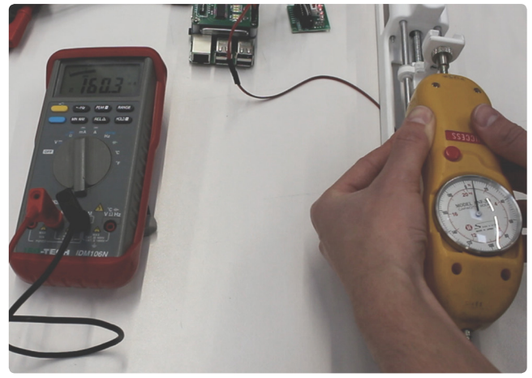

Figure G-2. Setup for evaluating the effect of the motor mode and driver on performance.

press against the static force gauge. Once the stepper motor stopped turning, the maximum force exerted was read from the force gauge. After this, the syringe holder was returned to its original position and the next measurement was performed. For each speed and for each motor driver, a minimum of three consecutive measurements were performed ($n \geq 3$). Additional measurements were performed if the initial values were considered inconsistent. The tolerance of the obtained values was determined using the minimum and maximum values observed during the measurements. The resulting driving forces and current draws can be seen in Table G-1.

As can be seen, the bipolar motor performed better at three of the four measurable rotational speeds. Surprisingly, the power consumption of the bipolar motor during usage was lower than that of the unipolar motor. During the initial validation discussed in Appendix

F.4, the maximum speed of the lead screw rod did not exceed 35°/sec. Therefore, the bipolar motor performed better than the unipolar motor for the speed required, and would be used in the improved prototype. Still, as the resting current of the bipolar motor driver was quite high, a transistor was to be placed on the final motor driver circuit board to interrupt the board's power supply when not in use.

G.2. Reducing the resistance of the fluid insertion system

Another approach for increasing the maximum force that could be exerted on the syringe was to decrease the resistance of the fluid insertion system. The main source of both resistance and play in the system seemed to be the connections of the syringe holder with both the lead screw rod and guiding optical axes. The play between the syringe holder and the rod and axes allowed the syringe holder to slightly rotate. This caused additional friction at the contact points, and was therefore to be prevented.

A means expected to reduce this rotation was to add a second nut or nylon plain bearing to the syringe holder. As the syringe holder also clearly had vertical play at its connection to the lead screw nut, it was decided to add a second nut that could be moved slightly to reduce play in the system. A second syringe holder with double M10 nut holder had been prototyped, and was compared to the initial syringe holder with a single M10 nut holder.

When evaluating the influence of this adaptation, the experimental method used was the same as that for evaluating the effect of motor mode and driver. In this, the maximum force that could be exerted on a syringe and the current draw of the motor were measured for different rotational speeds of the lead screw rod.

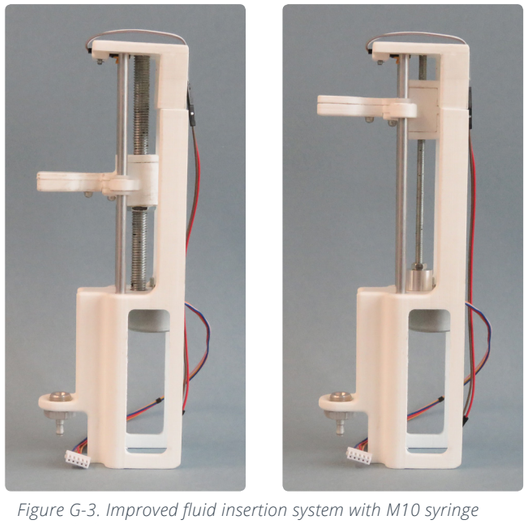

Figure G-3. Improved fluid insertion system with M10 syringe holder (Left) and M5 syringe holder (right) with according lead screw rods.

Using these conditions, it was quickly noticed that slight misalignments between the two nuts after placement in the 3D-printed parts resulted in a large amount of friction. This resulted in a clear reduction in the maximum force, as can be seen in Table G-2.

As the same slight misalignments can be expected when placing a double layer of nylon plain bearings in 3D-printed parts, this approach for decreasing the resistance was abandoned for this prototyping phase. Still, it might be worth exploring this means of reducing friction once other production methods are available. As no clear alternative method for reducing friction was identified for the current prototype, this approach was discontinued.

G.3. Evaluating the effect of the pitch of the lead screw rod

The third means to potentially increase the maximum force that could be exerted on the syringe was to reduce the pitch of the lead screw rod. For this, a third syringe holder was created with a double M5 nut holder, which had a 0.8mm pitch. Besides this, an according M5 lead screw rod was made and connected to the stepper motor using a manually turned aluminum shaft coupler. This was manually made, as it allowed one side to be threaded at M5 with a perpendicular hole threaded at M3 for further fixation via adjusting bolts. This was to be compared with the earlier introduced second syringe holder with double M10 nut holder, which had a 1.5mm pitch. The two syringe holders and their according lead screw rods can be seen in Figure G-3.

To assess the effect of the lead screw rod pitch on the maximum force that could be exerted on the syringe, a comparison was made between the M10 syringe holder with a pitch of 1.5mm and the M5 syringe holder with a pitch of 0.8mm. The experimental method used was again the same as that for evaluating the effect of motor mode and driver, and for evaluating the effect of a second nut holder. In this, the maximum force that could be exerted on a syringe and the associated current draw were measured for different rotational speeds of the lead screw rods. As can be seen in Table G-3, the results were quite surprising. The M5 syringe holder with smaller pitch actually exerted a smaller maximum force on the syringe than the M10 syringe holder. This could be partially attributed to the M5 lead screw rod and nut having a tighter connection with more friction. Using a double nut holder further increased the friction due to slight misalignments of the two nuts, as was also found earlier with the M10 syringe holder with double nut holder.

Still, when removing the secondary nut from the M5 syringe holder, the maximum forces were closer to the original M10 syringe holder with single nut holder, as can be seen in Table G-4. Due to this, the single nut M5 syringe

Table G-1. Driving force and current draw for different motor drivers.

	Unipolar ULN2003 [a]		Bipolar L293D [b]	
Speed	**Driving force**	**Current draw**	**Driving force**	**Current draw**
Resting	N/A	0.025 ± 0.025 mA	N/A	51 ± 2mA
18°/sec	8 ± 1N	159 ± 1mA	13 ± 1N	135 ± 1mA
36°/sec	7 ± 1N	150 ± 2mA	11 ± 1N	120 ± 1mA
54°/sec	7 ± 1N	142 ± 2mA	9 ± 1N	103 ± 1mA
72°/sec	7 ± 1N	131 ± 1mA	7 ± 1N	88 ± 2mA
90°/sec	N/A [c]	157 ± 1mA	N/A [c]	127 ± 3mA
108°/sec	N/A [c]	154 ± 1mA	N/A [c]	126 ± 2mAv

Each value was obtained using a minimum of three consecutive measurements (n≥3). Additional measurements were performed if the initial values were considered inconsistent. The obtained values only provide basis for relative comparison, and not for absolute performance. This, as the current sensor negatively influences the performance of the motor, and the current sensors available gave different values for the same conditions (±30mA). Repositioning of the lead screw rod may have affected relative performance.
a. Driver type ULN2003 in combination with the unipolar stepper motor type 28BYJ-48, pitch 1.5mm, and the 8-step full-wave control sequence.
b. Driver type L293D in combination with the adapted bipolar stepper motor type 28BYJ-48, pitch 1.5mm, and the 4-step full-wave control sequence.
c. No rotation could be achieved by the motor for these conditions.

Table G-2. Driving force and current draw for syringe holders with single and double M10 nut holders.

	Single M10 nut [a]		Double M10 nut [b]	
Speed	**Driving force**	**Current draw**	**Driving force**	**Current draw**
Resting	N/A	51 ± 2mA	N/A	50 ± 1mA
18°/sec	13 ± 1N	135 ± 1mA	11 ± 1N	126 ± 1mA
36°/sec	11 ± 1N	120 ± 1mA	9 ± 1N	113 ± 1mA
54°/sec	9 ± 1N	103 ± 1mA	7 ± 1N	97 ± 3mA
72°/sec	7 ± 1N	88 ± 2mA	4.5 ± 1N	84 ± 1mA
90°/sec	N/A [c]	127 ± 3mA	N/A [c]	121 ± 1mA
108°/sec	N/A [c]	126 ± 2mA	N/A [c]	119 ± 1mA

Each value was obtained using a minimum of three consecutive measurements (n≥3). Additional measurements were performed if the initial values were considered inconsistent. The obtained values only provide basis for relative comparison, and not for absolute performance. This, as the current sensor negatively influences the performance of the motor, and the current sensors available gave different values for the same conditions (±30mA). Repositioning of the lead screw rod may have affected relative performance.
a. Single nut M10 syringe holder with 1.5mm pitch in combination with the adapted bipolar stepper motor type 28BYJ-48 and the 4-step full-wave control sequence.
b. Double nut M10 syringe holder with 1.5mm pitch in combination with the adapted bipolar stepper motor type 28BYJ-48 and the 4-step full-wave control sequence.
c. No rotation could be achieved by the motor for these conditions.

Table G-3. Driving force and current draw for different pitches on threaded rods with double nut holder.

	M5 with 0.8mm pitch [a]		M10 with 1.5mm pitch [b]	
Speed	**Driving force**	**Current draw**	**Driving force**	**Current draw**
Resting	N/A	50 ± 1mA	N/A	50 ± 1mA
18°/sec	5 ± 1N	127 ± 1mA	11 ± 1N	126 ± 1mA
36°/sec	5 ± 1N	114 ± 2mA	9 ± 1N	113 ± 1mA
54°/sec	3.5 ± 0.5N	98 ± 2mA	7 ± 1N	97 ± 3mA
72°/sec	2 ± 0.5N	86 ± 3mA	4.5 ± 1N	84 ± 1mA
90°/sec	N/A [c]	121 ± 1mA	N/A [c]	121 ± 1mA
108°/sec	N/A [c]	119 ± 1mA	N/A [c]	119 ± 1mA

Each value was obtained using a minimum of three consecutive measurements (n≥3). Additional measurements were performed if the initial values were considered inconsistent. The obtained values only provide basis for relative comparison, and not for absolute performance. This, as the current sensor negatively influences the performance of the motor, and the current sensors available gave different values for the same conditions (±30mA). Repositioning of the lead screw rod may have affected relative performance.
a. M5 threaded rod with 0.8mm pitch and double nut syringe holder in combination with the adapted bipolar stepper motor type 28BYJ-48 and the 4-step full-wave control sequence.
b. M10 threaded rod with 1.5mm pitch and double nut syringe holder in combination with the adapted bipolar stepper motor type 28BYJ-48 and the 4-step full-wave control sequence.
c. No rotation could be achieved by the motor for these conditions.

Table G-4. Driving force and current draw for different pitches on threaded rods with single nut holder.

	Single M5 with 0.8mm pitch [a]		Single M10 with 1.5mm pitch [b]	
Speed	**Driving force**	**Current draw**	**Driving force**	**Current draw**
Resting	N/A	50 ± 1mA	N/A	51 ± 2mA
18°/sec	10 ± 1N	128 ± 1mA	13 ± 1N	135 ± 1mA
36°/sec	9 ± 1N	112 ± 2mA	11 ± 1N	120 ± 1mA
54°/sec	7.5 ± 1N	99 ± 1mA	9 ± 1N	103 ± 1mA
72°/sec	5 ± 1N	89 ± 1mA	7 ± 1N	88 ± 2mA
90°/sec	N/A [c]	121 ± 1mA	N/A [c]	127 ± 3mA
108°/sec	N/A [c]	119 ± 1mA	N/A [c]	126 ± 2mA

Each value was obtained using a minimum of three consecutive measurements (n≥3). Additional measurements were performed if the initial values were considered inconsistent. The obtained values only provide basis for relative comparison, and not for absolute performance. This, as the current sensor negatively influences the performance of the motor, and the current sensors available gave different values for the same conditions (±30mA). Repositioning of the lead screw rod may have affected relative performance.
a. M5 threaded rod with 0.8mm pitch and single nut syringe holder in combination with the adapted bipolar stepper motor type 28BYJ-48 and the 4-step full-wave control sequence.
b. M10 threaded rod with 1.5mm pitch and single nut syringe holder in combination with the adapted bipolar stepper motor type 28BYJ-48 and the 4-step full-wave control sequence.
c. No rotation could be achieved by the motor for these conditions.

holder could be a suitable alternative to the single nut M10 syringe holder. The reduced vertical play enabled directional changes with less play. The smaller pitch enabled an increased vertical positioning accuracy, yet reduced the maximum vertical speed achievable by the system. With the current system, there was no need for accurate directional changes and the vertical positioning accuracy of the system was already sufficient. Therefore, there was no need to switch to the single nut M5 syringe holder, as this would only further reduce the maximum vertical speed.

G.4. Improved support and guidance to the syringe

Another main recommendation for the improved fluid insertion system design was to provide improved support and guidance to the syringe. This, as the initial design showed undesirable deflections at the connection between the barrel and plunger of the syringe. In addition, the funnel was too small to consistently guide the nozzle of the syringe.

Therefore, a new design was made to support the barrel of the syringe. This was realized by reducing the size of the opening in which the syringe can be placed. To allow placement of the syringe in this now limited space, the support was only added to the top of the syringe barrel, as most deflection occurred here. To ensure that the syringe remained well positioned within the opening after placement, a spring loaded button was placed on one side of the support for the syringe. On top of this button, a sloped surface was placed that fixated the syringe after placement. This also allowed the system to determine whether a syringe had been placed successfully, contributing to its ability to self-diagnose its condition (wish 10).

As the current designs were only temporary in nature and the improved support could fit on the initial prototype, the parts for the improved support were designed to be attached to this initial prototype. This to conserve both materials and time.

During the consecutive testing of the improved support, it was quickly noticed that the syringe no longer showed the undesirable deflections seen before. However, the friction of the support had increased such that the syringe was often being emptied before being well positioned in the funnel. Therefore, the height of the tightly fitting support was severely reduced. This quick iteration solved the problem of friction whilst preventing the undesirable deflections. Both versions of the improved support and guidance can be seen in Figure G-4.

G.5. Validation of the improved system

Validation of the improved fluid insertion system was performed together with the validation of the improved diagnostic setup embodiment to assess the combination of the components, as can be seen in Figure D-3.

The performance of the fluid insertion system had improved significantly compared to the initial design. The system was now able to completely compress a syringe filled with urine. However, it was noticed that air bubbles tended to remain in the flow cell after a flow cell was previously contaminated. These bubbles had a disruptive effect on the footage obtained, and prevented the desirable laminar flow. When compressing the syringe by hand, this problem could easily be overcome by pushing the air bubbles out. This was done by moving urine at a high speed through the flow cell for a short period of time. As the speed of the current system was highly limited, it was unable to push these bubbles out.

Recommendations for the next design iterations

For the next design iteration, it was recommended to increase the speed of the stepper motor, as the current stepper motor was not able to push out the air bubbles in the flow cell.

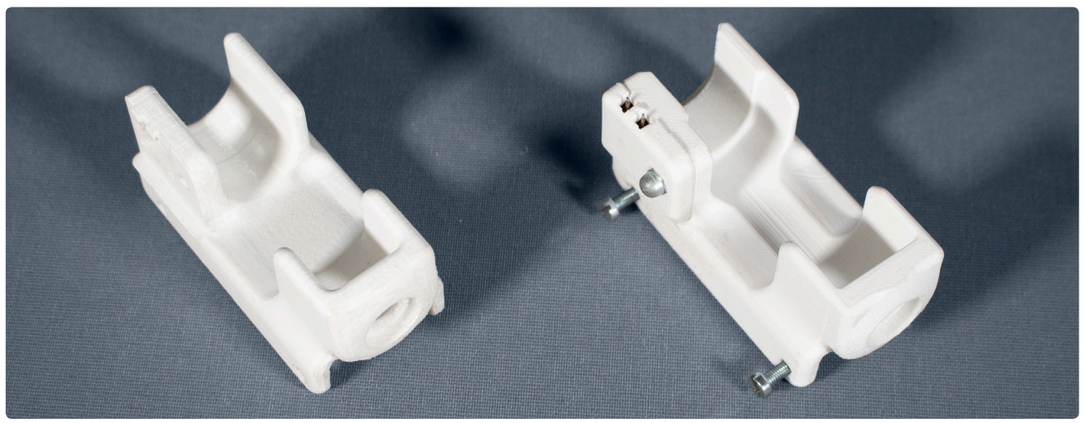

Figure G-4. The first (Left) and second (Right) version of the improved support and guidance to the syringe.

Appendix H. Integrated fluid insertion system design

During the previous design iteration, only a single design recommendation remained. Therefore, it was decided that the design was sufficiently developed to perform this design iteration as an integrated design. This meant that this design of the fluid insertion system would be combined with the other separately developed sub-system designs to form a single functional and interactive prototype.

Besides this, the fluid insertion system must be partially directly exposed to the outside of the integrated prototype. This, as the syringe holder must be accessible to the user. Therefore, this part should be user friendly, compact, and resistant to external conditions.

These general design considerations applied to the integrated prototype in general, and will therefore be discussed together in Part C of the thesis. In this section, the previously made recommendation for increasing the stepper motor's maximum speed will be discussed.

H.1. Increasing the stepper motor's maximum speed

The currently used stepper motor of the type 28BYJ-48 had an internal gearbox to reduce its step size. This increased its accuracy and force, but limited its speed to 72°/s. With the currently used single nut M10 syringe holder, a maximum vertical speed of 0.2 mm/s could be achieved without causing the stepper motor to skip. Based on experimentation with manually compressing a syringe through the flow cell, it was estimated that this speed needed to be increased to 4 mm/s or 960°/s for short periods of time to push out the air bubbles in contaminated flow cells.

As this was far beyond the capabilities of the 28BYJ-48, different options were explored. As the exact requirements in terms of achievable speed and force were not known, it was decided to use standardized stepper motor sizes. This means that stepper motors of varying current draws and step sizes have the same standardized connection points and outer dimensions, except for the depth of the motor. This allowed the redesign to be suitable for different stepper motor types, and allowed experimentation with different current draws and step sizes.

NEMA17 stepper motors of 350mA and 1200mA were obtained. As these stepper motors were designed to be operated at 12V, a voltage converter 5V-12V and a suitable motor driver were implemented in the integrated design. Upon experimentation, it was quickly noticed that the listed current draw was for stationary conditions only, and greatly deviated from the current draw during motion, due to the inertia of the motor's coils. In this, the faster the stepper motor rotated, the less current it drew. As a result, a 1200mA stepper motor consumed only around 340mA when moving at 960°/s, whilst this was just 130mA for a 350mA stepper motor. At this speed, the 350mA stepper motor was lacking in force, and was not always able to move the syringe. Still, as the stepper motor was only to be activated during motion, and the force of the stepper motor was sufficient to allow direct acceleration to a high speed, the 1200mA stepper motor could be used without disturbing the system. To prevent power problems, the software had been adapted to ensure shutdown of the motor when it was no longer being ordered to move.

In addition, the syringe was quickly compressed at the start of the measurement to completely fill the flow cell with urine. After this, the measurement continued as normal. Between capturing frames, the movement of the syringe was kept at a low speed to prevent blurry images from occurring. This caused a slight increase in power consumption to 500mA, but this was deemed acceptable within the current design of the integrated prototype.

The increased maximum speed of the stepper motor also allowed the automatic rinsing of the system after a measurement. Up to this point, this procedure was always envisioned, but not yet elaborated upon due to the limited maximum speed of the motor and overall stage of development. With the increased maximum speed, this could now be realized. By automating this cleaning procedure, it became easier to clean the system, reducing the chance of user error. A relatively simple script had been developed for this purpose.

H.2. Validation of the integrated fluid insertion system

The prototype of the integrated fluid insertion system can be seen in Figure H-1. During the initial validation of the integrated fluid insertion system, it seemed well capable of pushing the air bubbles out of the flow cell. Still, heavily contaminated flow cells could not always be cleared of air. In addition, air bubbles were also found to rise from the bottom of the flow cell during measurements.

Therefore, experiments were performed with the quick movement of urine in an already filled flow cell containing some air bubbles. Yet, this method was not always able to clear the flow cell. In addition, a lot of urine was disregarded when frequently using this method. Therefore, experiments were performed with the repetitive up and down movement of urine, as this does not disregard urine. During this, the barrel of the syringe was manually fixated, as retraction of fluid into the syringe would otherwise not be possible within the current design. It was quickly noticed that the upward motion of urine allowed the air bubbles to rise in the urine towards the syringe, whilst the downward motion had little effect. The larger the upward motion was, the further the air bubbles could rise. Still, the current syringe holder had a lot of vertical play to allow placement of the syringe. This would be undesirable when the direction of movement was to be alternated, as it would introduce inaccuracies in the amount of fluid retraction. Besides this, the speed at which fluid was retracted seemed to have little influence

In addition, the newly created automated cleaning procedure seemed to work well, but its efficiency in cleaning was difficult to assess in this stage of development.

Recommendations for the next design iteration

There were several recommendations for the next design iteration. Namely, the system should be redesigned to reliably fixate the syringe barrel during usage and to remove the vertical play of the syringe holder during usage. This, to allow reliable retraction of urine.

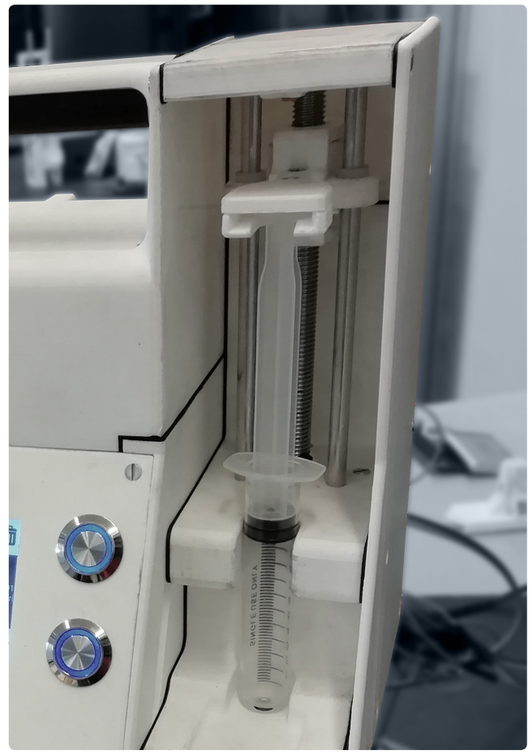

Figure H-1. Setup for validating the performance of the initial fluid insertion system.

Appendix I. Improved integrated fluid insertion system

During the previous design iteration, it was recommended to redesign the system to reliably fixate the syringe barrel and to remove the vertical play of the syringe holder. Both aspects must only be present during usage, as placement and removal of the syringe would otherwise become impossible. Therefore, the state of the system must change at the start and end of both cleaning and measuring procedures. This could be performed manually by the user, but this would introduce a large potential for user error. User errors were already a noticeable occurrence when testing the handling of fluids with the integrated prototype (Part B, section 1.1). Because of these reasons, automated possibilities were explored.

Adding additional actuators to change the state of the system would be possible, but would increase the complexity and cost of the system. However, the existing stepper motor and the connected syringe holder could also be used. As the syringe should only be movable when the syringe holder is completely at the top, this change in distance could be used to realize the required change in state. To do so, a new design and prototype was created in which springs were used to remove the vertical play and fixate the barrel, as can be seen in Figure I-1 and Figure 17 of the thesis (p.28).

For removing the vertical play, the syringe holder was split up in an upper and lower part. The upper part was directly connected to the nut holder and optical axes, whilst the lower part was connected to the upper part via a hinge. Tension springs were placed between the upper and lower part so the two were pulled together. They both contained rubber padding on the inner sides, and fitted closely together to hold the syringe once placed without vertical play. To allow the syringe to be removed when the syringe holder was at the top, two upward pins were present on the lower part of the syringe. These pins came into contact with the top of the fluid insertion system when the syringe holder came close to the top. This pushed the lower part away from the upper part, allowing the syringe to be removed.

To fixate the barrel of the syringe, an addition clamping part was designed that slided over the optical axes of the fluid insertion system and rested on top of the barrel. In this, the connections between the part and the optical axes were located above those of the syringe holder. This caused the part to be lifted as a whole when the syringe holder came close to the top. To ensure that the clamping part fixated the barrel when the syringe holder had moved down, compression springs were placed over the optical axes, between the clamping part and the top of the fluid insertion system.

During the design of the clamping part, it was noticed that the plain nylon bearings also used for the syringe holder actually had a diameter of 6.3mm rather than 6.0mm. As a result, there was a relatively large amount of play between the clamping part and the 6.0mm optical axes. Therefore, a cut was sawed into the side of the nylon plain bearing and strips of tape were placed on its outer side to reduce the inner diameter of the bearing. After this, the bearings could be compressed into place. As there was also significant play in the redesigned syringe holder, this was also performed here.

As discussed in the validation of the integrated diagnostic embodiment (Appendix E.6), another point for improvement identified was to improve the smoothness of the integrated fluid insertion system. The step size of this faster stepper motor was so severely reduced by the switch to the NEMA17 stepper motor that the motion became interrupted at low speeds, and caused vibrations of the stepper motor. To reduce this, a shock absorber had been added between the stepper motor and the main body of the fluid insertion system. In addition, as the maximum speed of the stepper motor was no longer required for removing air bubbles, a switch could be made from the M10 syringe holder to the M5 syringe holder. This doubled the number of steps between capturing frames.

I.1. The Anti-Bubble System (ABS)

It was discovered during the validation of the integrated fluid insertion system (Appendix H.2), that air bubbles could be easily removed from the flow cell when retracting the urine back into the syringe. With the redesigned fluid insertion system, it was now possible to push the urine past the flow cell at the start of a measurement, and then retract a small amount of urine back into the syringe to pull the air bubbles that could still be present in the flow cell up into the syringe. How far the urine should be pushed past the flow cell, and how much the urine should be retracted was experimentally determined.

Still, it was previously also found that air bubbles could be present in the flow cell after urine had been pushed through, or can float up from the bottom of the flow cell. As these air bubbles could have a disruptive effect on a measurement, they must either be prevented or removed throughout the measurement. As there was currently no known way to prevent these air bubbles from occurring, a system was made to automatically detect and remove air bubbles; the Anti-Bubble System, or ABS in short.

The detection algorithms of the ABS had been developed by Patrick. In this, every frame that is captured is resized to a small grid of 4 by 4. For every element in the grid, the value is compared to the mean and medium value of that element over time. As a result, sudden changes can be detected, indicating the presence of an air bubble. This approach had been selected as it is very fast and not computationally demanding, which is preferable for a script that is to be executed for every frame captured.

If no air bubble was detected after capturing a frame, the value of the element was used to adapt the mean and median of the element over time with a low learning factor, and the captured frame was passed on to the analysis or storage algorithms. This allowed the ABS to account for changes in the flow cell's condition. As the ABS does not know by default what the values of the specific flow cell and fluid should be, the first 10 frames of a measurement must be manually assessed for the presence of air bubbles. This was expected to be removable upon further improvement in the ABS algorithms, but these have not yet been explored.

If an air bubble was detected, the captured frame would not be passed on to the analysis or storage algorithms, as this would have a disrupting effect on the measurement. Instead, the syringe would be moved up and down by exactly 3.0mm to retract the bubbles. After this, another frame would be captured at the same position. If another bubble would be detected, the syringe would be moved again until the bubble is gone.

I.2. Validation of the improved integrated fluid insertion system

Initially, the improved integrated fluid insertion system seemed to work perfectly, and no potential improvements could be found. Fluids could now be retracted accurately and reliably, air bubbles had become easy to remove, and movement of the stepper motor was relatively smooth and did no longer seem to disturb the quality of the footage. In addition, the automatic fixation of the syringe forced the user to only place or remove a syringe when the syringe holder was at the very top. This further reduced the chance of user error and protected the user against potential urine spillage, addressing the recommendation identified during the initial design cycle.

However, over time the play between the syringe holder and optical axes that was earlier removed by reducing the diameter of the nylon plain bearings returned worse than ever. This increased the friction of the system to such a degree that the stepper motor was no longer able to move the syringe. It was found that the adjusted nylon plain bearings wore out over time.

Further reducing the hole size and adding grease temporarily solved the issue, but was not considered a viable long-term solution.

The Anti-Bubble System (ABS) worked very well after some tuning of the parameters. It was capable of removing nearly all bubbles. So far, it only seemed to fail in instances where the syringe tip did not maintain an airtight connection with the funnel, as all urine would flow out of the system and the measurement must be restarted. These were rare instances, and only seemed to occur when the syringe barrel was moved by force after the measurement had begun, or when a damaged syringe was used.

I.3. Improved bearing selection

To permanently solve the problems with the optical axes and its bearings, linear ball bearings were obtained as a replacement. In addition, the aluminum extrusion rods were exchanged with hardened steel rods, as these maintain a more accurate diameter. As the linear ball bearings were a lot larger in both diameter and height than the nylon plain bearings, the syringe holder was once again to be redesigned. As the clamping part and its compression springs were still to be placed above the syringe holder, the design was to be extended downwards. Due to this limited space above the syringe holder, the clamping part did not have its nylon plain bearings replaced. This is acceptable, as play had little effect on the functioning of this part. The resulting design can be seen in Figure I-1.

Figure I-1. The adapted syringe holder of the improved integrated fluid insertion system.

I.4. The maximum pressure in the system

With the final adaptations being made, it may be useful to determine the maximum pressure that may be present on the entire urine pathway. This, to assess the possibilities and effects of potential worst case scenarios. To do so, two values were to be determined; the effective cross-sectional area of the syringe plunger, and the maximum vertical force exerted by the syringe holder on the syringe during use.

The syringe barrel had an inner diameter of 14.8mm without deflection, and thus a cross-sectional area of 172mm^2. The outer diameter of the syringe plunger rubber cap is 15.1mm without compression, representing a cross-sectional area of 179mm^2, but due to compression of the rubber cap by the syringe barrel this will not be present during usage and the 172mm2 was more likely to be representative of the cross-sectional area during usage.

To determine the maximum vertical force exerted by the syringe holder during usage, the same method was used as during the evaluation of the effect of motor mode and driver on performance of the improved fluid insertion system (Appendix G). In this, the setup shown in Figure G-2 was recreated for the improved integrated fluid insertion system.

During measurement procedures, a maximum vertical speed of 0.25mm/s was maintained to prevent excessive flow rates. This was equal to a stepper motor speed of 72°/sec. Therefore, the maximum vertical force was to be determined for this speed. However, the maximum torque that could be provided by the stepper motor proved to be very high. As the syringe holder was divided in two parts in the improved integrated fluid insertion system, the upper half started to break due to the stress and the measurement was discontinued at 28N.

In contrast, cleaning procedures maintained a maximum vertical speed of 2.5mm/s. This was with 720°/sec the

maximum stepper motor speed that could be reliably achieved. For this speed, the maximum torque that could be provided by the stepper motor was less, causing the stepper motor to skip when providing 24-26N.

Using the cross-sectional area of the syringe and the maximum forces exerted on the syringe, the maximum pressure could be established. During measurements, the maximum pressure of the urine pathway was 163kN/m^2. For cleaning procedures, this was 140-151kN/m^2.

This was significantly higher than with the improved fluid insertion system design. As the maximum force that could be exerted by the improved fluid insertion system on the syringe was established to be 14N (Appendix G), the maximum pressure that could be exerted on the urine pathway was 81kN/m^2.

Discussion

The high maximum pressure could be present during measurements if the urine pathway becomes seriously obstructed. This could either result in the obstruction being removed due to the pressure, or could result in an undesirable alternative outlet of urine. The latter is considered a worst case scenario. So far, no obstructions or alternative urine outlets have been experienced. With the good fixation of the syringe in the fluid insertion system, this is also not expected to occur. Still, it is recommended to perform tests with different types of potential obstructions in the system to determine their effect on the functioning of the device and the safety of the user.

Appendix J. Initial flow cell placement tool design

To create the initial flow cell placement tool design, a list of requirements and wishes was created, as can be seen in Part C, section 4.1 of the thesis (p.36). Based on this, an initial design was made, validated, and iterated upon. As this was considered a relatively small part of the project as a whole, and only seen as a temporary solution until the flow cell could be redesigned, no conceptual exploration was performed.

J.1. Initial embodiment design

Based on the requirements set out, a design was created with the potential to meet the requirements and wishes. A render of this design can be seen in Figure J-1. The tool consisted of three main parts; the basis and two arms.

The basis contained a flat surface on which the flow cell could be laid. In the center of this surface, a deepened slot was present to prevent contact with the vulnerable center of the flow cell. This prevented both contamination of the area of interest (req. 2), and the exertion of external forces on the vulnerable center during placement (req. 4.b). The top and bottom sides of the flat surface were extended and fitted with holes. These holes could later be used to place bolts with a specific length on the side of the flow cell. During placement, these bolts would limit the depth of placement by coming in contact with the laser side of the box. This, to ensure that the flow cell would be placed in the flow cell connectors at the specific depth required for optimal performance (req. 4.a).

On the back side of the flat surface, two partially knurled extensions were present. Between the two, a bolt could be placed. These extensions allowed the user to hold on to the tool and exert forces during placement and removal, as suggested by the knurling. Besides this, the bolt between the two extensions formed the axis for the hinge holding the two arms.

The arms were responsible for holding the flow cell in place without relying on external forces (req. 1), and for exerting the forces required for removal of the flow cell on non-vulnerable areas (req. 4.c). The choice was made to use the arms, as the flow cell was to be placed in a relatively confined space and usage could become difficult if the placement tool required a lot of place to function (req. 3). To reduce the stresses during removal, the contact area was maximized without complicating the usage. This was enabled by holding on to the long sides of the flow cell. As it must still be possible to release the flow cell from the arms once it was placed, only the edges of the flow cell could be hold on to. It must be experimentally validated whether the resulting stresses were sufficiently low to prevent damage to the flow cell. To allow the arms to hold the flow cell in place without relying on external forces, a small spring was placed between the two arms.

The arms could be opened by compressing the surfaces on the back of the arms, as suggested by these surfaces being knurled. As a result, the working principle of the tool was comparable to that of a regular clothespin.

J.2. Initial prototype creation

The prototype of the flow cell placement tool was mostly created using the 3D printing of regular PLA at the TU Delft. In addition, cheap off-the-shelf components were used as described. The resulting prototype can be seen in Figure J-2.

J.3. Envisioned usage of the initial prototype

The envisioned usage of the initial flow cell placement tool prototype can be seen in Figure J-3. In this, the flow cell could be easily held in the tool (1), after which the tool could be aligned with the flow cell connectors (2), and pressed into place (3). The tool could then be released to check its positioning (4), or removed by compressing the arms (5-6). The envisioned usage during flow cell removal was the inverse of the envisioned usage during flow cell placement (6 to 1).

J.4. Validation of the initial embodiment design

Validation of the flow cell placement tool prototype had to be performed on two major aspects: functionality and interaction.

In terms of functionality, repetitive testing had shown that the prototype was well capable of holding a flow cell without external forces (req. 1) or contaminating the area of interest (req. 2). It was also very capable in placing the flow cell in the flow cell connectors (req. 4), yet excessive use of force during both the placement and removal of the flow cell could still result in stresses being present in the vulnerable center of the flow cell (req. 4.b and 4.c), and had resulted in damage to old flow cells.

Besides this, there was also the requirement that the positioning of the flow cell after placement must be constant (req. 4.a). As also discussed in Appendix D.3, this was not always the case with the current prototype

Figure J-1. Digital design of the initial flow cell placement tool.

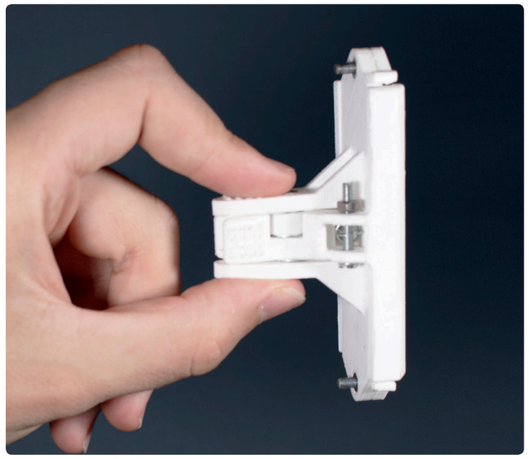

Figure J-2. The initial flow cell placement tool prototype.

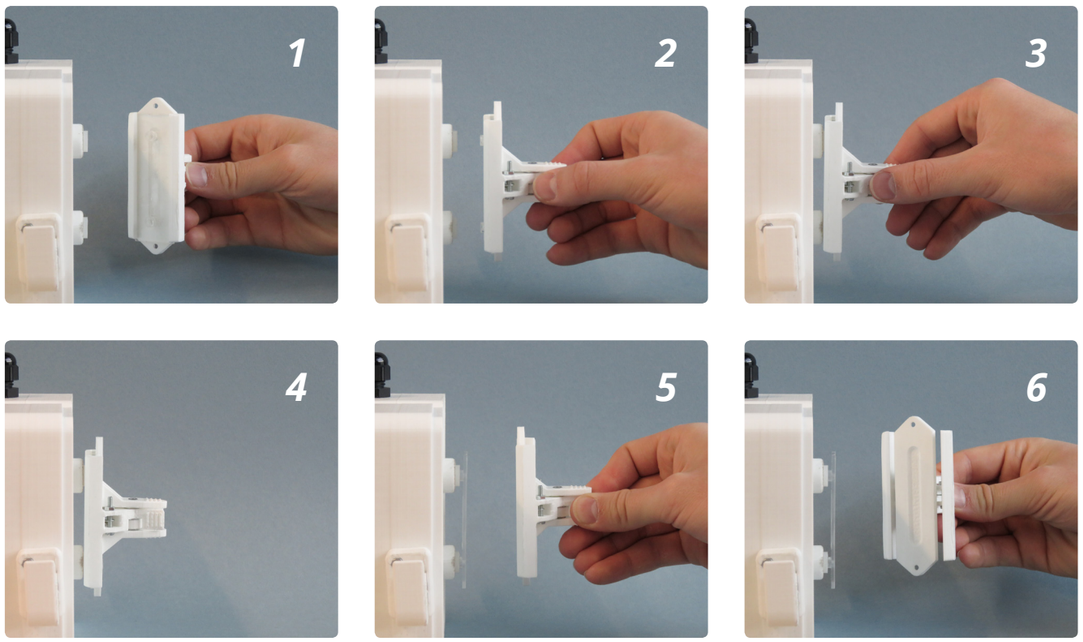

Figure J-3. Envisioned usage of the initial flow cell placement tool on the initial diagnostic setup embodiment.

due to variations in the depth of the flow cell in its connectors. It was possible to limit the depth of the flow cell in its connectors by placing bolts in the intended holes of the prototype. Still, this would introduce the risk of incomplete connections and potentially result in leakages over time. Therefore, it was decided to abandon requirement 4.a and to implement the automatic adjustment system introduced in Appendix E.1.

In terms of usage, the main wishes were that the flow cell placement tool should be intuitive to use (wish 1.a) and that the placement and removal of the flow cell should be user friendly (wish 1.c and 1.b1.d). To validate whether the prototype met these wishes, short user tests were performed with fellow students not familiar with the design and the envisioned usage described in Figure J-3.

The subjects were given explanations on the general goal of the device and the vulnerabilities of the flow cell. They were then instructed to use the flow cell placement tool to hold a flow cell, to place it in the connectors of the integrated prototype, and to remove the flow cell placement tool from the flow cell. After this, they were again asked to hold the flow cell, to remove it from the connectors and to remove the flow cell from the flow cell placement tool. They were asked to think out loud whilst performing these actions.

It could be observed that the subjects had different approaches for placing the flow cell in the flow cell placement tool. Whilst some placed the flow cell by holding open the arms and moving the flow cell perpendicular to the flat surface, others attempted to slide the flow cell in from the bottom or top of the placement tool. The placement tool was not designed for this approach, as the deepened slot did not extend to the end of the flat surface. As a result, this approach could cause scratching of the surface. In addition, some found the alignment of the flow cell with the tool difficult to achieve, and the necessity of the alignment not clear by design. Also, the arms did not always successfully hold on to the flow cell without manually positioning them, making removal prone to failure and user errors.

In addition, some subjects did not notice the knurled interfaces. If the knurled interfaces were notices, subjects indicated that it did suggest an interaction was possible, but not which interaction.

Aside from this, all subjects were hesitant of applying a large amount of force. This was likely due to the vulnerabilities of the flow cell being stressed during the briefing.

Recommendations

Due to the prototype not meeting the functional requirements of preventing stresses being exerted on the vulnerable center of the flow cell (req. 4.b-c), it was recommended to reconsider the general design to better distribute the forces applied to it.

Aside from this, the arms were not always capable of holding on to the flow cell without manual positioning, and the envisioned usage was not intuitive by design. Therefore, the redesign should always hold the flow cell in the intended manner, and better guide the user towards the intended usage.

Appendix K. Improved flow cell placement tool design

As the initial embodiment design was not able to prevent stresses being exerted on the vulnerable center and the arms were not capable of holding on to the flow cell, the use of arms to hold the flow cell was reconsidered all together. As discussed, there was only limited space available for the placement tool to be used, especially in the integrated prototype of the diagnostic device. In this, obstructions were located close to the top and bottom of the flow cell connectors, and space to the sides is limited as well.

When considering a general holding mechanism this limited space should be considered, as well as that a larger contact area should be enabled to better distribute the stresses. It was realized that non-perpendicular movement of the placement tool release mechanism relative to the flow cell surface would result in a limited contact area with the flow cell, as was the case in the current design using arms. Therefore, a perpendicular release mechanism was selected. The resulting design can be seen in Figure K-1.

In this, the front and back side of the placement tool could move relative to one another when desired to hold or release the flow cell. This movement could be controlled from the back of the placement tool. To enable the placement tool to hold the flow cell without relying on external forces, a compression spring was added inside the placement tool (req. 1). The contact area with the flow cell was maximized on both sides, with the exception of the clean area of interest (req. 2), the vulnerable center of the flow cell (req. 4.b and 4.c), and the areas required for reaching the flow cell connectors. If the front and back side of the placement tool were

Figure K-1. Digital design of the improved flow cell placement tool design

pushed away from one another, the flow cell could be slided in and out to the side within the space available of the integrated prototype. This had been designed such that there was no alternative approach for placing the flow cell in the placement tool (wish 1.b). To reduce peak stresses on the flow cell, the entire potential contact area with the flow cell had been covered with 1mm rubber.

To make the placement tool more intuitive in its usage, all interfaces on the back had been fitted with 1mm rubber with indication of the intended usage (wish 1.a). The faces had been placed such that it could be used with a single hand (wish 1.e). There were two opposing faces with arrows towards the flow cell that should be hold during placement (wish 1.c). Perpendicular to that were two opposing faces with arrows away from the flow cell that should be hold during removal (wish 1.d). On the end of the latter part was another interface with the word “open” in it, that was to be compressed in order to open the placement tool mechanism and allow the flow cell to be slides in and out.

K.1. Improved prototype creation

The improved prototype was again created using 3d-printing. In addition, 1mm rubber was laser cut to cover the entire potential contact area and all user interfaces. The arrows on these interfaces and the word “open” were cut out using laser cutting. In addition, a standard compression spring was used to automatically push the two sides together.

K.2. Envisioned usage of the improved prototype

The envisioned usage of the improved flow cell placement tool was slightly more detailed than that of the initial flow cell placement tool. The envisioned usage for placement can be seen in Figure K-2. In this, the flow cell could be placed into the tool by holding the flow cell with one hand whilst opening the tool with the other by pressing the “open” button, and sliding the flow cell in (1). After this, the tool could be aligned with the flow cell connectors (2), and pressed into place using the faces with the arrows pointed towards the flow cell connectors (3). The tool could then be released to check its positioning (4), or removed by pressing the “open” button whilst holding the top and bottom faces and sliding the flow cell out (5-6).

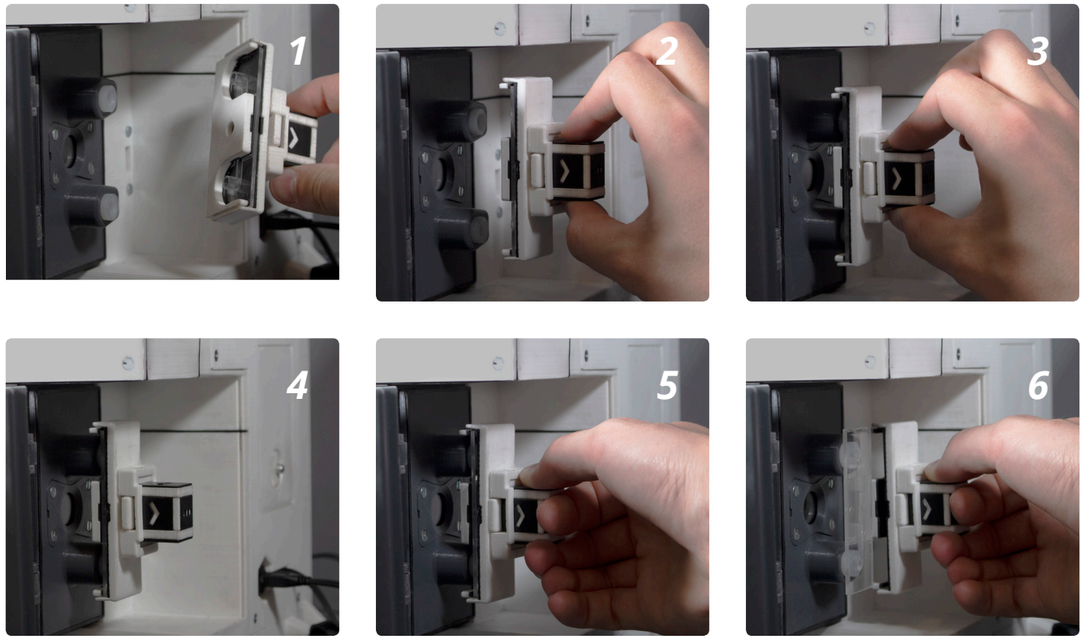

Figure K-2. Envisioned usage of placement with the improved flow cell placement tool on the integrated diagnostic setup embodiment.

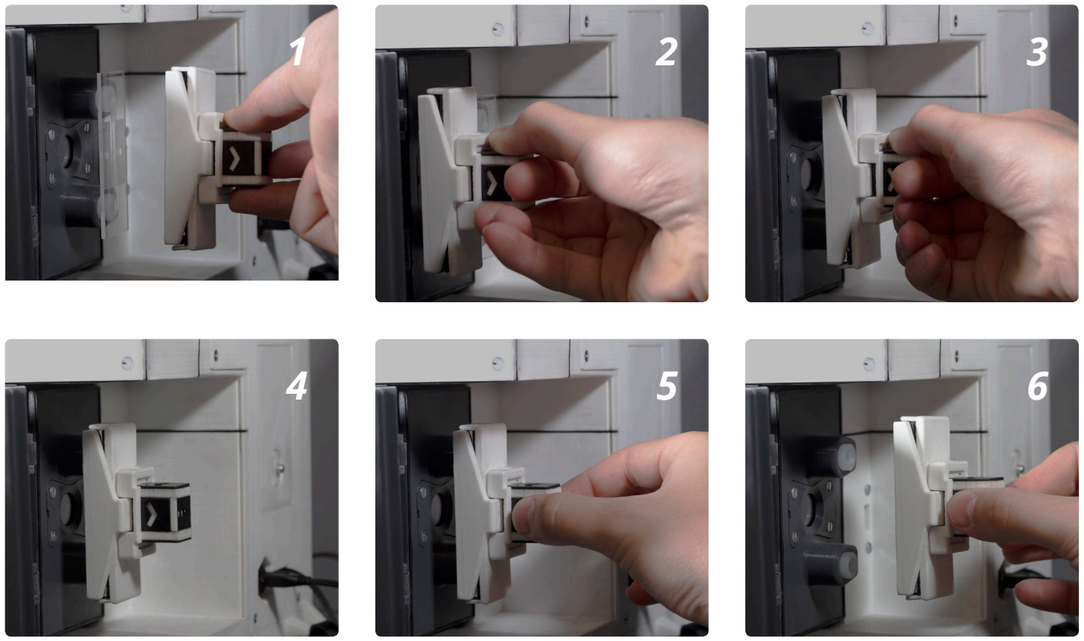

Figure K-3. Envisioned usage of removal using the improved flow cell placement tool on the integrated diagnostic setup embodiment.

The envisioned usage for removal can be seen in Figure K-3, and differs slightly. In this, the improved flow cell placement tool prototype was being held upside down to illustrate that this does not affect the functioning of the tool. First, the tool's opening side was put to the side of the flow cell (1). After this, the "open" button was pressed, and the opening was aligned with the flow cell (2) and the tool could be slided over the flow cell (3). The tool could then be released if desired (4). The flow cell could then be removed by pulling on the faces with the arrows pointing away from the flow cell connectors (5-6).

K.3. Validation of the improved embodiment design

Validation of the improved flow cell placement tool prototype again had to be performed on two major aspects: functionality and interaction.

Just like the initial prototype, the improved prototype had demonstrated to be well capable of holding a flow cell without external forces (req. 1) or contaminating the area of interest (req. 2). It was also well capable of placing the flow cell in the flow cell connectors (req. 4). Besides this, and in contrast to the initial prototype, it was capable of handling excessive forces during both placement and removal sufficiently to prevent apparent damage to old flow cells (req. 4.b and 4.c).

In terms of interaction, the usage still remained relatively unintuitive for fellow students. This was due to the prototype having only a single usage scenario in which it could be used. However, once the envisioned usage was explained to the user, placement could be performed reliably. For some students, this required multiple trials due to the limited faces that could be hold on to whilst pressing the "open" button.

Besides this, it was noticed that an excessive amount of force was required to overcome the internal friction between the 3D-printed parts. As a result, some students required the use of two hands to press the "open" button. This complicated the interaction and should be prevented. The friction could be easily reduced by sanding the 3D-printed parts. After this, the prototype was tested again with the same students who could now easily press the "open" button with a single hand. Due to users being able to place the flow cell reliably without causing damage, and the limited importance of the flow cell placement tool, no further iterations will be performed.

Appendix L. Initial digital interaction embodiment design

To create the initial digital interaction embodiment design, a list of requirements and wishes was first created, as can be seen in Part B, section 2.1 of the thesis (p.45). Based on this, an initial design was to be made, validated, and iterated upon if necessary.

L.1. Conceptual exploration

Based on the requirements and wishes set out, a wide variety of concepts could still be envisioned. To systemically process the various options, a morphological chart was created. First, all aspects that had to be designed for based on the lists of requirements and wishes and for which multiple feasible solutions could be envisioned were reformulated into questions in the form of "how can you ...?". This resulted in five questions for which solutions were listed. The five aspects and their most realistic solutions have been combined to the morphological chart seen in Figure L-1.

Using the morphological chart, concepts could be created for the digital interaction embodiment by combining sub-solutions for the different aspects that were to be designed for. As can be seen in Figure L-1, the conceptual interactive design created by Mirte was also included. Besides this, four more concepts were created using the morphological chart; basic, extended, rotary, and touch. For most design aspects, the same sub-solutions were used for most concepts. This, as these sub-solutions were considered most feasible and realistic in regards to the lists of requirements and wishes.

Elaborated visualizations of the four concepts can be found in Figure L-2. In this, the double circle indicates the use of a momentary switch, the single circle with arrows indicates the use of a rotary encoder, and the hand indicates the use of a touchscreen. In addition, potential configurations for the digital interface designs were added in gray.

L.2. Concept evaluation

To select a concept for the digital interaction embodiment design, the concepts were evaluated against the lists of requirements and wishes. For this, wishes on which the concepts performed differently were cost (wish 2), durability (wish 1, 3), cleanability (wish 4), and ease of interaction (wish 1.b, 5).

Figure L-1. Morphological chart for the digital interaction embodiment.

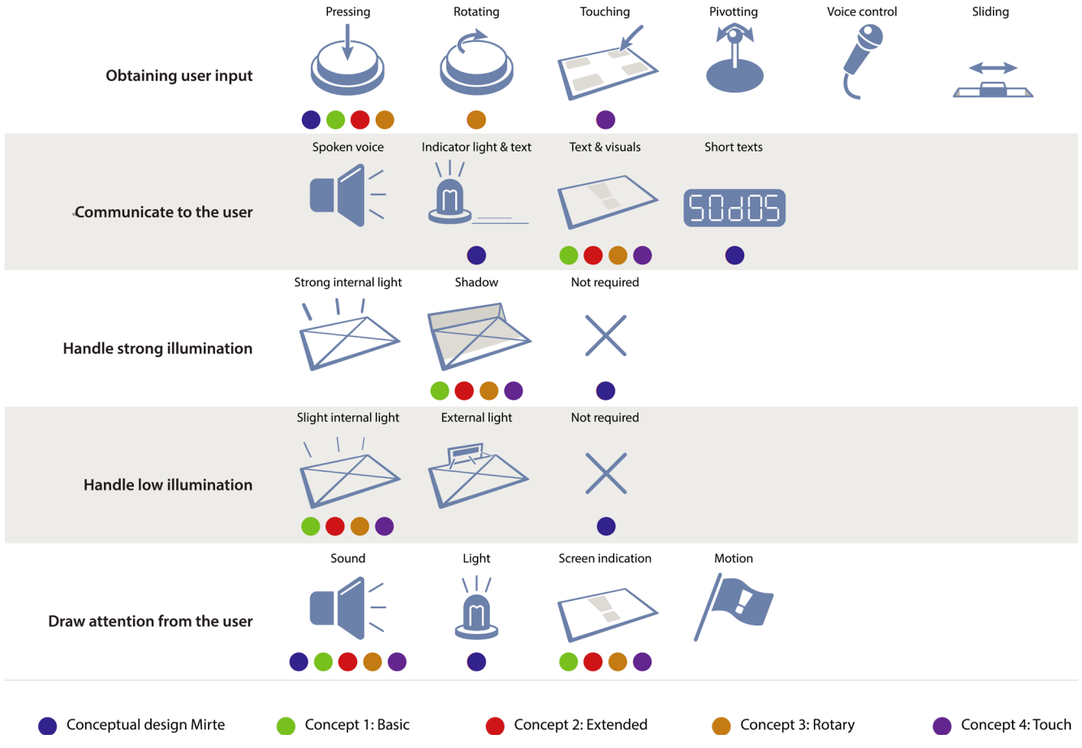

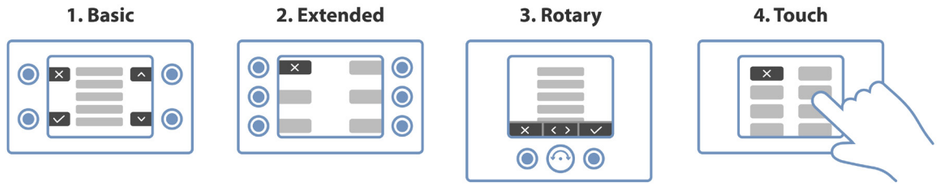

Figure L-2. Conceptual designs for the digital interaction embodiment.

For cost, a clear comparison can be made. In this, it should be noted that there was a wide range of display types available for concepts 1-3. For concept 4, less options were available, as this was to be a touchscreen. Based on a comparison of potential solutions and the expected digital interaction required, a custom segmented LCD display could be the most preferable solution for concepts 1-3 [36]. This display could be a passive matrix monochrome LCD display. This, as this solution is relatively energy efficient, durable, and affordable when produced in larger quantities. Still, as the digital interaction was not yet defined and this type of screen could best be made for a specific purpose, a regular TFT LCD screen would be used for prototyping purposes.

In terms of durability, touchscreens were deemed relatively vulnerable for rough handling. In contrast, momentary switches could easily be made highly durable and waterproof. Rotary encoders could be considered more vulnerable than momentary switches, as they protrude from the device by design and would require a rotary shaft seal to be made waterproof.

When considering the cleanability, touchscreens were also deemed relatively prone to contamination, and malfunctioning as a result. In contrast, the waterproof momentary switches could be easily cleaned. The rotary encoder could be comparable in terms of cleanability, if made waterproof and when accounted for in the selection of the knob cap.

Defining the ease of interaction

As the digital interaction is not yet defined, the ease of interaction could not be assessed at this stage. Therefore, before a selection could be made amongst the four concepts, the digital interaction was to be further defined. After this, the required interaction for each of the concepts could be estimated to determine the ease of interaction and a final selection could be made.

Concept selection

Based on the essential digital interaction flowchart as seen in Figure N-1, the ease of interaction could be assessed. It could clearly be seen that at any moment during usage, a maximum of four interactive options are present. Therefore, interaction with concepts 1, 2, and 4 only requires a single action. For concept 3, one or two actions are required, as a selection must be confirmed by pressing a button.

This resulted in a complete Harris profile, as can be seen in Figure L-3. It could clearly be seen that concept 1, Basic, scored best on each of the wishes. Therefore, this concept would be elaborated into a functional embodiment design and prototype that could be used to evaluate the digital interaction design.

L.3. Initial embodiment design

The embodiment design that was to be created for the concept should be suitable for all potential digital interaction designs that were still to be prototyped. As discussed before, a custom segmented, passive matrix, monochrome LCD display would be highly suitable for the final embodiment of the display. However, as the digital interaction was not yet defined and this type of screen can best be made for a specific purpose, a regular TFT LCD screen is used for prototyping purposes.

More specifically, a 3.5 inch TFT LCD touchscreen was chosen with a resolution of 480x320 pixels and a screen size of approximately 74x49 mm. This, as it was subjectively considered a suitable size for the chosen application, readily available, and highly compatible with the Raspberry Pi. In addition, a passive speaker was directly connected to the Raspberry Pi in order to draw the user's attention when deemed necessary.

Figure L-3. Harris profile for the digital interaction embodiment.

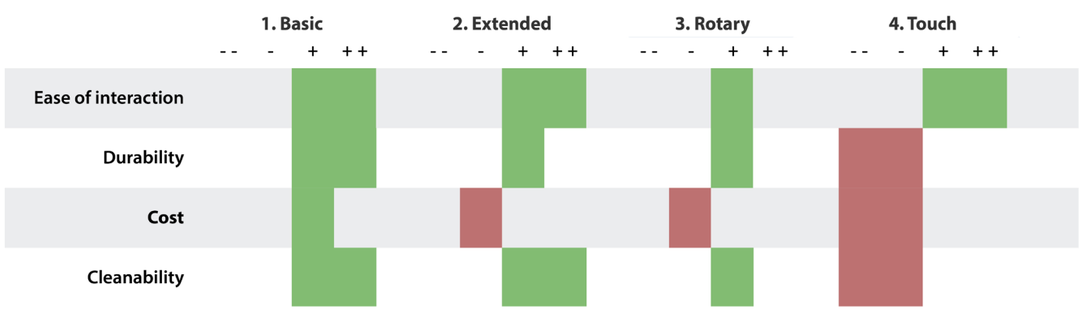

The four buttons should be watertight, resistant to chemicals potentially used for cleaning purposes, and able to handle rough handling. In addition, they should also be preferably able to draw and guide attention when interaction is required. Therefore, existing buttons were explored and assessed. Eventually, watertight momentary switches with build-in LEDs and a diameter of 12mm were selected for this purpose. An alternative method, potentially more suitable for the final embodiment design is the use of membrane switches with LED backlight, which can be integrated with passive matrix, monochrome LCD displays.

As shown in the visualization of concept 1 in Figure L-2, the four buttons were placed horizontally adjacent to the four corners of the display. This was to clearly visually separate the buttons and their labels on the display from one another, whilst not obstructing the view of the display by movement of the user's hand. To hold the TFT LCD screen and the four buttons, a small frame was designed. This contained attachment points for the screen, holes for the button, and side wall to let the screen rest on a surface without resting on the electronics.

L.4. Initial prototype

Using the components described above, an initial prototype was created using the 3D printing of regular PLA at the TU Delft. The resulting prototype was directly connected to the Raspberry Pi 3B+ used for prototyping.

Within the prototype, it should be possible to turn each of the build-in LEDs of the momentary switches on or off depending on whether interaction would be possible. This means that four General-purpose input/output (GPIO) pins were required to control the individual LEDs, whilst another four GPIO pins were required to detect whether a button was pressed. With a growing number of components requiring a large number of GPIO pins, an IO expansion HAT using I^2C communication was purchased for increasing the number of GPIO pins available. Still, the build-in LEDs required a 5V input, which could not be provided by the GPIO pins of both the Raspberry Pi and IO expansion HAT. Therefore, transistors with according resistors were added to control the LEDs. To reduce the complexity of the system required to control the LEDs, the top two and bottom two LEDs were controlled by a single transistor. This was deemed acceptable, as most interaction would have two or four interactions. This resulted in the prototype seen in Figure F-3, Figure F-4, and Figure 28 of the thesis.

L.5. Validation of the initial embodiment design

The prototype of the initial digital interaction embodiment was validated together with the fluid handling and initial digital interaction design, as can be seen in Figure 28 in the thesis. During this, eight fellow students were asked to simulate a measurement using the digital interfaces and were asked to think out loud whilst doing so. Afterwards, they were asked specifically about their opinion of the initial digital interaction embodiment design.

Regarding this prototype, the participants considered themselves to be able to navigate through the interfaces. Still, a majority considered the 12mm watertight momentary switches to be too small for comfortable usage. Besides this, some participants indicated to like the fact that they could place their fingers on the back side of the prototype frame to hold the device whilst using the buttons. They also indicated that it was best to hold the screen at a slight upward angle, as this makes the screen more perpendicular to the user's face. The passive speaker was used to get the user's attention when required, but as the user was already focused on the interaction this had no apparent effect during the user tests.

The positioning of the momentary switches next to their according labels on the screen was considered clear. However, as there were some interfaces having an uneven number of interactions, the indications given by the build-in LEDs of the momentary switches were not always correct. This was considered contradicting and needed to be improved.

Besides this, it could be noted that the currently used clamping mechanism for attaching the screen to the frame did not yet result in a watertight system. As a result, it was likely not capable of resisting the environmental conditions present in the envisioned context (req. 3).

Recommendations for the next design iteration

For the next design iteration, it was recommended to increase the diameter of the momentary switches, to change the electronics for individual control of the build-in LEDs of the switches, and to maintain a feature for placement of the fingers during usage of the buttons. Besides this, the attachment of the screen to the frame should be improved to withstand the environmental conditions present in the envisioned context.

Appendix M. Integrated digital interaction embodiment design

As the recommendations given for the digital interaction embodiment design did not require fundamental changes to the design, it was decided that the design was sufficiently developed to perform this design iteration as an integrated design. This means that this design of the digital interaction embodiment design was combined with the other separately developed sub-system designs to form a single functional and interactive prototype.

In the integrated design, the 12mm momentary switches had been replaced with 19mm switches of the exact same type. As a result, no additional changes were required of the frame other than a larger diameter for placement. For the electronics, no additional changes were required, other than the LED transistor design being adapted to enable individual control of the LEDs.

For the attachment of the screen to the frame, a completely new design was made. This, as the touchscreen was considered relatively vulnerable and should not be usable in the final prototype. Due to this, a protective transparent PMMA plate was added on top of the touch screen, and rubber padding was added on both sides of the plate for insulation and shock absorbance. Also, between the touchscreen and the 3D printed supports, rubber foam had been added for shock absorbance. Due to the screen being well protected in this new design, and the screen being directly connectable to the 40 pin GPIO header of the Raspberry Pi 3B+, these supports had been extended to also hold the Raspberry Pi, the GPIO splitter HAT, and the GPIO expansion HAT. These general design choices for the electronics of the Sodos are further discussed in Part C, section 2.1 of the thesis and Appendix P.

Besides this, a feature for placing fingers during usage of the buttons should be maintained. As the frame for holding the screen had been reduced to a flat surface with rubber padding along its edges for integration with other components, these features must be integrated with other parts. To do so, two slots were added to the product embodiment design on the sides of the screen. To quickly determine the distance between the screen and the slots and the overall dimensions of the slot, cardboard was folded in the eventual outer shape of a side, and fellow students with different hand sizes were asked which was most comfortable. Besides this, the frame for holding the screen was placed at a slight upward angle.

M.1. Validation of the integrated embodiment design

The validation of the integrated digital interaction embodiment was performed together with the validation of the improved digital interaction and the fluid handling. In this, the most complex interactions within the improved digital interaction design were tested with the participants being asked to think out loud, without setting the focus on the embodiment design. As the participants were not actively made conscious of their physical interaction with the prototype, their unbiased behavior could be observed. Afterwards, specific questions regarding their opinion of the digital interaction embodiment were asked.

From this, it became clear that the momentary switches could now be comfortably used, and individual control of the build-in LEDs had improved the clarity of the interactions possible. Still, not all users intuitively used the slots designed for placing the fingers. Instead, they either controlled the interface with one hand on the back of the integrated prototype or without providing support to the prototype at all. The latter was considered potentially undesirable, as it would increase the chance of the prototype moving or falling over. When asking the participants why they did not use the slots, some stated not noting the slots whilst others indicated that they were not sure about the purpose of the slots. This is understandable, as the slots have a near rectangular shape and do not suggest being designed for placement of the fingers.

Recommendations for future design iterations

For future design iterations, it is recommended to redesign the slots for placement of the fingers to suggest their intended use. This can for example be achieved by creating a slope on the side of the slot not intended for placement of fingers, by adapting the shape of the side intended for placing fingers to match the rough shape of finger tips, and by giving this side a diverging appearance to indicate the possibility of an interaction.

For the latter, the surface could for example be covered with the same rubber used to cover the interaction surface of the handle in the product embodiment design. This, as the resemblance between the two surfaces would suggest a resemblance in function. A digital render of what this would look like can be seen in Figure M-1. Of this design, no prototype has been created.

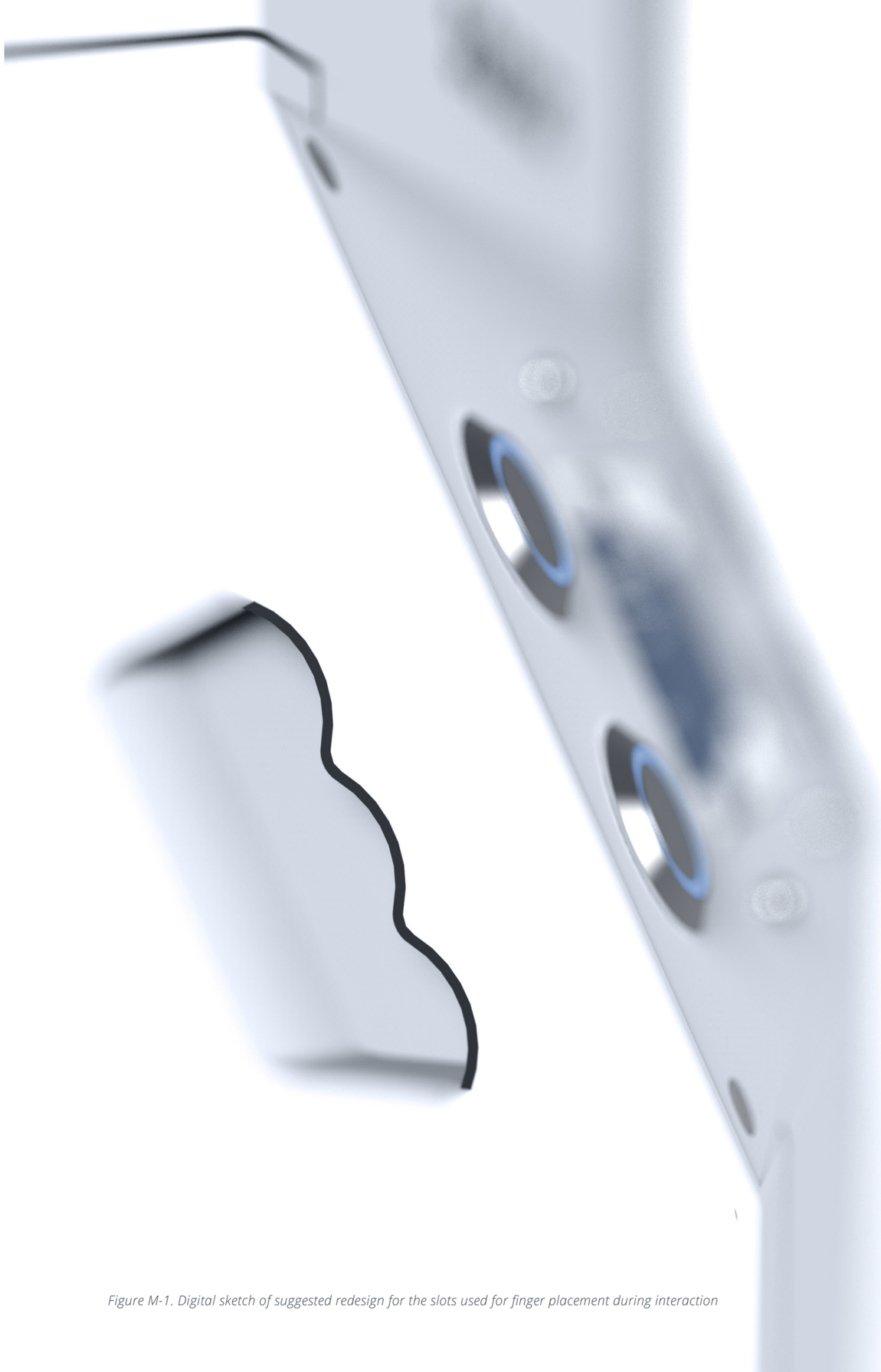

Figure M-1. Digital sketch of suggested redesign for the slots used for finger placement during interaction

Appendix N. Initial digital interaction design

To create the initial digital interaction design, a list of requirements and wishes was first created, as can be seen in Part B, section 3.1 of the thesis (p.49). Based on this, an initial design was made, validated, and iterated upon if necessary.

N.1. Defining the digital interaction flowchart

Based on the list of the requirements and the list of wishes, the essential digital interaction flowchart was created, as can be seen in Figure N-1. In this, the required interaction for performing a measurement was based on the expected interaction required and the fluid handling procedure. Brief validation of the digital interaction flowchart was obtaining during discussions with fellow students.

Using this flowchart, concept selection could be performed for the initial digital interaction embodiment, as discussed in Appendix L.2. The resulting design and prototype were used for creating and validating the digital interaction design.

N.2. Initial digital interaction design

Using the digital interaction flowchart introduced in Figure N-1, and the digital interaction embodiment design and prototype introduced in Appendix L.3-4, the digital interaction design could be created and validated.

First, various layouts potentially meeting the requirements and wishes were set out. Besides the requirements and wishes originally set out, button labels should be horizontally adjacent to the four buttons in the corners. The layout should only use two colors

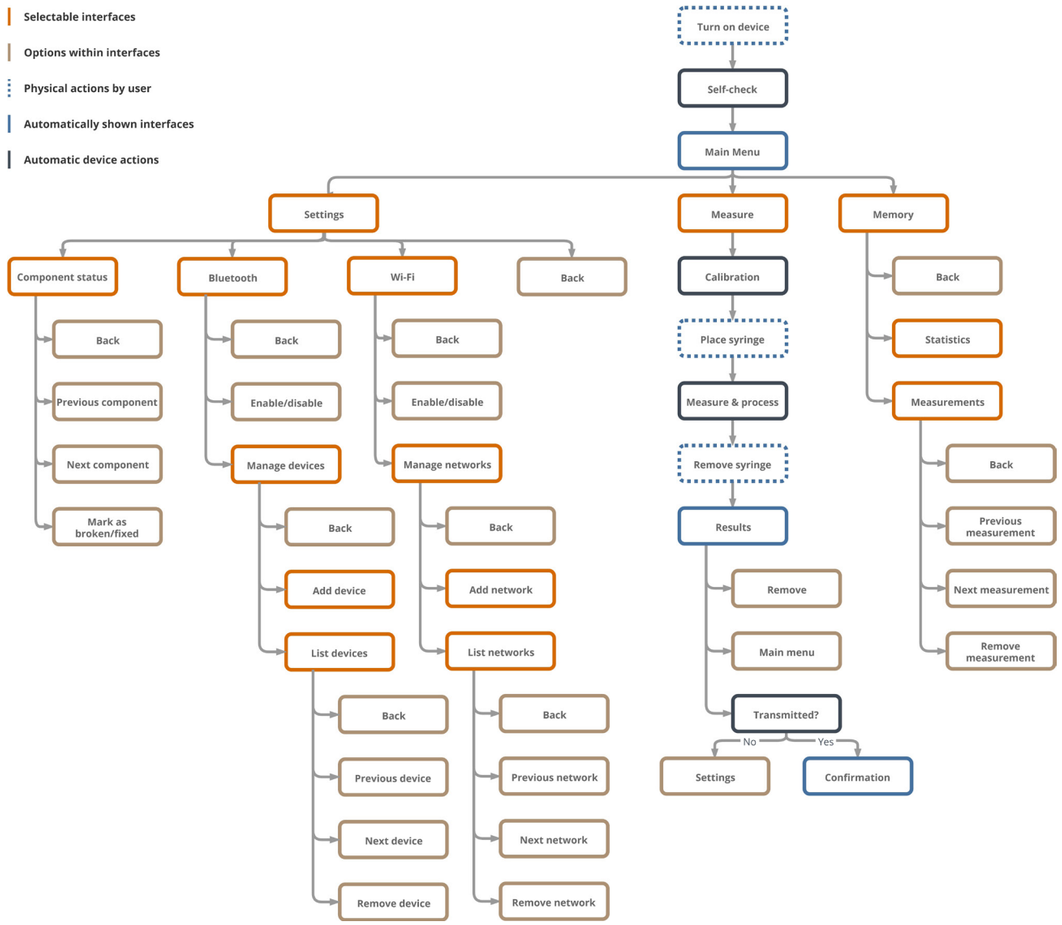

Figure N-1. Flowchart of the essential interactions for the digital interaction.

Figure N-2. General layout options for the digital interaction design.

(req. 1.a), which were subjectively chosen and validated with fellow students. Also, to minimize the risks of user error (wish 1), and to make the presented information (partially) interpretable for illiterate users (wish 3.a), icons were added. Of the various options envisioned, the most feasible were elaborated into digital layout designs, as can be seen in Figure N-2. Based on discussion with fellow students, layout 4 was selected and applied to the interfaces required for enabling the interactions introduced in Figure N-1.

This resulted in a complete flowchart of visual interfaces, as seen in Figure N-4. In this, one interaction that was not fully elaborated when assessing the ease of interaction in Appendix L.2 was connecting to a Wi-Fi network.

Namely, regular Wi-Fi networks can require a password of up to 63 characters to be entered [37]. As the digital interaction design must enable the configuration of Wi-Fi networks (req. 4c), this should be possible using the digital interaction embodiment design. Still, Wi-Fi passwords can contain each of the 95 printable ASCII characters [14]. Therefore, the relatively rare interaction of entering a Wi-Fi password would be difficult to perform with every concept proposed in Figure L-2.

There are other applications where complex passwords must be entered using basic input devices. Examples include modern televisions, game consoles, and digital cameras. Here, virtual keyboards were designed to enable the interactions required. Often, uppercase and complex characters were accessible via dedicated keyboards. A similar virtual keyboard was designed for entering Wi-Fi passwords, as can be seen in Figure N-3. Still, the interface and its interaction should be validated during user tests.

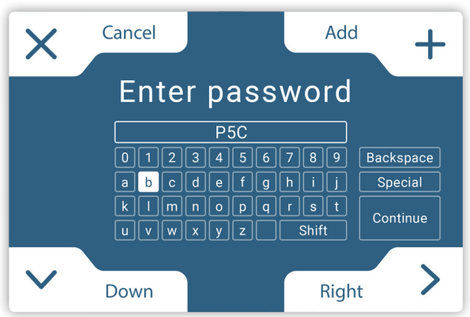

Figure N-3. Initial interface with virtual keyboard for entering Wi-Fi passwords shown on scale 1:1.

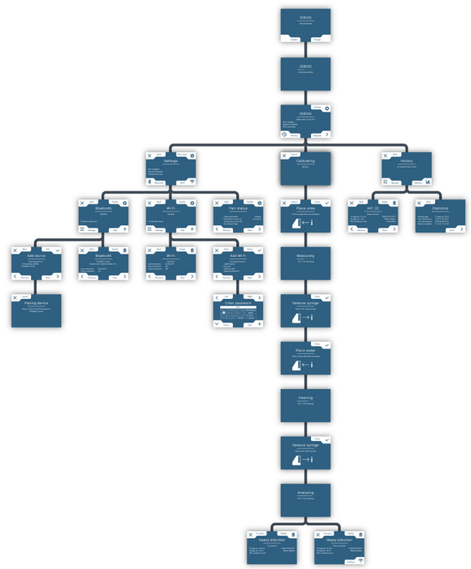

Figure N-4. Interface flowchart for the digital interaction design

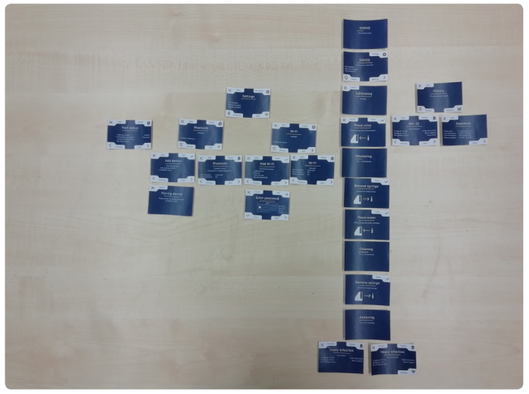

Figure N-5. Initial interface with virtual keyboard for entering Wi-Fi passwords shown on scale 1:1.

N.3. Cognitive Walkthrough of the digital interaction design

To assess the general setup of the interface flowchart in Figure N-1, various discussions were held with fellow students. Besides this, it was recommended to perform an individual Cognitive Walkthrough to quickly validate the explicit user tasks that were to be performed using the digital interaction design [38]. In this, the user profile was obtained from the context analysis described in Part 2.3 of Vendel [9].

In addition, the tasks that were to be considered during the Cognitive Walkthrough should be selected. As the number of tasks that could be performed using the device was limited, all eight task paths were included. Within these paths, a larger number of tasks could be performed.

For the Cognitive Walkthrough, the designed screens were printed at their eventual size. They were laid out on the table to match the interface flowchart of Figure N-1, as can be seen in Figure N-5. After this, each of the eight task paths were reflected upon. To do so, every screen in each path was physically brought to the front of the table and the four questions of a Cognitive Walkthrough were reflected upon [38]:

1. Will the user try to achieve the right effect?
2. Will the user notice that the correct action is available?
3. Will the user associate the correct action with the effect that the user is trying to achieve?
4. If the correct action is performed, will the user see that progress is being made towards the solution of the task?

Design changes resulting from the Cognitive Walkthrough

After an individual Cognitive Walkthrough was completed in accordance with the recommended literature [38], various changes were made to the design. These were mostly changes to the choice of words on the interfaces and the visual appearance of the icons, and adding details to the functional behavior of the interfaces. It was decided that the latter could best be implemented into the design by turning the design into a functional prototype.

N.4. Prototyping the digital interaction design

The digital interaction was to be displayed using the same Raspberry Pi used for controlling all other digital applications and electronic components. As discussed before, all electronic components were controlled using algorithms made in Python 3. To ensure an effective cooperation of the algorithms with the digital interaction, the interfaces were also to be made using Python 3.

To do so, an interface library should be used. After online comparisons of the different libraries available for Python 3, it was decided to use the Kivy library. The Kivy library uses special kv files with its own syntax and rules in combination with regular Python 3 scripts to create controllable interfaces. In order to use the library correctly, an online course was followed.

To assess whether the designs were really suitable for the screen, Kivy was used to display each individual interface of the interface flowchart as an image. Upon confirming that the designs were suitable for the screen, it was decided to code the interfaces. This, as the size of the images often resulted in Kivy crashing, and it was not possible to have dynamic changes in the interfaces.

Building on personal experience as a freelance web designer and developer, a template with all required layouts and components was first created. Using this, the required interfaces could easily be created. The template enabled central control of components and prevents a lot of work during iterative design processes. In addition, a special Python 3 class was created that controlled the LEDs of the momentary switches, and binded the input of the momentary switches to the activated interface.

In the end, over 2700 lines of code were required for creating and controlling the interfaces. The most complex part of this was creating the virtual keyboard as seen in Figure N-3, as there are a lot of actions possible.

N.5. Validation of the initial digital interaction design

The prototype of the initial digital interaction design was validated together with the fluid handling and initial digital embodiment design, as can be seen in Figure 28 of the thesis. To do so, fellow students were asked to simulate a measurement during individual sessions using the initial digital interaction design communicated via the initial digital embodiment design.

For this, the participants were given written instructions explaining the functional capabilities of the device. After this, they were given three written assignments; to perform a diagnosis of a simulated urine sample, to transmit the results over a Wi-Fi network new to the device, and to find back the diagnosis of an earlier measurement. They were asked to think out loud whilst performing these assignments.

The feedback obtained during each individual session was discussed with the participant after the session, and implemented in the digital interaction design before the next session was started. New sessions were started until no more points for improvements were found for multiple sessions. This resulted in a total of eight participants and individual sessions. The resulting adapted design formed the improved digital interaction design.

Appendix O. Improved digital interaction design

The iterative validation of the initial digital interaction design had resulted in consecutive changes that gradually transformed the initial design into an improved design.

In this improved design, changes were made to the icons and specific words used in the digital interaction design. Most changes were made to the virtual keyboard design for entering Wi-Fi passwords. In this, the cancel button was made a part of the keyboard instead of being a separate button. As a result, a directional button to the left could be added to enable faster and more intuitive handling of the keyboard. Additionally, holding down one of the directional buttons for a longer period of time caused the button action to be repeated at a high rate until the button was released. This was suggested during the validation of the initial digital interaction design as it is a standard function for physical buttons such as keyboard and remotes. Also, the add/select button had been moved to the lower right position, as this had proven to be a more intuitive location. The original virtual keyboard design can be seen in Figure N-3, whilst the improved virtual keyboard design can be seen in Figure O-1.

Besides this, the digital interaction design had been extended upon to include control of the fluid insertion system in the integrated prototype. Algorithms were developed to track the progress of syringe actions and to visualize countdowns in the interfaces.

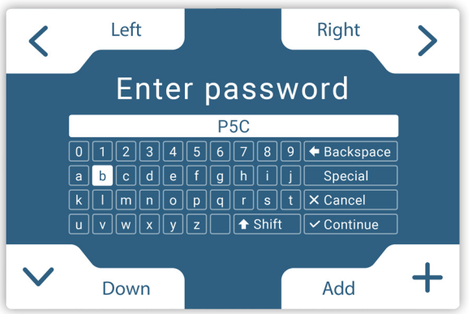

Figure O-1. The improved virtual keyboard design created for entering Wi-Fi passwords.

In preparation for the field research in Ivory Coast, the interfaces have also been translated to French by using MO and PO files. The language used by the interfaces could now be selected after starting the program. To validate the accuracy of the translations, all interfaces were discussed with a native French speaking student.

O.1. Validation of the improved digital interaction design

To validate the improved digital interaction design, short user tests with fellow students were performed together with the validation of the fluid handling and integrated digital interaction embodiment. Based on findings related to the handling of fluids, the texts of the digital interaction design were slightly changed to highlight the filling of the syringe and the necessity of placing cups. Aside from this, no significant points for improvement could be identified.

O.2. Recommendations for future development

For future development, it is recommended to further expand on the software for the digital interaction design by implementing direct measurement control, Wi-Fi control, Bluetooth control, and database control. In the current design, simulated control is deemed sufficient for the purpose the digital interaction design serves.

For a future redesign in which the regular TFT LCD screen will be replaced by a custom segmented LCD display, a complete redesign and optimization of the digital interaction design is recommended.

Appendix P. Electronic optimization of the product embodiment design

For optimizing the internal electronics of the product embodiment design, it was first important to create an overview of the electrical functionalities the design should enable. As discussed in Part C, section 2.1 of the thesis (p.56), this included a functional screen, passive speaker, laser diode, optical sensor, stepper motor, and (momentary) switches. In addition, various sensors were to be included to provide additional information on the performance and conditions of the design, including temperature, humidity, and GPS sensors.

Besides this, the design was to have a suitable power supply for the envisioned context. For this, the main requirements set out were that it must be able to handle an insufficient power supply and electrical disturbances in the electrical grid, and it should be able to keep the device functional for multiple hours if the power supply is insufficient (req. 3.a-b and wish 2, p.54). In addition, the battery capacity could not exceed the maximum levels allowed for transportation by airplane (req. 8, p.54). To meet these requirements, the power requirements of the device were to be established first.

As discussed in Part C, section 2.1, all components were to be controlled by a single Raspberry Pi. The use of a Raspberry Pi was a predetermined aspect of the Sodos. I personally agree with this decision, as the Raspberry Pi is a broadly applicable, powerful, standardized, and well-documented prototyping computer with native support for Python 3. This coding language was to be used for enabling all desired functionalities. As the computational demands for the existing Python algorithms developed by Patrick were high, the most powerful Raspberry Pi was obtained for this project, being the Raspberry Pi 3B+.

To enable the described functionalities, standard components were used as much as possible throughout the development process. Using these components, the desired configuration was first determined by using multiple breadboards, as can be seen in Figure P-1. Once the desired configuration of the components was determined, custom circuit boards were created to simplify the design. Once all boards were completed, the components were organized and fixed on either laser cut PET-G panels or as part of the electronics package shown in Figure 36 of the thesis. This resulted in the configuration illustrated in Figure P-2 and Figure P-3.

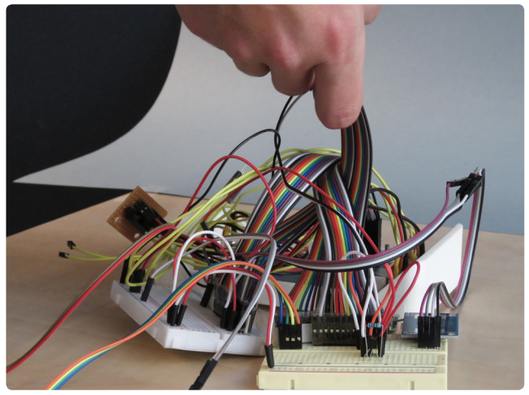

Figure P-1. Determining the desired configuration of electronics using breadboards.

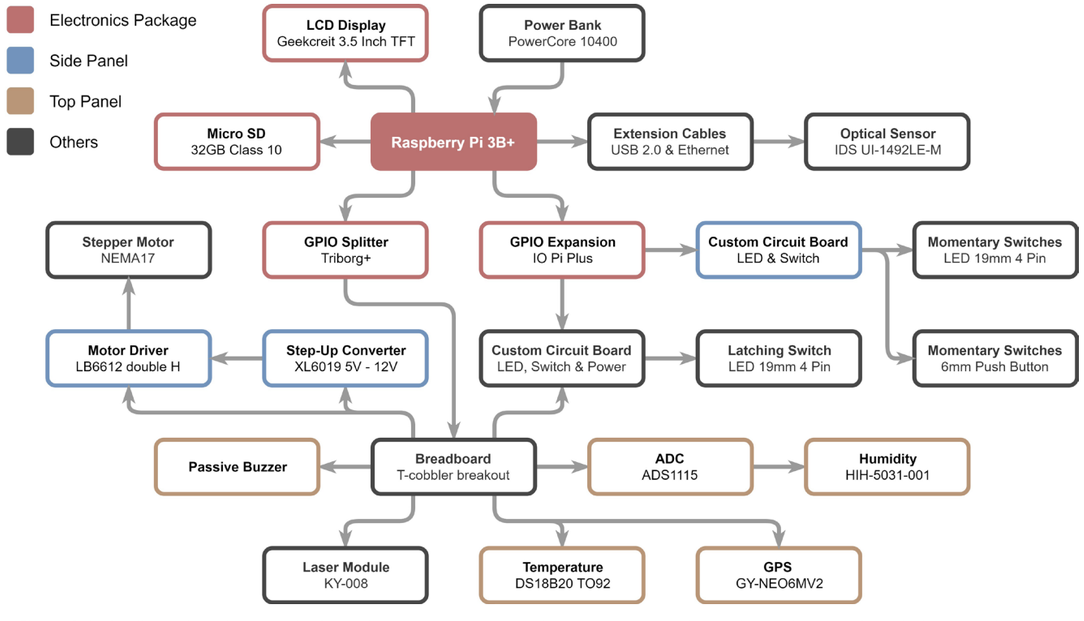

Figure P-2. Configuration of electronics in the integrated prototype with colors representing their physical location within the design.

P.1. The configuration of electronics

To create the configuration of electronics illustrated in Figure P-2, the individual components required for enabling the described functionalities using the Raspberry Pi 3B+ were to be determined.

For the screen, a standard TFT LCD touchscreen with a resolution of 480x320 pixels was selected due to its suitable size, its compatibility with the Raspberry Pi and the option to directly place it as a Hardware Attached on Top (HAT) on the general-purpose input/output (GPIO) pins of the Raspberry Pi [39]. Still, this meant that a large number of GPIO pins would become both physically and digitally unavailable for other functionalities. Therefore, two additional HAT boards were obtained, being a GPIO splitter board and a GPIO expansion board. The GPIO expansion board used I^2C communication with the Raspberry Pi to set the pin modes and communicate the values of input pins.

As I^2C was also used by various other components, only infrequently changed components were controlled via the GPIO expansion board, being the LEDs and some of the switches. As the used LEDs required 5V to function accordingly and the GPIO pins only supplied 3.3V with a limited current, NPN transistor configurations were designed to provide power to the LEDs directly from the 5V power supply.

In addition, it was decided to add a power button to the design using a latching switch with build-in LED. For this, an additional circuit was required, as the wake-up pin of the Raspberry Pi (pin 5) was also required for I^2C communication with the HATs. Therefore, a PNP based transistor setup was designed to automatically disable the wake-up pin connection once the Raspberry Pi was waking up. This was designed such that the I^2C communication would not be disrupted, whilst the state of the switch could still be read by the GPIO expansion board to initiate shutdown when pressed again.

Besides the GPIO expansion board, other components using the I^2C communication were the TFT LCD touchscreen and the analog-to-digital converter (ADC) required to obtained the humidity within the design. This ADC could also be potentially used to read the voltage level of the power supply. Other sensors within the design used other methods for communication. The GPS module used the UART protocol, whilst the temperature sensor used the 1-Wire protocol.

Anther electrical component within the design is the NEMA17 stepper motor. For the stepper motor to function accordingly, a suitable motor driver was selected. To provide this motor driver with the according voltage, a step-up converter was included and configured to convert the 5V provided by the power supply to the 12V for which the stepper motor was designed. The use of a stepper motor resulted in peak current draws. This could be reduced by placing a suitable capacitor at the 12V side of the step-up converter. Still, as the stepper motor was functional without the capacitor and limited time was available, this was not explored.

Also included in the design was the laser diode required for measurements. For the laser diode, a constant currently supply was originally implemented and used with the U-LD-630551A laser diode. However, now that the KY-008 laser diode was being used instead, the constant current supply could be exchanged for the constant voltage of 3.3V supplied by the Raspberry Pi. The constant current supply is still present in the design in case the laser diode is to be changed again in the future.

With most electronic components determined, it was now possible to determine the power requirements of the device and select a suitable power supply for the envisioned context. It was experimentally determined that the device drew 0.8A during rest (4.0W). During measurements, peak current draws by the stepper motor caused the device's draw have a range of 1.0-1.4A (5.0-7.0W). Therefore, having the device function without external power for an entire day would consume 56Wh at most, being well below the maximum of 100Wh for transport by plane [16].

For this, an Uninterruptable Power Supply (UPS) in the form of a Raspberry Pi HAT was obtained with a maximum charging and discharging rate of 2.0A. The battery status of the UPS could be digitally read by the Raspberry Pi over I^2C, allowing it to shut down automatically before the battery was completely emptied. However, it was quickly discovered that the UPS was not able to provide the indicated discharge rate or that the required discharge rate was higher than measured, as the UPS was not able to reliably power the Raspberry Pi. This caused brownouts to occur even when using the Raspberry Pi without additional electronics. In addition, the UPS could not be controlled by the Raspberry Pi, preventing automatic activation and shutdown of the UPS. As there were few off-the-shelf UPS systems addressing these shortcomings, different options were explored. Still, a potentially viable system worth exploring in the future was later found [40].

Instead of an UPS, two 5.0V power banks with a maximum discharge rate of 3.0A and a capacity of 10400mAh at 3.7V were obtained. These power banks were specifically selected due to their maximum discharge rate of 3.0A, which is much higher than the 2.0A of the malfunctioning UPS. These power banks would allow the prototype to function for 5 to 6 hours per power bank. After this, the power bank could be charged whilst the other power bank could be used, as the power banks do not support pass-through charging. It would be preferable to use power banks with pass-through charging, but these were often found to be interrupted when switching between discharging and pass-through charging, and to result in a disruptive voltage drop during pass-through charging.

Having all electronic components fully determined and the custom circuit boards prototyped, the components could now be organized and placed in the product embodiment design. The Raspberry Pi and its HATs were stacked on the back of the digital interaction embodiment with additional support, forming an electronics package. Other components were distributed over two laser cut PET-G panels which could be bolted onto the inside of the embodiment, as indicated by color in Figure P-2 and seen in Figure P-3 and Figure 36 of the thesis. The remaining components were either placed on other specific locations within the design or kept unfixed within the general electronics housing to maintain accessibility. The power banks were kept outside the product embodiment design to ease replacement for charging.

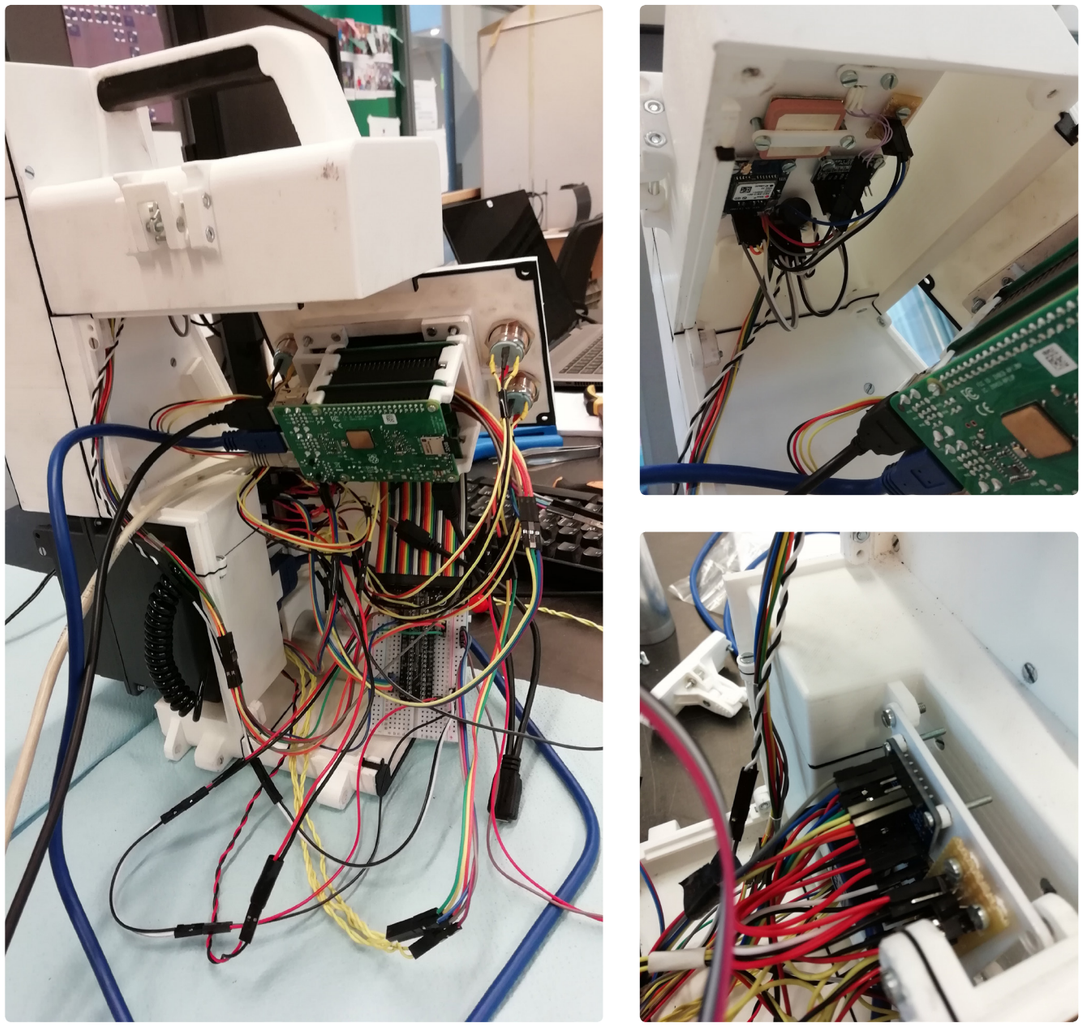

Figure P-3. Configuring the internal electronics of the integrated prototype. Left; the overall complexity of the partially assembled integrated prototype and the electronics package. Bottom right; a close-up of the side panel. Top right; a close-up of the top panel.

Appendix Q. Summarized anonymized urine sample data

In Table Q-1, all urine samples obtained during the field research in Ivory Coast have been documented. In this, the urine number or participant number is noted to match the urine number in the measurement data (Appendix R). The duration of manual diagnosis is measured as the time between filling the syringe with urine for the first time to the moment the final number of SH eggs is determined. The number of eggs is the total number of SH eggs found in the analyzed part of the urine sample and the cleaning water. Participant age and gender are included in the table, but participant names are excluded to safeguard the identity of the participants. Notes were only added if abnormalities occurred or if the entire sample was also analyzed for reference.

Table Q-1. Summarized anonymized urine sample data.

Urine ID	Collected at	Duration	Eggs	Volume	Analyzed	Age	Gender	Notes
101	23/06/2019 - 24/06/2019		0	12ml	Yes	42	Male	Time not recorded
102	23/06/2019 - 24/06/2019		2	12ml	Yes	27	Male	Time not recorded
103	23/06/2019 - 24/06/2019	00:04:53	21	12ml	Yes	28	Female	
104	23/06/2019 - 24/06/2019	00:04:20	1	12ml	Yes	50	Female	
105	23/06/2019 - 24/06/2019	00:04:20	1	12ml	Yes	25	Female	
106	23/06/2019 - 24/06/2019	00:05:10	3	12ml	Yes	28	Male	
107	23/06/2019 - 24/06/2019	00:04:32	4	12ml	Yes	65	Female	
108	23/06/2019 - 24/06/2019	00:02:36	46	12ml	Yes	69	Female	
109	23/06/2019 - 24/06/2019	00:02:30	7	12ml	Yes	57	Female	
110	23/06/2019 - 24/06/2019	00:01:02	0	12ml	Yes	79	Male	
111	23/06/2019 - 24/06/2019	00:01:29	1	12ml	Yes	42	Male	
112	23/06/2019 - 24/06/2019	00:01:19	1	12ml	Yes	41	Female	
113	23/06/2019 - 24/06/2019	00:01:41	6	12ml	Yes	32	Male	
114	23/06/2019 - 24/06/2019	00:03:12	105	12ml	Yes	20	Female	
115	23/06/2019 - 24/06/2019	00:02:11	9	12ml	Yes	17	Male	
116	25/06/2019 - 26/06/2019	00:02:24	0	12ml	Yes	27	Female	
117	23/06/2019 - 24/06/2019	00:04:17	4	12ml	Yes	19	Female	
118	23/06/2019 - 24/06/2019	00:03:30	0	12ml	Yes	45	Female	
119	23/06/2019 - 24/06/2019	00:02:41	0	12ml	Yes	77	Male	
120	23/06/2019 - 24/06/2019	00:02:45	0	12ml	Yes	32	Male	
121	24/06/2019 - 25/06/2019	00:03:57	1	12ml	Yes	56	Male	
122	24/06/2019 - 25/06/2019	00:03:34	1	12ml	Yes	46	Male	
123	24/06/2019 - 25/06/2019	00:03:11	0	12ml	Yes	39	Female	
124	24/06/2019 - 25/06/2019	00:03:57	2	7ml	Yes	55	Male	Drinking water added due to sample having only 7 ml of urine
125	24/06/2019 - 25/06/2019	00:04:09	0	12ml	Yes	46	Female	
126	24/06/2019 - 25/06/2019	00:03:35	0	12ml	Yes	20	Female	
127	24/06/2019 - 25/06/2019	00:02:47	0	12ml	Yes	50	Female	
128	24/06/2019 - 25/06/2019	00:04:02	0	9ml	Yes	24	Female	Drinking water added due to sample having only 9 ml of urine
129	24/06/2019 - 25/06/2019	00:03:18	0	12ml	Yes	29	Male	
130	24/06/2019 - 25/06/2019	00:03:20	0	12ml	Yes	18	Female	
131	24/06/2019 - 25/06/2019	00:03:22	0	12ml	Yes	20	Male	
132	24/06/2019 - 25/06/2019	00:02:44	0	12ml	Yes	36	Male	
133	24/06/2019 - 25/06/2019	00:02:45	0	12ml	Yes	40	Male	
134	24/06/2019 - 25/06/2019	00:03:22	0	12ml	Yes	28	Female	

Urine ID	Collected at	Duration	Eggs	Volume	Analyzed	Age	Gender	Notes
135	24/06/2019 - 25/06/2019	00:03:20	0	12ml	Yes	42	Male	Filter holder dropped before measurement
136	24/06/2019 - 25/06/2019	00:02:50	0	12ml	Yes	50	Male	
137	24/06/2019 - 25/06/2019	00:03:50	1	12ml	Yes	17	Female	
138	24/06/2019 - 25/06/2019	00:02:54	0	12ml	Yes	46	Female	
139	24/06/2019 - 25/06/2019	00:03:17	0	12ml	Yes	50	Female	
140	24/06/2019 - 25/06/2019	00:02:34	0	12ml	Yes	62	Male	
141	25/06/2019 - 26/06/2019	00:02:27	0	12ml	Yes	19	Male	
142	25/06/2019 - 26/06/2019	00:02:36	0	12ml	Yes	19	Female	
143	25/06/2019 - 26/06/2019	00:02:30	0	12ml	Yes	26	Female	
144	25/06/2019 - 26/06/2019	00:03:30	4	12ml	Yes	18	Female	
145	25/06/2019 - 26/06/2019	00:03:04	0	12ml	Yes	60	Female	
146	25/06/2019 - 26/06/2019	00:03:05	0	12ml	Yes	35	Female	
147	25/06/2019 - 26/06/2019	00:03:10	0	12ml	Yes	49	Male	
148	25/06/2019 - 26/06/2019	00:03:03	0	12ml	Yes	45	Female	
149	25/06/2019 - 26/06/2019	00:03:17	4	12ml	Yes	17	Male	
150	25/06/2019 - 26/06/2019	00:02:47	0	12ml	Yes	15	Female	
151	25/06/2019 - 26/06/2019	00:03:32	0	12ml	Yes	46	Female	
152	25/06/2019 - 26/06/2019	00:02:14	0	12ml	Yes	45	Female	
153	25/06/2019 - 26/06/2019	00:02:25	0	12ml	Yes	60	Female	
154	25/06/2019 - 26/06/2019	00:02:41	0	12ml	Yes	50	Male	
155	25/06/2019 - 26/06/2019	00:03:11	0	12ml	Yes	48	Female	
156	25/06/2019 - 26/06/2019	00:02:40	0	12ml	Yes	56	Female	
157	25/06/2019 - 26/06/2019	00:02:15	0	12ml	Yes	49	Female	
158	25/06/2019 - 26/06/2019	00:02:54	0	12ml	Yes	19	Male	
159	25/06/2019 - 26/06/2019	00:03:28	173	12ml	Yes	18	Male	
160	25/06/2019 - 26/06/2019	00:02:55	1	12ml	Yes	37	Male	
161	25/06/2019 - 26/06/2019	00:02:19	0	12ml	Yes	41	Male	
162	25/06/2019 - 26/06/2019	00:02:20	0	12ml	Yes	29	Male	
163	25/06/2019 - 26/06/2019				No	24	Female	Insufficient time for analysis
164	25/06/2019 - 26/06/2019				No	48	Female	Insufficient time for analysis
165	26/06/2019 - 27/06/2019	00:04:54	3	12ml	Yes	18	Male	1 Schistosoma Mansoni egg, 6 eggs in whole sample
166	26/06/2019 - 27/06/2019	00:02:08	0	12ml	Yes	48	Male	0 eggs in whole sample
167	23/06/2019 - 24/06/2019	00:02:04	0	12ml	Yes	31	Male	
168	26/06/2019 - 27/06/2019	00:04:59	0	12ml	Yes	39	Male	0 eggs in whole sample
169	26/06/2019 - 27/06/2019	00:04:30	0	12ml	Yes	47	Male	0 eggs in whole sample
170	26/06/2019 - 27/06/2019	00:02:10	0	12ml	Yes	40	Male	0 eggs in whole sample
171	26/06/2019 - 27/06/2019	00:03:10	0	12ml	Yes	45	Female	0 eggs in whole sample
172	26/06/2019 - 27/06/2019	00:02:08	0	12ml	Yes	42	Male	0 eggs in whole sample
173	26/06/2019 - 27/06/2019	00:02:30	0	12ml	Yes	25	Male	0 eggs in whole sample
174	26/06/2019 - 27/06/2019	00:02:10	0	12ml	Yes	35	Female	0 eggs in whole sample
175	26/06/2019 - 27/06/2019	00:02:10	0	12ml	Yes	61	Male	0 eggs in whole sample
176	26/06/2019 - 27/06/2019	00:02:10	0	12ml	Yes	35	Female	0 eggs in whole sample
177	26/06/2019 - 27/06/2019				No	22	Female	Insufficient time for analysis
178	26/06/2019 - 27/06/2019				No	40	Male	Insufficient time for analysis

Urine ID	Collected at	Duration	Eggs	Volume	Analyzed	Age	Gender	Notes
179	26/06/2019 - 27/06/2019				No	20	Male	Insufficient time for analysis
180	26/06/2019 - 27/06/2019				No	18	Male	Insufficient time for analysis
181	27/06/2019 - 28/06/2019	00:02:11	0	12ml	Yes	59	Female	Urine spilled over table, returned into cup for analysis, 0 eggs in whole sample
182	27/06/2019 - 28/06/2019	00:02:12	0	12ml	Yes	48	Female	0 eggs in whole sample
183	27/06/2019 - 28/06/2019	00:02:02	0	12ml	Yes	63	Female	0 eggs in whole sample
184	27/06/2019 - 28/06/2019	00:02:23	0	12ml	Yes	34	Female	0 eggs in whole sample
185	27/06/2019 - 28/06/2019	00:02:29	0	12ml	Yes	59	Male	0 eggs in whole sample
186	27/06/2019 - 28/06/2019	00:02:08	0	12ml	Yes	44	Male	0 eggs in whole sample
187	27/06/2019 - 28/06/2019	00:02:10	0	12ml	Yes	62	Female	1 egg in whole sample
188	27/06/2019 - 28/06/2019	00:02:12	0	12ml	Yes	51	Male	2 eggs in whole sample
189	27/06/2019 - 28/06/2019	00:02:31	1	12ml	Yes	42	Female	1 egg in whole sample
190	27/06/2019 - 28/06/2019	00:02:20	0	12ml	Yes	33	Male	0 eggs in whole sample
191	27/06/2019 - 28/06/2019				No	18	Female	Insufficient urine available, 3 eggs in whole sample in 2:20
192	27/06/2019 - 28/06/2019	00:02:10	0	12ml	Yes	20	Female	0 eggs in whole sample
002	26/06/2019 - 27/06/2019	00:02:38	0	12ml	Yes	8	Male	2 eggs in whole sample, see photo
004	26/06/2019 - 27/06/2019	00:03:09	32	12ml	Yes	10	Male	92 eggs in whole sample, see photo
008	26/06/2019 - 27/06/2019	00:02:08	10	12ml	Yes	14	Female	50 eggs in whole sample
009	26/06/2019 - 27/06/2019		60	12ml	Yes	10	Male	Time not recorded, 122 eggs in whole sample
021	26/06/2019 - 27/06/2019	00:02:14	27	12ml	Yes	6	Female	45 eggs in whole sample
028	26/06/2019 - 27/06/2019	00:02:24	30	12ml	Yes	12	Male	180 eggs in whole sample
029	26/06/2019 - 27/06/2019	00:02:09	39	12ml	Yes	9	Male	61 eggs in whole sample
033	26/06/2019 - 27/06/2019	00:02:40	61	12ml	Yes	8	Male	
066	26/06/2019 - 27/06/2019	00:02:40	19	12ml	Yes	14	Male	40 eggs in whole sample
067	26/06/2019 - 27/06/2019	00:02:35	0	12ml	Yes	6	Male	6 eggs in whole sample

Appendix R. Summarized urine sample measurement data

In Table R-1, all measurements performed during the field research in Ivory Coast have been documented. In this, the measurement number (#), urine sample number, and flow cell slide number have been given. In addition, the local time at the start of the measurement, validated by the digital records of the Sodos has been given. The duration is measured as the time between the placement of the syringe filled with urine and the last holographic photo being captured. The file size is the total size of the folder containing all raw data and additional photos of detected air bubbles. The volume is measured as the total volume of urine being examined by the Sodos during the measurement and is therefore less than the total volume of the syringe (12.0ml). Notes were only added if abnormalities were observed.

Table R-1. Summarized urine sample measurement data.

#	Urine ID	Slide ID	Local time	Duration	File size	Volume	Complete	Notes
1	101	3	24/06/2019 09:40		42,91MB	0,2ml	No	Too many false ABS, remove transmit, heavily contaminated sample
2	101	3	24/06/2019 10:40	00:28:20	2,07GB	10ml	Yes	Too many false ABS, remove transmit, heavily contaminated sample
3	102	3	24/06/2019 10:26	00:27:08	1,98GB	10,7ml	Yes	ABS thresholds set to 50
4	103	3	24/06/2019 11:02	00:24:51	2,03GB	10,7ml	Yes	
5	104	3	24/06/2019 11:35		0MB	0ml	No	Failed due to cv2 not opening separate windows
6	104	3	24/06/2019 11:38		0MB	0ml	No	Failed due to cv2 not opening separate windows
7	104	3	24/06/2019 11:45	00:22:47	2,1GB	10,6ml	Yes	
8	105	3	24/06/2019 12:14	00:25:03	1,93GB	10,7ml	Yes	
9	106	3	24/06/2019 12:46		62,58MB	0,3ml	No	Incorrect multiprocessing closure, reboot required
10	106	3	24/06/2019 12:52		3,39MB	0ml	No	Label error by classifier by Patrick, disabled classifier, analyser, and reconstructor
11	106	3	24/06/2019 12:58		0MB	0ml	No	Confused with measurement 12, empty
12	106	3	24/06/2019 13:05	00:23:48	2,04GB	10,7ml	Yes	
13	107	3	24/06/2019 13:35		258,56MB	1,4ml	No	Process error, possible cause to_usb.py in parallel terminal
14	107	3	24/06/2019 13:46		0MB	0ml	No	Camera error stuck on freeze
15	107	3	24/06/2019 13:51		11,88MB	0,1ml	No	Camera error stuck on freeze
16	107	3	24/06/2019 13:57	00:21:34	1,96GB	10,7ml	Yes	
17	108	3	24/06/2019 14:29	00:22:42	1,98GB	10,7ml	Yes	
18	109	3	24/06/2019 14:56	00:22:52	1,99GB	10,7ml	Yes	
19	110	3	24/06/2019 15:23	00:23:19	2,08GB	10,7ml	Yes	Flow cell switch afterwards
20	111	4	24/06/2019 15:53	00:23:57	2,01GB	10,7ml	Yes	Power bank switch afterwards
21	112	4	24/06/2019 16:23	00:21:27	1,92GB	10,7ml	Yes	
22	113	4	24/06/2019 16:48	00:22:38	1,94GB	10,7ml	Yes	Small image capture & transfer disabled to reduce recording & transfer time
23	114	4	24/06/2019 17:36	00:22:22	1,97GB	10,7ml	Yes	
24	115	4	24/06/2019 18:02	00:22:50	1,88GB	10,7ml	Yes	
25	117	4	24/06/2019 18:30	00:24:51	1,9GB	10,5ml	Yes	
26	118	4	24/06/2019 18:58	00:23:12	2,12GB	10,6ml	Yes	Busfout before performing cleaning procedure, reboot required, transfer of 2
27	119	4	24/06/2019 19:37		1,66GB	9,6ml	No	Camera error stuck on freeze
28	119	4	24/06/2019 20:06		277,96MB	1,6ml	No	Camera error, stuck on freeze, reboot attempted
29	119	4	24/06/2019 20:14	00:22:00	1,87GB	10,7ml	Yes	Success, transfer of 1
30	120	4	24/06/2019 20:45	00:23:09	1,87GB	10,5ml	Yes	
31	167	4	24/06/2019 21:13	00:22:19	2,01GB	10,7ml	Yes	
32	121	5	25/06/2019 08:46	00:22:17	1,8GB	10,7ml	Yes	FreezeVideo set to is_ DontWait to allow timeout of missed signal
33	122	5	25/06/2019 09:17	00:21:49	1,99GB	10,7ml	Yes	DB transmit limited to 10 per category, to prevent memory error during upload
34	123	5	25/06/2019 09:50	00:24:28	1,79GB	10,7ml	Yes	
35	124	5	25/06/2019 10:22	00:23:05	1,81GB	10,7ml	Yes	Sample only has 7 ml of urine. Water has been added to allow analysis
36	125	5	25/06/2019 10:51	00:25:07	1,84GB	10,6ml	Yes	
37	126	5	25/06/2019 11:20	00:26:49	1,79GB	10,7ml	Yes	
38	127	5	25/06/2019 11:51		0MB	0ml	No	Too much air in flow cell, possibly due to the syringe not being filled completely
39	127	5	25/06/2019 11:55	00:24:02	1,91GB	10,7ml	Yes	
40	128	5	25/06/2019 12:24	00:23:31	1,87GB	10,7ml	Yes	
41	129	5	25/06/2019 12:54	00:21:28	1,82GB	10,7ml	Yes	
42	130	5	25/06/2019 13:19	00:22:20	1,9GB	10,7ml	Yes	
43	131	6	25/06/2019 14:18	00:23:32	1,83GB	10,7ml	Yes	Power bank switch afterwards
44	132	6	25/06/2019 14:46	00:21:35	1,84GB	10,7ml	Yes	Spider walked into collection cup, could be removed before reaching urine
45	133	6	25/06/2019 15:13	00:22:49	1,82GB	10,7ml	Yes	
46	134	6	25/06/2019 15:40	00:22:47	1,87GB	10,7ml	Yes	
47	135	6	25/06/2019 16:26	00:22:33	1,85GB	10,7ml	Yes	
48	136	6	25/06/2019 16:53	00:23:46	1,86GB	10,7ml	Yes	
49	136	6	25/06/2019 17:28		0MB	0ml	No	Too much air in flow cell
50	137	6	25/06/2019 17:31	00:28:56	1,95GB	10,4ml	Yes	Camera showed errors, resolved by disconnecting USB 60s and reconnecting
51	138	6	25/06/2019 18:05	00:24:28	1,97GB	10,7ml	Yes	Restart prior to run to force restart IDS Daemon
52	139	6	25/06/2019 18:33	00:22:46	1,97GB	10,7ml	Yes	
53	140	6	25/06/2019 19:00	00:25:55	1,98GB	10,6ml	Yes	
54	116	7	26/06/2019 08:15	00:21:43	1,8GB	10,7ml	Yes	
55	141	7	26/06/2019 08:40	00:22:21	1,81GB	10,7ml	Yes	
56	142	7	26/06/2019 09:06	00:22:01	1,84GB	10,7ml	Yes	
57	143	7	26/06/2019 09:33	00:22:05	1,88GB	10,7ml	Yes	
58	144	7	26/06/2019 09:59	00:26:50	2,23GB	10,7ml	Yes	Camera showed errors, resolved by disconnecting USB 20s and reconnecting
59	145	7	26/06/2019 10:31	00:21:41	1,83GB	10,7ml	Yes	Restart prior to run to restart IDS Daemon
60	146	7	26/06/2019 10:57	00:23:43	1,82GB	10,7ml	Yes	

#	Urine ID	Slide ID	Local time	Duration	File size	Volume	Complete	Notes
61	147	7	26/06/2019 11:25	00:22:34	1,8GB	10,7ml	Yes	
62	148	7	26/06/2019 11:51	00:23:06	1,97GB	10,6ml	Yes	
63	149	7	26/06/2019 12:18	00:23:00	1,86GB	10,7ml	Yes	Power bank switch afterwards
64	150	8	26/06/2019 13:12	00:21:27	1,87GB	10,7ml	Yes	User test drop afterwards during transfer
65	151	8	26/06/2019 14:52	00:22:58	2,06GB	10,7ml	Yes	
66	152	8	26/06/2019 15:19	00:24:46	2,05GB	10,7ml	Yes	
67	153	8	26/06/2019 15:47	00:24:34	2,03GB	10,7ml	Yes	
68	154	8	26/06/2019 16:15	00:23:41	2,03GB	10,7ml	Yes	
69	155	8	26/06/2019 16:41	00:24:52	2,03GB	10,6ml	Yes	
70	156	8	26/06/2019 17:32	00:22:41	2,1GB	10,7ml	Yes	Busfout before starting measurement, restart required
71	157	8	26/06/2019 17:59	00:22:47	2,1GB	10,7ml	Yes	
72	158	8	26/06/2019 18:26	00:24:46	2,3GB	10,7ml	Yes	
73	159	8	26/06/2019 19:25	00:22:44	2,28GB	10,7ml	Yes	
74	160	9	26/06/2019 19:53	00:23:06	2,05GB	10,7ml	Yes	
75	161	9	26/06/2019 20:19	00:22:39	2,06GB	10,7ml	Yes	
76	162	9	26/06/2019 20:45	00:24:51	2,13GB	10,7ml	Yes	
77	163	9	26/06/2019 21:27		7,04MB	0ml	No	Too much air in flow cell
78	163	9	26/06/2019 21:30		0MB	0ml	No	Too much air in flow cell
79	163	9	26/06/2019 21:36		0MB	0ml	No	Too much air in flow cell, stopped for the day due to team being tired and failing flow cell
80	002	10	27/06/2019 08:59	00:24:27	2,06GB	10,7ml	Yes	Cleaning with alcohol prior to start
81	004	10	27/06/2019 09:27	00:24:48	2,22GB	10,7ml	Yes	
82	008	10	27/06/2019 09:56	00:33:26	2,43GB	10,7ml	Yes	Camera showed error, resolved by disconnecting USB 20s and reconnecting
83	009	10	27/06/2019 10:34	00:27:14	2,48GB	10,7ml	Yes	Restart prior to run to restart IDS Daemon
84	021	10	27/06/2019 11:06	00:28:23	2,76GB	10,7ml	Yes	
85	028	10	27/06/2019 11:36	00:26:11	2,91GB	10,7ml	Yes	
86	029	10	27/06/2019 12:07	00:27:30	3,03GB	10,7ml	Yes	
87	033	10	27/06/2019 12:40		202,88MB	0,7ml	No	Cancelled due to the storage having unexpected little storage space
88	033	10	27/06/2019 12:55	00:23:36	2,51GB	10,7ml	Yes	
89	066	10	27/06/2019 13:25		0MB	0ml	No	Too much air in flow cell
90	066	10	27/06/2019 13:27	00:23:38	2,92GB	10,7ml	Yes	
91	067	10	27/06/2019 14:17		338,81MB	1,7ml	No	Camera kept showing error
92	067	10	27/06/2019 14:33	00:23:17	2,34GB	10,7ml	Yes	
93	165	10	27/06/2019 15:01				No	Forgot to change flow cell for next measurement
94	165	11	27/06/2019 15:08	00:24:22	2,2GB	10,7ml	Yes	
95	166	11	27/06/2019 15:35	00:25:54	2,35GB	10,7ml	Yes	
96	168	11	27/06/2019 16:20	00:22:26	2,18GB	10,7ml	Yes	
97	169	11	27/06/2019 16:48	00:24:22	2,33GB	10,7ml	Yes	
98	170	11	27/06/2019 17:16	00:24:05	2,39GB	10,7ml	Yes	
99	171	11	27/06/2019 18:01	00:22:00	2,23GB	10,7ml	Yes	
100	172	11	27/06/2019 18:26	00:23:38	2,29GB	10,7ml	Yes	
101	173	11	27/06/2019 18:54	00:23:00	2,34GB	10,7ml	Yes	
102	174	11	27/06/2019 19:20	00:27:23	2,32GB	10,7ml	Yes	
103	175	11	27/06/2019 20:10	00:24:15	2,29GB	10,7ml	Yes	
104	176	12	27/06/2019 20:41	00:23:30	2,07GB	10,7ml	Yes	
105	181	13	28/06/2019 08:09	00:27:15	1,97GB	10,7ml	Yes	
106	182	13	28/06/2019 08:42	00:27:48	2,06GB	10,2ml	Yes	
107	183	13	28/06/2019 09:13	00:26:09	1,98GB	10,7ml	Yes	
108	184	13	28/06/2019 09:43	00:24:30	2,01GB	10,6ml	Yes	
109	185	13	28/06/2019 10:10	00:24:07	2,03GB	10,6ml	Yes	
110	186	13	28/06/2019 10:39	00:26:00	1,99GB	10,7ml	Yes	Busfout before cleaning
111	187	13	28/06/2019 11:08	00:23:20	2GB	10,7ml	Yes	
112	188	13	28/06/2019 11:37	00:23:56	2,01GB	10,7ml	Yes	
113	189	13	28/06/2019 12:02		0MB	0ml	No	Too much air in flow cell
114	189	13	28/06/2019 12:06	00:22:55	2,1GB	10,7ml	Yes	
115	190	13	28/06/2019 12:46	00:22:52	2,01GB	10,7ml	Yes	
116	192	14	28/06/2019 13:14	00:23:58	1,97GB	10,7ml	Yes	Busfout before cleaning

Appendix S. Summarized maintenance data

In Table S-1, all actions involving the movement of flow cell slides during the field research in Ivory Coast have been documented. In Table S-2, all local maintenance actions during the field research in Ivory Coast excluding flow cell slide movement have been documented. For both tables, the time noted at which the action was performed was the local time at the start of the action.

Table S-1. Summarized urine sample measurement data.

Slide ID	Action	Performed at	Completed	Notes
3	Placement	24/06/2019 09:35	Yes	Sterile
3	Removal	24/06/2019 15:55	Yes	Stored contaminated
4	Placement	24/06/2019 15:56	Yes	Sterile
4	Removal	24/06/2019 23:47	Yes	Stored contaminated
5	Placement	25/06/2019 08:36	Yes	Sterile
5	Removal	25/06/2019 14:14	Yes	Stored contaminated
6	Placement	25/06/2019 14:16	Yes	Sterile
6	Removal	25/06/2019 19:35	Yes	Stored contaminated
7	Placement	26/07/2019 08:10	Yes	Sterile
7	Removal	26/06/2019 12:45	Yes	Stored contaminated
8	Placement	26/06/2019 12:46	Yes	Sterile
8	Removal	26/06/2019 19:50	Yes	Stored contaminated
9	Placement	26/06/2019 19:51	Yes	Sterile
9	Removal	26/06/2019 21:43	Yes	Stored contaminated
10	Placement	27/06/2019 08:57	Yes	Sterile
10	Removal	27/06/2019 15:06	Yes	Stored contaminated
11	Placement	27/06/2019 15:07	Yes	Sterile
11	Removal	27/06/2019 20:39	Yes	Stored contaminated
12	Placement	27/06/2019 20:40	Yes	Sterile
12	Removal	27/06/2019 21:09	Yes	Stored contaminated
13	Placement	28/06/2019 08:04	Yes	Sterile
13	Removal	28/06/2019 13:12	Yes	Stored contaminated
14	Placement	28/06/2019 13:13	Yes	Sterile
14	Removal	28/06/2019 13:47	Yes	Stored contaminated

Table S-2. Summarized urine sample measurement data.

Action	Performed at	Duration	Notes
Dry cleaning	24/06/2019 22:40	10 minutes	Camera acrylic layer showed contamination, removed using dry cotton
Emergency repairs	26/06/2019 13:20	90 minutes	Falling of the prototype caused damage to the prototype, requiring repairs
Alcohol cleaning	27/06/2019 08:43	15 minutes	Camera acrylic layer showed contamination, removed using 90% ethanol and cotton

References

1. Vos, T., Allen, C., Arora, M., Barber, R. M., Bhutta, Z. A., Brown, A., Chen, A. Z. (2016). Global, regional, and national incidence, prevalence, and years lived with disability for 310 diseases and injuries, 1990–2015: a systematic analysis for the Global Burden of Disease Study 2015. *The Lancet, 388*(10053), 1545-1602.
2. Gryseels, B., Polman, K., Clerinx, J., & Kestens, L. (2006). Human schistosomiasis. *The Lancet, 368*(9541), 1106-1118.
3. Colley, D. G., Bustinduy, A. L., Secor, W. E., & King, C. H. (2014). Human schistosomiasis. *The Lancet, 383*(9936), 2253-2264.
4. World Health Organization Expert Committee on the Control of Schistosomiasis. (2002). Prevention and control of Schistosomiasis and soil-transmitted helminthiasis. *World Health Organization Technical Report Series*. Geneva: World Health Organization.
5. International Agency for Research on Cancer. (1994). *Schistosomes, liver flukes and Helicobacter pylori* (Vol. 61): IARC Lyon.
6. King, C. H., & Dangerfield-Cha, M. (2008). The unacknowledged impact of chronic schistosomiasis. *Chronic illness*, 4(1), 65-79.
7. World Health Organization. (2017). Annex 10: Urine filtration SOP, Diagnosis of Schistosoma Haematobium. Retrieved 12-07-2019, from https://www.who.int/neglected_diseases/training/Session_9.3.2_learners_guide.pdf
8. Lengeler, C., Utzinger, J., & Tanner, M. (2002). Screening for schistosomiasis with questionnaires. *Trends in parasitology*, 18(9), 375-377.
9. Vendel, M. (2018). *The EC: a device to diagnose urinary schistosomiasis in Ghana*. Delft University of Technology, Repository. Retrieved from http://resolver.tudelft.nl/uuid:3a13cddc-d766-49e2-8363-3c0162aaa086 (3a13cddc-d766-49e2-8363-3c0162aaa086)
10. Pahl, G., & Beitz, W. (2013). *Engineering design: a systematic approach*: Springer Science & Business Media.
11. Katz, J., & Sheng, J. (2010). Applications of holography in fluid mechanics and particle dynamics. *Annual Review of Fluid Mechanics*, 42, 531-555.
12. Zubair, A. R. (2010). Biomedical Instruments: safety, quality control, maintenance, prospects & benefits of African Technology. *African journal of medicine and medical sciences*, 39, 35-40.
13. Law, E. L.-C., Roto, V., Hassenzahl, M., Vermeeren, A. P., & Kort, J. (2009). *Understanding, scoping and defining user experience: a survey approach*. Paper presented at the Proceedings of the SIGCHI conference on human factors in computing systems.
14. DePaul University. ASCII Table - Printable Characters. Retrieved 17-05-2019, from https://www.netspotapp.com/wifi-encryption-and-security.html
15. Samsonite. (2019). Find hand luggage size by airline. Retrieved 26-07-2019, from https://www.samsonite.co.uk/hand-luggage-size-restrictions-dimensions/
16. International Civil Aviation Organization. (2018). Technical instructions for the safe transport of dangerous goods by air. Retrieved 17-05-2019, from https://www.icao.int/safety/DangerousGoods/AddendumCorrigendum%20to%20the%20Technical%20Instructions/Doc%209284-2017-2018.AddendumNo2.en.pdf
17. Owens, M. (2006). *The definitive guide to SQLite*: Apress.
18. The MagPi Magazine. (2018). Raspberry Pi 3B+ Specifications and Benchmarks. Retrieved 15-07-2019, from https://www.raspberrypi.org/magpi/raspberry-pi-3bplus-specs-benchmarks/
19. The MagPi Magazine. (2019). Raspberry Pi 4 Specifications and Benchmarks. Retrieved 15-07-2019, from https://www.raspberrypi.org/magpi/raspberry-pi-4-specs-benchmarks/
20. Raspberry Pi Dramble. (2019). microSD Card Benchmarks. Retrieved 15-07-2019, from http://www.pidramble.com/wiki/benchmarks/microsd-cards#3-model-b-plus
21. Minich, D. M., & Bland, J. S. (2007). Acid-alkaline balance: role in chronic disease and detoxification. *Alternative therapies in health and medicine*, 13(4), 62.
22. Granta Design Limited. (2018). CES EduPack 2018.
23. Occupational Safety and Health Administration. (1991). *Guidelines for laser safety and hazard assessment*: Occupational Safety and Health Administration, U.S. Dept. of Labor.
24. LaserDiodeControl. (2019). Laser Diode Driver Basics. Retrieved 06-05-2019, from https://www.laserdiodecontrol.com/laser-diode-driver-basics-and-fundamentals
25. Malzahn, U. M. (2006). Driving Laser Diodes. Retrieved 06-05-2019, from https://ichaus.de/upload/pdf/laser-handout2ups.pdf
26. Union Optronic Corp. (2019). U-LD-630551A Series Laser Diode. Retrieved 17-05-2019, from http://www.uocnet.com/pdf/LD/U-LD-630551A.pdf
27. Imaging Development Systems. (2019). IDS Software Suite. Retrieved 17-05-2019, from https://en.ids-imaging.com/download-ueye-win32.html
28. Raspberry Pi Foundation. (2019). Usage of Python. Retrieved 17-05-2019, from https://www.raspberrypi.org/documentation/usage/python/
29. PyPi. (2019). PyuEye - Python bindings for uEye API. Retrieved 17-05-2019, from https://pypi.org/project/pyueye/
30. Wong, T. Y. (1981). Fluid flow control system. US4277832A.
31. Philbin, B. (1993). Control apparatus and method for controlling fluid flows and pressures.
32. Michaels, M. B., Robinson, J. C., Claude, J. P., & Alden, D. L. (1994). Automated fluid pressure control system.
33. Blomquist, M. L., & Bynum, G. B. (2006). Syringe pump control systems and methods.
34. Wijnen, B., Hunt, E. J., Anzalone, G. C., & Pearce, J. M. (2014). Open-source syringe pump library. *PloS one*, 9(9), e107216.
35. Adriaensen, J. Change unipolar 28BYJ-48 to bipolar stepper motor. Retrieved 10-03-2019, from http://www.jangeox.be/2013/10/change-unipolar-28byj-48-to-bipolar.html
36. PC Magazine. Definition of LCD. Retrieved 17-05-2019, from https://www.pcmag.com/encyclopedia/term/60488/lcd-types
37. NetSpot. WEP, WPA, WPA2, and WPA3 and their differences. Retrieved 24-05-2019, from https://www.netspotapp.com/wifi-encryption-and-security.html
38. Usability Body of Knowledge, Cognitive Walkthrough. Retrieved 13-04-2019, from http://www.usabilitybok.org/cognitive-walkthrough
39. Raspberry Pi Foundation. (2014). Introducing Raspberry Pi HATs. Retrieved 31-07-2019, from https://www.raspberrypi.org/blog/introducing-raspberry-pi-hats/
40. The Pi Hut. (2016). UPS PIco - Uninterruptible Power Supply (HV3.0B+). Retrieved 31-07-2019, from https://thepihut.com/products/ups-pico?variant=20063191203902